

Manuscript Details

Manuscript number	EARTH_2017_327_R1
Title	Origin of post-collisional magmas and formation of porphyry Cu deposits in southern Tibet
Article type	Invited review article

Abstract

The recent discovery of large porphyry copper deposits (PCDs) associated with Miocene (22–12 Ma) granitoid magmas in the eastern section of the Paleocene-Eocene Gangdese magmatic arc in the Himalaya-Tibetan orogenic belt raises new questions about the origin of water-rich (≥ 4.5 wt.%), oxidized (ΔFMQ 1–3) magmas in continental collisional settings and their mineralization potential. We review the literature and compile available data on whole rock and isotope geochemistry for Cenozoic igneous rocks from Tibet, and add new zircon $\text{Ce}^{4+}/\text{Ce}^{3+}$ and Ti-in-zircon thermometry data to better understand variations in oxidation state and thermal evolution of these suites, which are key controls on Cu mineralization. Six distinct Cenozoic igneous suites are defined: Paleocene-Eocene syn-collisional Gangdese magmatic arc rocks (ΔFMQ = -1.2 to +0.8) (suite I), and five broadly contemporaneous Miocene suites. A distinct change in magmatism along the length of the belt occurs at around 88°E in the Miocene suites: to the east, porphyry copper mineralization is associated with a moderately oxidized, high-Sr/Y granitoid suite (suite II, ΔFMQ = +0.8 to +2.9) with minor occurrences of transitional (hybrid) monzonitic (suite III) and trachytic rocks (suite IV; both with zircon $\text{Ce}^{4+}/\text{Ce}^{3+} > 50$ –100, $\text{EuN}/\text{EuN}^* \approx 0.5$, and $\Delta\text{FMQ} \approx +1$ to +2). To the west of 88°E , trachytic volcanic rocks (suite V) are more voluminous but more reduced (zircon $\text{Ce}^{4+}/\text{Ce}^{3+} < 50$, $\Delta\text{FMQ} < +1$), and are associated with sparse, poorly mineralized high-Sr/Y granitoids (suite VI) which are moderately oxidized (zircon $\text{Ce}^{4+}/\text{Ce}^{3+} = 20$ –100, $\Delta\text{FMQ} \approx +1$ to +3). The Miocene high-Sr/Y granitoids have many compositional and isotopic similarities to the Paleocene-Eocene Gangdese arc rocks, and are interpreted to have been derived by melting of the hydrated arc root, with minor mantle input. In contrast, the highly evolved isotopic signatures of the Miocene trachytic rocks, combined with deep seismic profiles and a xenolith-derived geotherm, suggest their derivation from the underthrust Indian Proterozoic subcontinental lithospheric mantle (SCLM) or old fore-arc Tibetan SCLM during phlogopite breakdown at temperatures of $\sim 1100^\circ\text{C}$. Based on published geophysical data and tectonic reconstructions, we develop a model that explains the origin of the various Miocene magmatic suites, their spatial differences, and the origin of related PCDs. Following the early stages of continental collision (Eocene–Oligocene), shallow underthrusting of the Indian continental lithosphere and subcretion of Tethyan sediments (including oxidized carbonates and possibly evaporites) under eclogite facies conditions promoted the release of aqueous fluids, which hydrated and oxidized the base of the overlying Tibetan plate. This metasomatism rendered the Tibetan lower crust fusible and fertile for metal remobilization. During the mid-Miocene, the Indian slab steepened in the eastern sector (east of $\sim 88^\circ\text{E}$). In this eastern belt, deeply derived trachytic magmas were trapped in melt zones at the base of the Tibetan crust, and variably mixed with the crustally-derived, high Sr/Y granitoid magmas. They may also have released water that contributed to fluid-fluxed melting of the lower crust, producing voluminous high-Sr/Y granitoid magmas, which were associated with significant PCD mineralization. Hybridization between the trachytic magmas and lower crustal partial melts is indicated by intermediate isotopic compositions, enriched Cr and Ni contents, and high Mg# in some intermediate-to-felsic (56–70 wt. % SiO_2) high-Sr/Y granitoids. Trapping of the trachytic melts in deep crustal melt zones explains the relatively small volumes of trachytic magmas erupted at surface in the east. In contrast, to the west of $\sim 88^\circ\text{E}$, subduction of the Indian plate has remained flat to the present day, preventing incursion of hot asthenosphere. Consequently, cooler conditions in the deep Tibetan lithosphere resulted in limited crustal melting and the production of only small volumes of high-Sr/Y granitic magmas. Trachytic melts ascending from the underthrust Indian or Tibetan plate were able to pass through the cooler lower crust and erupted in greater volume at surface, whereas only small volumes of high-Sr/Y granitoid magma were generated and are not associated with significant PCD mineralization.

Keywords	high-Sr/Y granitoids, trachytic magmatism, Indian subduction geometry, water-fluxed melting, Gangdese, porphyry copper deposits
Corresponding Author	Rui Wang
Corresponding Author's Institution	CSIRO
Order of Authors	Rui Wang, Roberto Weinberg, William Collins, Jeremy Richards, Di-Cheng Zhu
Suggested reviewers	Mark Allen, Massimo Chiaradia, Yongjun Lu, Yildirim Dilek

Origin of post-collisional magmas and formation of porphyry Cu deposits in southern Tibet

Rui Wang^{1,2*}, Roberto F. Weinberg³, William J. Collins⁴, Jeremy P. Richards⁵, and Di-cheng Zhu¹

¹State Key Laboratory of Geological Processes and Mineral Resources, and School of Scientific Research, China University of Geosciences, Beijing 100083, China

²CSIRO Mineral Resources, Perth, WA 6151, Australia

³School of Earth, Atmosphere and Environment, Monash University, Building 28, Clayton, Victoria 3800, Australia

⁴The Institute for Geoscience Research (TIGeR), Department of Applied Geology, Curtin University, GPO Box U1987 Perth WA 6845, Australia

⁵Harquail School of Earth Sciences, Laurentian University, Sudbury, Ontario, P3E 2C6, Canada

The recent discovery of large porphyry copper deposits (PCDs) associated with Miocene (22–12 Ma) granitoid magmas in the eastern section of the Paleocene-Eocene Gangdese magmatic arc in the Himalaya-Tibetan orogenic belt raises new questions about the origin of water-rich (≥ 4.5 wt.%), oxidized (ΔFMQ 1–3) magmas in continental collisional settings and their mineralization potential. We review the literature and compile available data on whole rock and isotope geochemistry for Cenozoic igneous rocks from Tibet, and add new zircon $\text{Ce}^{4+}/\text{Ce}^{3+}$ and Ti-in-zircon thermometry data to better understand variations in oxidation state and thermal evolution of these suites, which are key controls on Cu mineralization. Six distinct Cenozoic igneous suites are defined: Paleocene-Eocene syn-collisional Gangdese magmatic arc rocks (ΔFMQ = -1.2 to +0.8) (suite I), and five broadly contemporaneous

Miocene suites. A distinct change in magmatism along the length of the belt occurs at around 88°E in the Miocene suites: to the east, porphyry copper mineralization is associated with a moderately oxidized, high-Sr/Y granitoid suite (suite II, $\Delta\text{FMQ} = +0.8$ to $+2.9$) with minor occurrences of transitional (hybrid) monzonitic (suite III) and trachytic rocks (suite IV; both with zircon $\text{Ce}^{4+}/\text{Ce}^{3+} > 50$ -100, $\text{Eu}_\text{N}/\text{Eu}_\text{N}^* = \sim 0.5$, and $\Delta\text{FMQ} = \sim +1$ to $+2$). To the west of 88°E, trachytic volcanic rocks (suite V) are more voluminous but more reduced (zircon $\text{Ce}^{4+}/\text{Ce}^{3+} < 50$, $\Delta\text{FMQ} < +1$), and are associated with sparse, poorly mineralized high-Sr/Y granitoids (suite VI) which are moderately oxidized (zircon $\text{Ce}^{4+}/\text{Ce}^{3+} = 20$ –100, $\Delta\text{FMQ} = \sim +1$ to $+3$).

The Miocene high-Sr/Y granitoids have many compositional and isotopic similarities to the Paleocene-Eocene Gangdese arc rocks, and are interpreted to have been derived by melting of the hydrated arc root, with minor mantle input. In contrast, the highly evolved isotopic signatures of the Miocene trachytic rocks, combined with deep seismic profiles and a xenolith-derived geotherm, suggest their derivation from the underthrust Indian Proterozoic subcontinental lithospheric mantle (SCLM) or old fore-arc Tibetan SCLM during phlogopite breakdown at temperatures of $\sim 1100^\circ\text{C}$.

Based on published geophysical data and tectonic reconstructions, we develop a model that explains the origin of the various Miocene magmatic suites, their spatial differences, and the origin of related PCDs. Following the early stages of continental collision (Eocene–Oligocene), shallow underthrusting of the Indian continental lithosphere and subcretion of Tethyan sediments (including oxidized carbonates and possibly evaporites) under eclogite facies conditions promoted the release of aqueous fluids, which hydrated and oxidized the base of the overlying Tibetan plate. This metasomatism rendered the Tibetan lower crust fusible and fertile for metal remobilization.

During the mid-Miocene, the Indian slab steepened in the eastern sector (east of $\sim 88^{\circ}\text{E}$). In this eastern belt, deeply derived trachytic magmas were trapped in melt zones at the base of the Tibetan crust, and variably mixed with the crustally-derived, high Sr/Y granitoid magmas. They may also have released water that contributed to fluid-fluxed melting of the lower crust, producing voluminous high-Sr/Y granitoid magmas, which were associated with significant PCD mineralization. Hybridization between the trachytic magmas and lower crustal partial melts is indicated by intermediate isotopic compositions, enriched Cr and Ni contents, and high $\text{Mg}^{\#}$ in some intermediate-to-felsic (56–70 wt. % SiO_2) high-Sr/Y granitoids. Trapping of the trachytic melts in deep crustal melt zones explains the relatively small volumes of trachytic magmas erupted at surface in the east.

In contrast, to the west of $\sim 88^{\circ}\text{E}$, subduction of the Indian plate has remained flat to the present day, preventing incursion of hot asthenosphere. Consequently, cooler conditions in the deep Tibetan lithosphere resulted in limited crustal melting and the production of only small volumes of high-Sr/Y granitic magmas. Trachytic melts ascending from the underthrust Indian or Tibetan plate were able to pass through the cooler lower crust and erupted in greater volume at surface, whereas only small volumes of high-Sr/Y granitoid magma were generated and are not associated with significant PCD mineralization.

Key words: high-Sr/Y granitoids, trachytic magmatism, Indian subduction geometry, water-fluxed melting, Gangdese, porphyry copper deposits

Table of contents

1. Introduction

2. Geological setting

2.1 Tectonics

178		
179		
180	75	2.2 Magmatism
181		
182	76	2.3 Metallogenesis
183		
184	77	3. Geodynamic evolution of the Himalayan orogen.
185		
186		
187	78	3.1 Onset of Indian-Asian collision
188		
189	79	3.2 Indian plate shallow subduction
190		
191	80	3.3 The nature of subducted Indian lithosphere
192		
193	81	3.4 Present-day configuration of the collision zone
194		
195	82	4. Six magmatic suite in the Gangdese belt
196		
197	83	4.1 Paleocene-Eocene Gangdese arc igneous rocks
198		
199	84	4.2 Eastern Miocene high-Sr/Y granitoids
200		
201	85	4.3 Western Miocene high-Sr/Y granitoids
202		
203	86	4.4 Western Miocene trachyte suite
204		
205	87	4.5 Eastern Miocene trachyte suite
206		
207	88	4.6 Eastern transitional monzonites
208		
209	89	5. Trace elements in zircons
210		
211	90	5.1 Trace element characteristics
212		
213	91	5.2 Magma oxidation state
214		
215	92	5.3 Magma temperature
216		
217	93	5.4 Petrogenesis implication
218		
219	94	6. Discussion
220		
221	95	6.1 Paleogene magmatism
222		
223	96	6.2 Post-Eocene Indian plate shallow subduction
224		
225	97	6.3 Origin of Miocene trachytes
226		
227	98	6.4 Tibetan or Indian lithospheric mantle melting as a source for trachytes?
228		
229		
230		
231		
232		
233		
234		
235		
236		

99	6.5 Fluid-fluxed melting and oxidation of Tibetan lower crust in the Miocene: the
100	origin of high-Sr/Y granitoids
101	6.6 Mixing model for Miocene high-Sr/Y magmas
102	6.7 Thermal structure of the Miocene Gangdese belt
103	6.8 Geodynamic model
104	6.9 Metallogenic implications

1. Introduction

Porphyry copper deposits (PCDs) are generally associated with oxidized and H₂O-rich magmas, typical features of magmatic arcs (Burnham, 1979; Candela, 1992; Richards, 2003; Sillitoe, 2010). In island arcs and continental arcs, where porphyry deposits form, it is generally thought that oxidized, sulphur-rich fluids released from subducting slabs migrate into the asthenospheric mantle wedge, where they cause partial melting and mobilization of metals (Richards, 2003; Audétat and Simon, 2012), and ultimately transfer these metals into the crust. Recently, large porphyry copper deposits (PCDs) have been found in association with post-collisional (Miocene; 22–12 Ma), high-Sr/Y granitoid plutons emplaced in the eastern section of the Paleocene-Eocene Gangdese magmatic arc in the Himalayan-Tibetan orogenic belt (Fig. 1; Hou et al., 2004, 2015; Yang et al., 2009, 2016; Lu et al., 2015; Wang et al., 2014a, b, 2015a). These discoveries raise questions about the nature of magmatic and metallogenic processes during continental collision.

In the Gangdese magmatic arc, the porphyry-related intrusions are coeval with a suite of Miocene potassic volcanic rocks (24–8 Ma), which have been collectively termed ultrapotassic volcanic rocks (UPVs) in the literature (Williams, 2000; Williams et al., 2001, 2004; Ding et al., 2003; Chung et al., 2005; Zhao et al., 2009; Zhou et al., 2010; Wang et al., 2014c; Guo et al., 2013, 2015; Liu D et al., 2014, 2015, 2017; Xu et al., 2017). In this paper,

we refer to this suite as trachytic. However, there is a puzzling difference in the spatial distribution of the Miocene intrusive (high-Sr/Y granitoid) and trachytic volcanic suites along the length of the Gangdese belt, with abundant PCD-hosting granitoids cropping out east of ~88°E, but only a few poorly mineralized granitoids to the west (Hou et al., 2004; Zhao et al., 2009; Li et al., 2011; Wang et al., 2014c; Yang et al., 2016). In contrast, trachytic volcanic rocks are relatively common along the Gangdese belt west of 88°E, but rare to the east (Fig. 1).

A number of hypotheses have been proposed to explain the unusual origin of these Miocene PCDs and their high-Sr/Y granitoid hosts (reviewed by Wang et al., 2015a, and Yang et al., 2016). These hypotheses typically link the deposits to recycling of the subduction-fertilized, deeper sections of the Paleocene-Eocene arc, and many ascribe the magmas to either the remelting of the Tibetan lower arc crust (Chung et al., 2003, 2009; Hou et al., 2004; Li et al., 2011) or metasomatized Tibetan lithospheric mantle (Lu et al., 2015), while some argue for hybrid magmas from both sources (Wang et al., 2015a; Yang et al., 2015, 2016). However, none of these models explain all the features (geochemistry, water content, redox state) of these Miocene granitoids, and especially their relationship with coeval trachytic volcanic rocks. Deep crustal and mantle xenoliths entrained by the Miocene trachytes provide direct information regarding crust-mantle hybridization (Chan et al., 2009; Liu CZ et al., 2011; Liu D et al., 2014; Wang et al., 2016), and suggest a link between the origin of high-Sr/Y granitoids and the coeval Miocene potassic volcanic rocks (Wang et al., 2017a).

The transition from subduction-related magmatism in the Paleocene to collisional magmatism in the Miocene is accompanied by significant changes in geochemical and isotopic (Sr-Nd-Hf-O) magmatic compositions (Wang et al., 2015a, b; Yang et al., 2016), suggesting that underthrusting of the Indian plate was a major control on the nature of

Miocene Gangdese magmatism. Following the Indian-Asian collision at ~55–50 Ma (Van der Voo et al., 1999; de Sigoyer et al., 2000; Meng et al., 2012; Ding et al., 2016; Zhu et al., 2015, 2017), the subsequent magmatic quiescence in the late Eocene–Oligocene reflects shallow angle underthrusting of the Indian continental margin (Guillot et al., 2008; Ji et al., 2009; Ding et al., 2016). However, recent seismic studies reveal contrasting Indian plate subduction geometry from west to east, with shallow underthrusting beneath the western Gangdese belt, and steep underthrusting in the east (Zhao et al., 2010). By combining the location of a high-velocity seismic anomaly corresponding to the subducted Indian plate in the deep mantle with the palaeogeographic position of India, Replumaz et al. (2010) suggested that steep subduction of India was initiated before 25 Ma. We suggest that the transition to steeper subduction in the east should have occurred in the Miocene, leading to the opening of an asthenospheric mantle wedge in the east but not in the west. Such differences impact the tectono-thermal regime of the evolving collisional system, and the impact on magmatism shown by the differences in the spatial distribution of intrusive and volcanic suites in the Miocene.

Here, we review major aspects of the geodynamic setting of the Himalayan-Tibetan orogen and the Miocene evolution of the Gangdese magmatic arc. We start with a brief summary of the geological setting followed by an overview of the geodynamic aspects of the orogen. We then use a compilation of 288 published geochemical and isotopic analyses to distinguish between six Cenozoic igneous suites exposed in the Gangdese belt. We add new titanium-in-zircon thermometry and zircon $\text{Ce}^{4+}/\text{Ce}^{3+}$ data to constrain the temperatures and redox states of these suites, and new plagioclase compositional data to constrain the magmatic water contents. These features are combined with geodynamic reconstructions to derive an integrated petrogenetic model for Miocene magmatism and mineralisation in the Gangdese belt.

2. Geological setting

2.1 Tectonics

The Himalayan-Tibetan orogen is composed of (from south to north) the Himalayas, Lhasa terrane, Qiangtang terrane, and Songpan-Ganze complex, separated from each other by the Indus-YarlungTsangpo, Bangong-Nujiang, and Jinsha River sutures, respectively (Yin and Harrison, 2000; Zhu et al., 2013). The Lhasa terrane is divided into northern, central, and southern Lhasa subterrane, bounded by the Shiquan River–Nam Tso Mélange zone and the Luobadui–Milashan fault, respectively (Fig. 1; Zhu et al., 2011, 2013). The core of the Lhasa terrane consists of Archean and Proterozoic crystalline basement (Zhu et al., 2011), which is considered to have rifted from the Gondwana margin in the Late Triassic (Zhu et al., 2013; Li et al., 2016). The Lhasa terrane is thought to have collided with the Qiangtang terrane to the north in the Early Cretaceous (Kapp et al., 2005; Zhu et al., 2016). Northward subduction of Neo-Tethyan oceanic lithosphere beneath its new northern margin, represented by the accreted Lhasa terrane, began in the Late Triassic or Early Jurassic (Chu et al., 2006). Whole rock Nd and zircon Hf isotopic compositions of the granitoid rocks in the Lhasa terrane suggest an old and isotopically evolved central Lhasa subterrane with juvenile northern and southern subterrane (Zhu et al., 2011; Hou et al., 2015).

The India–Asia collision started at ~55–50 Ma when the Greater India plate (Indian continental margin; Ali and Aitchison, 2005) first collided with the Lhasa terrane (Meng et al., 2012; van Hinsbergen et al., 2012; Zhu et al., 2015; Ding et al., 2016). The thicker and more rigid Indian craton continues to subduct beneath the Lhasa terrane to the present day (Kind and Yuan, 2010; Replumaz et al., 2010; Zhao et al., 2010). Seismic tomographic studies indicate that the Indian continental lithosphere (100 to 200 km thick) extends northward below the Tibetan plateau, where it is in direct contact with the base of the south Tibetan

crust, and where the Tibetan plate sub-continental mantle lithosphere (SCLM) appears to have been removed (Chung et al., 2009; Nábělek et al., 2009).

2.2 Magmatism

North-directed Neo-Tethyan subduction beneath southern Tibet produced voluminous Jurassic–Cretaceous calc-alkaline magmatism in the Lhasa terrane (Harris et al., 1986; Wen, 2007; Mo et al., 2008; Lee et al., 2011; Wang et al., 2017b; Zhu et al., 2017). In contrast to most Jurassic–Cretaceous igneous rocks that show typical continental arc features, a suite of ~90–85 Ma charnockites with adakite-like features have been reported from the eastern Gangdese belt (Wen et al., 2008; Zhang et al., 2010). These adakite-like rocks were interpreted to have been derived from partial melting of the lower crust during “flat-slab” subduction of the Neo-Tethyan ocean (Wen et al., 2008), or from the partial melting of a subducted oceanic slab in a mid-ocean ridge subduction setting (Guan et al., 2010; Zhang et al., 2010). A systematic geochronological study of Gangdese arc rocks reveals a magmatic gap or quiescent period between ca. 80 and 70 Ma (Wen et al., 2008; Ji et al., 2009). Afterwards, rollback of the Neo-Tethyan slab at ~69–53 Ma and possibly slab breakoff at ~53–50 Ma triggered a magmatic flare-up (Kapp et al., 2007; Wen, 2007; Wang et al., 2015b; Zhu et al., 2015), represented by extensive Paleocene–Eocene I-type intrusive rocks and widespread Linzizong volcanic successions (Mo et al., 2008; Zhu et al., 2015, 2017; Fig. 1). A magmatic gap or quiescent period from ~40–30 Ma was followed by emplacement of a large number of small-volume calc-alkaline to alkaline intrusions and potassic (trachytic) volcanic rocks in southern Tibet during the Oligo-Miocene (Ding et al., 2003; Hou et al., 2009; Lu et al., 2015; Wang et al., 2015a, 2016, 2017a; Yang et al., 2016).

2.3 Metallogenesis

Three episodes of porphyry-type mineralization are recognized in southern Tibet (Fig. 1): Jurassic, Paleocene-Eocene, and Miocene.

The Middle Jurassic Xietongmen (Xiongmen) district in the middle of the Gangdese magmatic belt is a large magmatic-hydrothermal centre (Tafti et al., 2009, 2014; Tang et al., 2015; Wang et al., 2017b) that hosts the Xietongmen (No. I: 219.8 Mt @ 0.43% Cu, 0.51g/t Au and 3.87g/t Ag) and Newtongmen (No. II: 388.9 Mt @ 0.32% Cu, 0.18g/t Au and 0.87g/t Ag) deposits, and a few smaller Cu-Au prospects (e.g., Tangbai and Zemoduola). The intrusions related to the ore-forming events are 176-171 Ma quartz diorite and granodiorite porphyries (Tafti, 2011; Tang et al., 2015; Wang et al., 2017b).

Only two small deposits are known to have formed in the Paleocene–Eocene: the Sharang porphyry Mo deposit (52.25 ± 0.31 Ma; 10 Mt @ 0.061% Mo; Zhao et al., 2014) and the Jiru porphyry Cu deposit (49.2 ± 1.7 Ma; 41.9 Mt @ 0.43 Cu; Zheng et al., 2014).

The largest porphyry copper deposits formed in the eastern Gangdese belt (east of 88°E) in the Miocene, and include the 16.4 ± 0.5 Ma Qulong porphyry Cu-Mo deposit (1,420 Mt @ 0.5% Cu; Yang et al., 2009), the 14.7 ± 0.3 Ma Jiama porphyry Cu-Mo deposit (1,054 Mt @ 0.44% Cu; Ying et al., 2014; Zheng et al., 2016), and the smaller Tinggong, Bangpu, Tangbula, and Zhunuo porphyry Cu-Mo deposits (Hou et al., 2011; Wang et al., 2015a; Fig. 1). The ore-forming intrusions are granodiorite porphyries or granite porphyries with high Sr/Y ratios (here termed high-Sr/Y granitoids), with ages between 21–13 Ma (Yang et al., 2016). In the western part of the belt (west of $\sim 88^{\circ}\text{E}$), Miocene plutons are sparse, and are associated with only a few, small porphyry deposits (e.g., Zhunuo porphyry Cu deposit; Zheng et al., 2007).

3. Geodynamic evolution of the Himalayan-Tibetan orogen

3.1 Onset of Indian-Asian collision

The timing of initial Indian-Asian collision is important for understanding the evolution of the Himalayan-Tibetan orogen. Based on the magmatic, metamorphic, biostratigraphic, and paleomagnetic data, most workers agree that the onset of Indian continental subduction below Asia occurred 55–50 Ma ago (de Sigoyer et al., 2000; Weinberg and Dunlap, 2000; Meng et al., 2012; DeCelles et al., 2014; Zhu et al., 2015; Ding et al., 2016). However, others have proposed ages ranging from ~70 to 35 Ma (e.g., Yin and Harrison, 2000; Aitchison et al., 2007). Palaeomagnetic data indicate that the Lhasa terrane was at a latitude of 24°N when it collided with Greater India at ~50 Ma (Meng et al., 2012). For the next 16 m.y., the southern margin of Asia remained almost fixed while the Greater India plate subducted beneath it (soft collision; Ali and Aitchison, 2005), causing shortening in the Himalaya and early uplift of the Tibetan Plateau. By the end of the Eocene (~34 Ma), the thicker Indian craton made contact with the Asian margin (hard collision: van Hinsbergen et al., 2012), increasing compressional stress and initiating northward displacement of the southern margin of the Asian plate (Meng et al., 2012).

3.2 Indian plate shallow subduction

The Indian plate is thought to have underthrust the Asian margin at a shallow angle in the Eocene-Oligocene, as indicated by the following lines of evidence: (1) igneous rocks formed between 50–41 Ma in the Gangdese arc on the southern Asian margin show more heterogeneous and lower $\epsilon_{\text{Hf}}(t)$ and $\epsilon_{\text{Nd}}(t)$ values than early Cretaceous-Eocene arc igneous rocks (Chung et al., 2005; Ji et al., 2009; Wang et al., 2015b), suggesting the involvement of old crustal material not previously present in this part of the Tibetan plate, such as the Indian

continental crust; (2) Indian plate upper crustal rocks in the Himalayan orogen (longitude 80°–95°E) show evidence for an early Eocene (48–45 Ma) medium-pressure amphibolite-facies metamorphic event, suggesting underthrusting to depths of ~20–30 km beneath southern Tibet (Guillot et al., 2008; Ding et al., 2016); and (3) the ages of Gangdese belt magmatic zircons record a magmatic gap between ~41 and 30 Ma (Ji et al., 2009), which is interpreted to represent cessation of Gangdese magmatism due to shallow subduction (Chung et al., 2005; Rowley and Currie, 2006).

3.3 Initiation of steep subduction

Based on the studies of Replumaz et al. (2004), Negredo et al. (2007), and Replumaz et al. (2010), the initiation of steep subduction can be estimated through combining the deepest part of the high wavespeed anomaly in the deep mantle and the palaeoposition of the subduction slab front. By combining the location of this anomaly with palaeogeographical positions of India, Replumaz et al. (2010) suggest the India initiated steep subduction before 15 Ma.

The geological evidence of steep subduction comes from the discovery eclogite in the central Himalaya around 88.5°E (the eastern Gangdese belt), and the only Lu-Hf date directly from Arun garnet is 20.7 ± 0.4 Ma (Corrie et al., 2010). The preservation of UHP metamorphism requires steep subduction to permit the rapid return of UHP rocks to the surface (Leech et al. 2005). Therefore, we suggest that the transition to steeper subduction in the east should have occurred in the Miocene, which led to the opening of an asthenospheric mantle wedge in the east but not in the west. This proposal is in line with the recent seismic data. The dip angle of the northward Indian lithospheric subduction is increasing from the west to east. The structure in the eastern Gangdese at the present is still steep subduction, farther west in the Pamirs, it is apparent that subduction breakoff is occurring now (Lister et al., 2008).

709
710
711 299
712
713 300
714
715
716 301
717
718 302
719
720 303
721
722 304
723
724 305
725
726 306
727
728 307
729
730 308
731
732 309
733
734 310
735
736 311
737
738 312
739
740 313
741
742 314
743
744 315
745
746 316
747
748 317
749
750 318
751
752 319
753
754 320
755
756 321
757
758 322
759
760 323
761
762
763
764
765
766
767

3.4 The nature of subducted Indian lithosphere

In order to understand the influence of the underthrust material on the post-collisional magmatic evolution of the Gangdese belt, it is necessary to consider the nature of the continental material involved. In addition to crystalline and clastic sedimentary rocks (such as limestone, mudstone, and chert; Phillips et al., 2013), evaporates and carbonates are reported in the Neoproterozoic sequence, NW Himalaya, India (Singh et al., 2006). Related carbonates are also reported in the Proterozoic stratigraphy of the Lesser Himalaya (Saha, 2013), and large volumes of Late Jurassic sabkhas containing evaporitic sulphates and minor chlorides were likely subducted. Such deposits occur widely on the southern margin of the former Tethys Ocean, and are found from across the Arabian Peninsula to Iran (Leeder and Zeidan, 1977). In addition, Cretaceous-Tertiary (K-T) boundary evaporites are found in the Malatya Basin on the Anatolide-Tauride plate of the Neo-Tethys Sea (Ayyıldız et al., 2015). Eocene Tethyan evaporites were very likely to have existed, especially at the leading edge of the subducting Indian plate where the sedimentary facies was shallow water and deposited during the “Eocene maximum”, when corals extended to latitudes 51°N. Northern India was ~20-30°S at this stage, probably close to the tropic of Capricorn. (Scheibner and Speijer, 2008). Carbonate-bearing coesite eclogite also occurs in the Tso-Moriri crystalline complex in eastern Ladakh, India, suggesting that the northern margin of the Indian continent was covered by carbonates and evaporites (Mukherjee et al., 2003; Johnston et al., 2011). Evidence for subduction of these materials is important, because unlike crystalline and clastic rocks, carbonates and sulphates are oxidants (Hattori, 2014), and their subduction could have affected the oxidation state of the orogen.

768
769
770 324 3.5 Present-day configuration of the collision zone
771

772 325 The Tibetan-Himalayan system is composed of three major parts: the Indian, Tibetan, and
773
774 326 Asian lithosphere, from south to north. A large number of seismic arrays have been operated
775
776
777 327 across large sections of the Tibetan plateau for over two decades to reveal the lithospheric
778
779 328 structure of the collision zone.

780
781 329
782
783 330 Indian lithosphere
784

785 331 There is abundant seismic evidence for subduction of the Indian plate below the southern
786
787 332 Tibetan Plateau. Seismic tomographic studies indicate that the Indian continental lithosphere
788
789 333 (100 to 200 km thick) dips northward below the Tibetan plateau, but that the extent of
790
791 334 underthrusting decreases from west ($\sim 31^\circ$ N, $\sim 85^\circ$ E) to east ($\sim 30^\circ$ N, $\sim 91^\circ$ E), with a NE-
792
793 335 directed convergence vector (Kumar et al., 2006; Li et al., 2008; Kind and Yuan, 2010; Zhao
794
795 336 et al., 2010; Shokoohi Razi et al., 2014; Liang et al., 2016).

796
797 337 The geometry and lateral continuity of the underthrust Indian plate lithosphere is debated,
798
799 338 limited by non-uniform seismic station coverage and the imprecision of existing tomographic
800
801 339 images (Liang et al., 2016). Receiver-function images (Kumar et al., 2006; Zhao et al., 2010)
802
803 340 and body and surface wave tomographic models (Nunn et al., 2014) suggest a west to east
804
805 341 increase in the dip-angle of the Indian plate lithosphere, a decrease of Indian plate
806
807 342 lithospheric thickness, and lack of Tibetan SCLM in the west (Fig. A1). The west–east
808
809 343 variability of P-normal velocities beneath the Himalayas and southern Tibet indicates that the
810
811 344 subducted Indian continental lithosphere is not homogeneous (Hearn et al., 2011). Fast
812
813 345 velocities (~ 8.4 km/s) were detected at a depth of ~ 90 km below the Tibetan plateau, which
814
815 346 are interpreted to correspond to localized formation of eclogite during underthrusting of
816
817 347 Indian lower crust in the Miocene (Huang et al., 2009; Shokoohi Razi et al., 2014). This
818
819 348 seismically fast material extends to the north of 32° N in western Tibet. In contrast, below
820
821
822
823
824
825
826

349 eastern Tibet north–south-trending low-velocity anomalies are dominant (Liang et al., 2012).
 350 Low-velocity anomalies in the upper mantle have been interpreted as evidence of
 351 fragmentation of the Indian lithosphere (Liang et al., 2016). Three dimensional iso-surface
 352 plots (Figure 8 in Liang et al., 2016) for the S-wave model reveal west-to-east variations of
 353 Indian lithosphere (high-velocity anomalies), characterized by a shallowly dipping and
 354 relatively intact lithosphere between longitude 85°E and 88°E, but a fragmented, steeply
 355 dipping lithosphere between 88°E and 91°E. This fragmentation appears to connect with N–
 356 S-trending rift faults and basins at surface in Tibet. Although there is some debate on the
 357 detailed 3D structure of the subducting Indian lithosphere under Tibet at present, the main
 358 feature revealed by geophysical data above is flat subduction occurring in the west and
 359 steepening to the east.

360

361 Tibetan lithosphere

362 Lithosphere structure inferred from elevation, gravity and geoid anomalies, and
 363 International Deep Profiling of Tibet and Himalaya (INDEPTH) surveys, reveal a Tibetan
 364 lithosphere with thickness of ~180–200 km beneath central and northern Tibet that thins
 365 southward where underlain by subducting Indian lithosphere (Kumar et al., 2006; Jiménez-
 366 Munt et al., 2008; Zhao et al., 2011).

367 Seismic data indicate that the crust in southern Tibet is ~75 km thick, consisting of ~50
 368 km of Tibetan crust underthrust by ~25 km of Indian crust (Owens and Zandt, 1997; Nábělek
 369 et al., 2009). Magnetotelluric data from the Tibetan–Himalayan orogen from 77°E to 92° E
 370 show an extensive low resistivity zone, interpreted to be a partially molten layer, along the
 371 southern margin of the Tibetan plateau (Unsworth et al., 2005). Numerical models suggest
 372 the possibility of channel flow of the partially molten layer under Tibet towards the
 373 Himalayan front driven by lateral pressure gradients due to the topographic elevation

differences (Clark and Royden, 2000; Beaumont et al., 2001). However, Miocene high-Sr/Y granitoid magmas derived from the lower crust in southern Tibet (Hou et al., 2004) and leucogranites in the High Himalayan Crystalline Series (Guo and Wilson, 2012) show very different geochemical compositions, and do not support a connected, homogeneous lower crustal melt sheet in the Miocene.

Based on the evidence summarized above, the Indian-Asian collision occurred at ~55–50 Ma, followed by shallow subduction of the Indian plate under the Asian margin. The subduction angle remained flat in the western Gangdese belt, but steepened in the east in the Miocene (Replumaz et al., 2010). Present-day configuration suggests that possible magmatic sources for Miocene igneous rocks in southern Tibet are the Tibetan and Indian lithospheres, and/or asthenosphere.

4. Six Cenozoic magmatic suites in the Gangdese belt

We have compiled published whole-rock geochemical data for 288 least-altered Paleocene-Eocene (65–42 Ma) intrusive rocks and Miocene (24–8 Ma) volcanic and intrusive rocks from the Gangdese belt in order to assess spatial differences in composition and petrogenesis along the belt. Because some sample locations in the eastern Gangdese belt are associated with porphyry-type alteration and mineralization, we excluded any samples with >2 wt. % LOI or which were described as significantly altered. Four samples from mine sites that showed extreme K/Na ratios were also excluded. Whole-rock geochemical and isotopic data are listed in Tables 1 and A1 together with references. During the Oligocene magmatic gap (Ji et al., 2009) only minor volumes of igneous rocks were formed, restricted to the Mingze-Chenba area, where small quartz monzonite and quartz monzonite plutons were emplaced at ~30 Ma (Zheng et al., 2012; Wang et al., 2014a). These have not been included in the Miocene suites.

Six Cenozoic igneous suites crop out along the Gangdese belt (Fig. 1): (1) a voluminous Paleocene–Eocene Gangdese arc calc-alkaline suite (including intrusive rocks and Linzizong volcanic rocks) that crops out along the length of the belt; and five Miocene suites that are subdivided at a longitude of $\sim 88^\circ\text{E}$: (2) a sparse western Miocene high-Sr/Y granitoid suite; (3) a more voluminous eastern Miocene high-Sr/Y granitoid suite; (4) a voluminous western Miocene trachytic suite (trachyandesitic to trachydacitic volcanic and subvolcanic rocks, commonly called ultrapotassic volcanic rocks, or UPV); (5) a sparse eastern Miocene trachydacitic (UPV) suite; and (6) a transitional (hybrid) Miocene monzonitic granitoid suite, which outcrops only to the east of $\sim 88^\circ\text{E}$. A summary of the main features of these six suites and their zircon and plagioclase elemental compositions is given in Table 1 and discussed below.

4.1 Paleocene–Eocene Gangdese arc igneous rocks

The first and oldest Cenozoic suite consists of voluminous Paleocene–Eocene I-type intrusive and volcanic rocks (Linzizong volcanic successions; 67.7–42.5 Ma; references for all ages are provided in Table A1) that cover nearly 50 % of the Gangdese arc (Fig. 1). Mafic to intermediate intrusive rocks (gabbros and diorites) are mainly composed of plagioclase, pyroxene, and amphibole, whereas granitoids are hornblende-bearing with minor biotite. The Linzizong volcanic successions extend in a 1600 km-long, E–W-trending belt and consist of calc-alkaline basaltic-andesitic lava flows, tuffs, and breccias, and dacitic to rhyolitic ignimbrites. Silica values range from 48–76 wt. % SiO_2 . They are calc-alkaline to high-K calc-alkaline (Fig. 2A, B), and are characterized by light rare earth element (LREE) and large-ion lithophile element (LILE) enrichments, with depletions of Nb, Ta, P, and Ti (Fig. 3A, B), and relatively low Sr/Y (mostly < 40 ; Fig. 4A) and low La/Yb ratios (mostly < 30 ; Fig. 4B). They have moderate to high $\epsilon\text{Nd}_{(t=15\text{Ma})}$ values (-4.4 to $+8.5$), low $(^{87}\text{Sr}/^{86}\text{Sr})_{t=15\text{Ma}}$

ratios (0.7036–0.7068) (calculated at $t = 15\text{Ma}$ to allow for direct comparison with Miocene suites, Fig. 5A). Zircon εHf_t values range from -5.3 to +13, with mantle-like $\delta^{18}\text{O}$ values (+5.0 to +7.1 ‰; Wang et al., 2015b), and Nd-depleted mantle model (Nd_{TDM}) ages generally $<1\text{ Ga}$ (Table A1). Combined, the large isotopic and compositional ranges indicate that the Paleocene–Eocene Gangdese arc rocks were a mix of mantle- and crustally-derived source rocks.

4.2 Western Miocene high-Sr/Y granitoids

The rare western Miocene high-Sr/Y granitoids (18.4–16 Ma) are intermediate to felsic in composition (granodiorite and quartz monzonite; Fig. 2A), with a restricted silica range (SiO_2 63–70 wt. %). They are subalkalic and plot in the calc-alkaline to high-K calc-alkaline field (Fig. 2B). They have higher Sr/Y ratios (44–99) and more significant LREE/HREE fractionation ($\text{La/Yb} = 26\text{--}51$) than the Paleocene-Eocene suite, but their incompatible element compositions are similar (Fig. 3A, B). The western high-Sr/Y granitoids have more evolved Sr-Nd isotopic compositions than the Gangdese arc igneous rocks (Fig. 5A), with $\varepsilon\text{Nd}_{(t=15\text{Ma})}$ values from -9.3 to -4.1, and $(^{87}\text{Sr}/^{86}\text{Sr})_{t=15\text{ Ma}}$ ratios from 0.7072 to 0.7100. Their zircon εHf_t values range from -12.5 to +4.3, and $\delta^{18}\text{O}$ values range from +6.2 to +8.1‰. Their Nd depleted mantle model (Nd_{TDM2}) ages cluster between 1.0 and 1.4 Ga (Table A1). These magmas were either derived from a crustal source slightly more evolved than the Gangdese arc, or from a relatively homogeneous mix of Gangdese arc crust and a more evolved source. Compositionally, they form a cluster between the more felsic components of Gangdese arc magmas and the western Miocene trachyte suite (Figs. 2, 4).

4.3 Eastern Miocene high-Sr/Y granitoids

The more abundant eastern Miocene high-Sr/Y granitoid suite (21.3–13.4 Ma) crops out east of 88°E as shallowly-emplaced, small-volume plugs, dikes, or sills of porphyritic rocks, locally associated with major porphyry copper deposits. The dominant lithologies are quartz monzonite, granodiorite, and granite with a silica range mainly between 63–73 wt.% SiO₂ (Fig. 2A). They are subalkaline and plot in the calc-alkaline to high-K calc-alkaline fields (Fig. 2B). They have arc-like geochemical features with LILE enrichments and depletions in Nb, Ta, and Ti (Fig. 3A, B), similar to the Paleocene–Eocene suite but with greater depletions of HREE (Fig. 3B). These rocks are commonly referred to as high-Sr/Y granitoids (Chung et al., 2003; Hou et al., 2004; Guo et al., 2007) because the great majority have Sr/Y ratios >50 (Fig. 4A) and high La/Yb ratios (26–80) (Fig. 4B). They have $\epsilon\text{Nd}_{(t=15\text{Ma})}$ values from -8.1 to +5.7, and $(^{87}\text{Sr}/^{86}\text{Sr})_{t=15\text{Ma}}$ ratios from 0.7046 to 0.7082 (Fig 5A), overlapping with their western counterparts but extending to more primitive compositions typical of the Paleocene–Eocene suite. Their Nd depleted mantle model (Nd_{TDM2}) ages range from 0.3–1.3 Ga (Table A1). They have more mantle-like zircon ϵHf_t (+1.4 to +8.7) and zircon $\delta^{18}\text{O}$ values (+5.5 to +6.5 ‰) compared to their western equivalents, and the range to more primitive Sr and Nd isotopic compositions suggest they have a large component of mantle-derived Gangdese arc crust as a source component (Fig. 5A,B).

4.4 Western Miocene trachyte suite

Miocene alkaline (trachytic) volcanic rocks (Fig. 2A) crop out mostly in the western Gangdese belt where they are locally related to N–S trending grabens or normal faults (Cogan et al., 1998; Williams et al., 2001, 2014; Lu et al., 2017); they are relatively rare in the east (see below). The volcanic rocks are porphyritic with phenocrysts mainly of olivine, clinopyroxene, phlogopite, and sanidine in a glassy or fine-grained groundmass. They plot as trachyandesite (latite) and trachydacite on a total alkali–silica (TAS) diagram (Fig. 2A) and

most analysed samples cluster between 53–71 wt.% SiO₂ (Fig. 2A). Their high K₂O contents place them in the shoshonite (SH) field (Fig. 2B), or the ultrapotassic field according to Foley et al. (1987). Based on the latter definition, more than 50% of the southern Tibet samples are ultrapotassic (Fig. 2C, D), and this suite of rocks has widely been referred to as ultrapotassic volcanic rocks, or UPV (Williams, 2001, 2014; Zhao et al., 2009; Liu et al., 2014; Wang et al., 2015a); however, we prefer the IUGS-consistent term “trachytic” (Le Bas and Streckeisen, 1991). The mafic end of this suite has 10–12 wt. % MgO at ~52–55 wt. % SiO₂ (Fig. 4E), and the intermediate compositions are similar to high magnesium andesites (Wood and Turner, 2009), indicating that they are primitive, mantle-derived magmas. The western trachytes have higher LREE contents than most of the Miocene granitoids (Fig. 3C, D), but similarly strong negative Nb-Ta anomalies. The more mafic rocks are particularly rich in Cr (up to 649 ppm) and Ni (up to 467 ppm), both of which show a strong positive correlation with Th (Fig. 4F). The more felsic (trachydacitic) rocks have compatible element and HFSE contents similar to the high-Sr/Y granitoids. They show variable Sr/Y (11–113) and La/Yb ratios (31–211), which overlap with the lower range of the Paleocene-Eocene suite, but extend to much higher ratios characterized by the high-Sr/Y granitoids. The trachytic suite is also characterized by high (⁸⁷Sr/⁸⁶Sr)_{t=15 Ma} ratios (0.7069–0.7393), strongly negative εNd_(t=15Ma) values (-18.5 to -7.1) (Fig. 5A), high Nd_{TDM2} values (1.2–2.5 Ga, Table A1), mostly negative zircon εHf_t values (-14.7 to +1.0), and crust-like zircon δ¹⁸O values (+6.9 to +8.3 ‰), all indicative of an old lithospheric source. This crust-like isotopic range contrasts with their mantle-like (¹⁸⁷Os/¹⁸⁸Os)_t values (0.156–0.188) and high Cr-Ni contents (Wang et al., 2015a), and is interpreted to reflect an ancient subcontinental lithospheric mantle (SCLM) source for the high MgO (10–12 wt.%) end-member.

4.5 Eastern Miocene trachyte suite

Upper Miocene (12–11 Ma) trachytic volcanic rocks are only known to occur in two locations in the eastern Gangdese region, at Yangying and Suojin (Fig. 1). They are essentially similar to the western trachytes, but are more silicic, with lower CaO and MgO contents, and lower Mg# (Fig. 4). They are classified on the TAS diagram as trachydacites (Fig. 2A) with K₂O contents above 3 wt. % (Fig. 2B), and plot in the shoshonitic field in Figure 2B. Phenocrysts include clinopyroxene, amphibole, plagioclase, and phlogopite, set in a fine-grained groundmass (Wang et al., 2015a). Like the western trachytes, these trachydacites are characterized by high (⁸⁷Sr/⁸⁶Sr)_t ratios (0.7119–7121), strongly negative εNd_t values (-9.8 to -9.2), variable zircon εHf_t values (-5.7 to +10.4), intermediate zircon δ¹⁸O values (+5.0 to +6.7 ‰), and mantle-like (¹⁸⁷Os/¹⁸⁸Os)_t values (0.153–0.210) (Wang et al., 2015a). They overlap in whole rock and isotope chemistry with the western trachytes, but their uniformly low MgO, Ni and Cr contents suggests they are more fractionated equivalents of those rock types.

4.6 Eastern transitional monzonites

The sixth igneous suite is transitional between the trachytes and high-Sr/Y granitoid rocks, and has ages between 16–14 Ma. They occur in the ore fields such as Qulong, Jiama, and Jiru mine in the eastern Gangdese belt, but they are not the ore-forming magmas in these deposits. They are post-mineralization, and cross cut ore-forming granitoids (high-Sr/Y granitoids). The Qulong transitional rocks have been investigated by Yang et al. (2015), who called them high-Mg diorites; however, they plot as monzonites in Figure 2A, and in the high-K calc-alkaline and shoshonitic fields in Figures 2B and 2D, respectively. They are silica oversaturated, with a primary mineral assemblage of plagioclase, quartz, amphibole, and minor biotite. Although silica contents range between of 59–63 wt. %, they have high K₂O (3.0–3.8 wt. %), relatively high MgO (4.1–5.4 wt. %) and Mg# (56 and 66), and high

CaO/Al₂O₃ ratios (0.30–0.36) (Fig. 4D). Their Mg[#] values are much higher than the high-Sr/Y granitoids (<50; Fig. 5A), but their LILE and HFSE contents, including high Sr/Y ratios (Fig. 4A), are similar to many of the eastern granitoids. Accordingly, we refer to these as “transitional” monzonites. Their transitional character is also evident in their isotopic characteristics. They have low to moderate (⁸⁷Sr/⁸⁶Sr)_{t=15 Ma} ratios (0.7057–0.7072), moderately negative εNd_(t=15Ma) values (-6.5 to -3.4), low (¹⁸⁷Os/¹⁸⁸Os)_t ratios (0.176–0.178), highly variable zircon εHf_t values (-1.1 to +7.1), and low mantle-like zircon δ¹⁸O values (+5.3 to +6.1 ‰). Thus, the transitional monzonites have affinities to both the trachytes and eastern Miocene high-Sr/Y granitoids (Figs. 2–5), suggesting melting in the deep crust, but with an additional component of trachytic magma.

5. Trace elements in zircons

We have compiled trace element analyses of zircon from the Gangdese Cenozoic magmatic suites from the literature, and added 44 new analyses from 7 new samples to constrain magmatic conditions. Analytical methods are described in the Appendix and the data are listed in Table A2.

5.1 Trace element characteristics

Trace elements in zircon reflect the characteristics of the magmas from which they crystallized (Ballard et al., 2002; Rubatto, 2002; Trail et al., 2012; Kirkland et al., 2015). Here, we are particularly interested in indicators of magmatic oxidation state, temperature, and evolution, and so focus on zircon Ce⁴⁺/Ce³⁺ ratios, Ti contents, and trace element patterns.

Ce⁴⁺/Ce³⁺ ratios have been used to distinguish between relatively oxidized ore-bearing porphyries (Ce⁴⁺/Ce³⁺ mostly > 50) from more reduced, barren intrusive suites (Ce⁴⁺/Ce³⁺ < 50; Ballard et al., 2002). Eu_N/Eu_N^{*} ratios (where Eu_N/Eu_N^{*} = Eu_N/(Sm_N*Gd_N)) in zircons

also correlate with oxidation state because Eu^{2+} is excluded from zircon relative to Eu^{3+} . Interpretation of magmatic redox state from the $\text{Eu}_\text{N}/\text{Eu}_\text{N}^*$ ratios in zircons is complicated by the effects of plagioclase crystallization, which preferentially partitions Eu^{2+} relative to Eu^{3+} . However, in water-rich magmas, plagioclase crystallization is delayed until late in the crystallization history (Naney, 1983), so should have minimal effect on zircon $\text{Eu}_\text{N}/\text{Eu}_\text{N}^*$ ratios in hydrous, intermediate composition rocks (Dilles et al., 2015).

Zircon Th/U ratios can also be used to assess the degree of crystal fractionation (Kirkland et al., 2015), and titanium (Ti) concentration can be used to estimate magmatic crystallization temperatures (Ti-in-zircon; Watson and Harrison, 2005). Figure 6 reports the mean values and standard deviation of zircons from each rock sample, and Fig. A2 illustrates single spot analytical results for each zircon grain investigated here.

5.2 Magmatic oxidation state

Paleocene-Eocene Gangdese arc rocks and the western trachyte suite are characterized by low zircon $\text{Ce}^{4+}/\text{Ce}^{3+}$ (mostly <50) over a wide spectrum of $\text{Eu}_\text{N}/\text{Eu}_\text{N}^*$ ratios (mostly <0.5) (Figs. 6B-C, A2A, Table 1). The western high-Sr/Y granitoids have higher zircon $\text{Ce}^{4+}/\text{Ce}^{3+}$ (up to 159) and $\text{Eu}_\text{N}/\text{Eu}_\text{N}^*$ ratios (up to 0.78). The eastern Miocene high-Sr/Y granitoids show similar zircon $\text{Ce}^{4+}/\text{Ce}^{3+}$ and $\text{Eu}_\text{N}/\text{Eu}_\text{N}^*$ ratios to the sparse western suite, but extend to slightly higher values in $\text{Eu}_\text{N}/\text{Eu}_\text{N}^*$ (up to 0.87).

The $\text{Ce}^{4+}/\text{Ce}^{3+}$ ratios can be used to indicate relative magmatic oxidation state, and the results reported here are consistent with a previous study of magnetite-ilmenite mineral pairs which showed that Paleocene-Eocene Gangdese arc rocks have low to moderate ΔFMQ values (-1.2 to +0.8; where ΔFMQ is measured in $\log f\text{O}_2$ units relative to the fayalite–magnetite–quartz oxygen buffer), whereas eastern Miocene high-Sr/Y granitoids are more oxidized ($\Delta\text{FMQ}+0.8$ to +2.9; Wang et al., 2014b).

Zircons from the eastern “transitional” monzonite suite show exceptionally high zircon $\text{Ce}^{4+}/\text{Ce}^{3+}$ ratios (up to 487; Fig. 6C, Table A2), but their $\text{Eu}_\text{N}/\text{Eu}_\text{N}^*$ ratios are not correspondingly high (~ 0.5). The sparse eastern trachytes also have elevated $\text{Ce}^{4+}/\text{Ce}^{3+}$ and $\text{Eu}_\text{N}/\text{Eu}_\text{N}^*$ ratios, but not as high as the western trachytes. The decoupling of zircon $\text{Ce}^{4+}/\text{Ce}^{3+}$ and $\text{Eu}_\text{N}/\text{Eu}_\text{N}^*$ ratios in the eastern transitional monzonites and trachytes suggest their oxidation states are not extremely high, likely close to $\Delta\text{FMQ} +1$ to $+2$ (Wang et al., 2014b; Lu et al., 2016).

In summary, $\text{Ce}^{4+}/\text{Ce}^{3+}$ and $\text{Eu}_\text{N}/\text{Eu}_\text{N}^*$ ratios in zircons show that a spatial and temporal distribution of oxidation state exists along the length of the Cenozoic Gangdese belt. Paleocene-Eocene and western Miocene suites are relatively reduced with low $\text{Ce}^{4+}/\text{Ce}^{3+}$ and scattered $\text{Eu}_\text{N}/\text{Eu}_\text{N}^*$ ratios, but all three eastern Miocene suites are relatively oxidized with $\text{Ce}^{4+}/\text{Ce}^{3+}$ ratios >50 . These observations suggest that oxidation of the deep Tibetan lithosphere occurred after Paleocene–Eocene magmatism ceased and continental collision began.

5.3 Magmatic temperature

The titanium-in-zircon geothermometer depends on the activity of Si and Ti in the host magma. Overestimation of $a\text{SiO}_2$ or $a\text{TiO}_2$ yields overestimates and underestimates of temperature, respectively, but values are generally considered to be correct within $\pm 50^\circ\text{C}$ if a Ti-bearing phase is present (McDowell et al., 2014). Rutile occurs in the trachytic rocks, titanite in the Gangdese arc rocks, and ilmenite and/or titanite in the high-Sr/Y granitoids, so that magma temperature estimates are thought to be reasonably accurate. Only some of the more mafic Gangdese arc rocks and most of the trachyte suite are likely to have underestimated temperatures because of high Zr solubility in mafic and alkaline magmas (Watson & Harrison, 1983).

Almost all calculations indicate temperatures $<900^{\circ}\text{C}$. The Paleocene-Eocene Gangdese arc zircons show a progressive decrease in temperature from $\sim 870^{\circ}\text{C}$ to 600°C as a function of decreasing Th/U (Figs. 6D, A2B), reflecting progressive fractional crystallization to subsolidus conditions (Kirkland et al., 2015). Zircons in the eastern high-Sr/Y granitoids have temperatures typically $<800^{\circ}\text{C}$ and no obvious trend with Th/U values (Fig. A2B), suggesting crystallisation from cooler magmas. Data from the sparse western high-Sr/Y granitoids overlap this range but extend to higher temperatures (up to 818°C) and Th/U ratios (up to 2.6) (Fig. A2B), suggesting crystallization from somewhat hotter melts than in the east. The trachytic rocks generally record higher temperatures than in the granitoid suites (980°C to 700°C ; Figs. 6D and A2B), as expected for mantle-derived magmas.

5.4 Petrogenetic implications

Chondrite-normalized zircon multi-element patterns are mostly steep for all magmatic suites, but some of the western trachytic rocks have flatter HREE patterns (Fig. 6A), particularly those trachytes with high Sr/Y ratios and large La/Yb variations. It is likely that these flat HREE patterns are a result of partial melting or crystallization in equilibrium with garnet (Rubatto, 2002). Such patterns are not observed in the high-Sr/Y granitoids, even though their high Sr/Y ratios might be taken to indicate melting in the garnet stability field (Macpherson et al., 2006). Instead, this lack of evidence for garnet fractionation in the zircon REE patterns, along with relatively low whole-rock La/Yb ratios, suggest that early amphibole fractionation and delayed plagioclase fractionation from hydrous melts was responsible for the observed trace element characteristics (Richards and Kerrich, 2007; Richards, 2011; Wang et al., 2014a).

The $\text{Ce}^{4+}/\text{Ce}^{3+}$ vs. T(ti-zr) (Ti-in-zircon) plot (Fig. 6E) shows two key features: (1) the Miocene high-Sr/Y granitoids have higher $\text{Ce}^{4+}/\text{Ce}^{3+}$ ratios than most western trachytic rocks

and Gangdese arc magmatic rocks; and (2) all Miocene granitoids show low T(ti-zr) below 750 °C. One eastern trachydacite sample records relatively high oxidation state (exceptionally high zircon Ce ratios but intermediate $\text{Eu}_\text{N}/\text{Eu}_\text{N}^*$) at high temperature, implying that the oxidation state of those magmas is not controlled by crystal fractionation, as could be implied from Fig. 6E. This disconnection with fractionation is further illustrated by the $\text{Ce}^{4+}/\text{Ce}^{3+}$ vs Th/U plot (Fig. 6F), which shows that oxidation state is independent of Th/U ratios for all the high-Sr/Y and transitional (monzonitic) granitoids. The data indicate that low and high temperature magmas can be associated with high oxidation state, independent of fractionation (Fig. 6F), and that the high-Sr/Y granitoids and eastern trachytic suites have higher oxidation states than the Paleocene–Eocene and western trachytic suites.

6. Discussion

Miocene high-Sr/Y granitoids bear many similarities to the Paleocene–Eocene Gangdese arc magmatic rocks, but crucial lithogeochemical and isotopic differences also suggest affinities with the Miocene trachytic suites. We hypothesize that in the Miocene, alkaline magmas hybridised with magmas generated by melting of the Gangdese arc root. Here, we review possible petrogenetic models, then discuss tectonic settings that could explain this magmatic evolution, as well as the implications for porphyry copper mineralization.

6.1 Paleogene magmatism

The onset of Paleocene magmas in the Gangdese belt has been ascribed to Neo-Tethyan slab rollback (Chung et al., 2005; Ji et al., 2009; Lee et al., 2009; Wen et al., 2008; Zhu et al., 2015). This is supported by southward migration of arc magmatism, an abrupt change of India–Asia convergence between ~69–58 Ma (Lee and Lawver, 1995), and the development of extension setting in the Qiangtang terrane characterized by east–west-trending sedimentary

basins (Chung et al., 2005).

The igneous rocks during this time (~69–58 Ma) have relatively homogeneous and juvenile isotopic compositions (ϵNd_i of -0.6 to +4.0, ϵHf_i of +3.8 to +7.1, and $\delta^{18}\text{O}$ of +5.0 to +6.5 ‰; Wang et al., 2015b), suggesting a significant juvenile crustal component mixed with a minor (if any) mantle component (Wen et al., 2008; Wang et al., 2015b). Significantly, the juvenile signatures highlight the absence of ancient Tibetan SCLM beneath the Gangdese arc throughout this interval.

Changes in Sr-Nd-Hf-O isotopic compositions for the Linzizong volcanic rocks and coeval intrusions in the Gangdese belt at ~53–50 Ma suggest mantle input and extensive crustal melting, possibly associated with Neo-Tethyan slab breakoff (Wen et al., 2008; Wang et al., 2015b; Zhu et al., 2015). The conclusion of slab breakoff at 53–50 Ma comes from many lines of evidence, which include: I) asthenospheric influx was triggered by slab breakoff. The Nd-Hf isotopic data of ~53–49 Ma igneous rocks show significant input from asthenospheric mantle with ϵNd_i values up to +9.8 and zircon ϵHf_i values up to +15.1, which are comparable with arc rocks from early periods (Wang et al., 2015b; Zhu et al., 2015); II) Voluminous magmatism emplaced during ~53–49 Ma. It is suggested by widespread outcrops of intrusions and Pa'na volcanic sequence at ~53–49 Ma (Fig. 2, Mo et al., 2003; Chung et al., 2005; Lee et al., 2009); III) anomalously high magmatic temperatures (T_{Zr} up to 800°C and $T_{(\text{ti-zr})}$ up to 980°C), reflecting a thermal anomaly at that time; IV) Bimodal volcanic rocks have been reported in the Pa'na and Nianbo formations of Linzizong volcanic rocks (Mo et al., 2003; Lee et al., 2009, 2011; Zhu et al., 2015); V) This high temperature event (or thermal anomaly) led to extensive crustal melting, and generated heterogeneous magmatic geochemistry during ~53–49 Ma. This is evidenced by heterogeneous whole-rock geochemical compositions, heterogeneous zircon Hf isotopic compositions ($\epsilon\text{Hf}_{(i)} = -5.3$ to 15.1)), and scattered magmatic temperatures; and VI) crustal deformation, characterized with

peak granulite-facies metamorphism from 66 to 52 Ma in the lower crust (Zhang et al., 2013). These early Paleogene rocks are associated with few porphyry-type deposits, possibly because the magmas were relatively anhydrous (Wang et al., 2014a) and less oxidized (ΔFMQ -1.2 to +0.8) than magmas typically associated with PCDs (ΔFMQ +2) (Wang et al., 2014b).

6.2 Post-Eocene flat Indian plate subduction

Crustal mass balance estimations suggest large-scale subduction of Indian continental crust during the India-Asia collision (Ingalls et al., 2016; Capitanio et al., 2010). The magmatic gap in the Gangdese belt between 40–30 Ma (section 3.2), and the gap in the histogram of U-Pb ages for zircons from crustal xenoliths in “ultrapotassic” trachytic rocks in the Himalayas (Liu et al., 2014), are consistent with flat subduction of the Indian plate throughout the Oligocene. This suggests the Indian continent was subducted below southern Tibet at a relatively shallow angle with little or no asthenospheric mantle wedge above the underthrust Indian lithosphere (Guillot et al., 2008; Ding et al., 2016).

This magmatic gap was followed at ~35 Ma by a jump to higher $\text{Dy}_\text{N}/\text{Yb}_\text{N}$ and U/Yb ratios in xenocrystic zircons from Miocene trachytic rocks, suggesting they formed in thickened crust, in equilibrium with eclogite and garnet-bearing granulitic mineral assemblages (Liu et al., 2014). Moreover, the jump to negative zircon ϵHf values indicates a major change to an isotopically evolved source for the trachyte suite at this stage. This is consistent with a recent, more comprehensive study of magmatic zircons from Tibet (Liu et al., 2017), which also shows an isotopically evolved source component added to the high-Sr/Y magmas between 32–28 Ma.

The underthrust Indian plate would have progressively dehydrated during continental collision (Massonne, 2016). Underthrust crustal rocks, including some sediments, are likely

sources of a hydrous fluid phase capable of metasomatising and/or melting the base of the lower Tibetan crust. In particular, Eocene evaporites and carbonates were common in the Neo-Tethys ocean, extending from Europe to SE Asia, and were prominent in the Great Kavir Basin of Iran (Mukherjee et al., 2003; Johnston et al., 2011). Extensive carbonates also existed on the leading edge of the Indian plate passive margin (Scheibner and Speijer, 2008). They presumably also existed on the leading edge of the Indian plate passive margin, and subduction of such oxidized materials could have affected the oxidation state of the Gangdese arc root. Water released during flat subduction could have affected the rheology and changed the mineralogy of the overriding lithospheric mantle, as revealed by high S-wave velocities (Sommer and Gauert, 2011; Wagner et al., 2005). When flat subduction ends, a hot asthenospheric mantle wedge opens between the two plates, which can cause partial melting of the hydrated and oxidized upper plate lithosphere, as has been proposed for the central Andes in the Miocene following a period of flat subduction (James and Sacks 1999; Kay et al., 1999; Kay and Mopodosis, 2001). We suggest a similar development for the Gangdese belt where initial flat subduction of the Indian plate was followed by steepening in the east (Kumar et al., 2006; Kind and Yuan, 2010; Zhang et al., 2010), allowing for voluminous high-Sr/Y granitoids to form in eastern Tibet. We will return to this idea when discussing the Miocene geodynamic evolution of the region in section 6.8.

6.3 Origin of Miocene trachyte suites

Several single-source models have been proposed for the origin of the trachyte suite (UPVs) in southern Tibet, including: (1) partial melting of the middle-lower crust of the Indian plate (Hébert et al., 2014); (2) melting of enriched Asian (Tibet) lithospheric mantle during delamination or convective thinning (Miller et al., 1999; Liu C et al., 2011), or due to

hydration by fluids from Indian plate subduction (Yang et al., 2016); or (3) derivation from metasomatized asthenospheric mantle (Guo et al., 2013).

Several lines of evidence suggest these volcanic rocks were derived from an ancient lithospheric mantle rather than crustal source: firstly, they carry not only lower-crustal but also mantle xenoliths (Liu C et al., 2011; Liu D et al., 2014; Wang et al., 2016); secondly, they have low SiO₂ contents (down to 45 wt.%), high Mg# (up to 76), and high Ni and Cr contents (467 and 649 ppm, respectively); and thirdly they have low, mantle-like Os isotopic compositions ($^{187}\text{Os}/^{188}\text{Os}$)_i = 0.154–0.210; Wang et al., 2015a). Indeed, the 10–12 wt. % MgO contents at 55–60 wt. % SiO₂ (Fig. 4E) require that these rocks were primary mantle-derived magmas (Grove et al., 2012). Most significantly, Figure 7C–F shows that the most evolved εNdi values are found in those rocks with highest values of MgO, Cr and Th, and lowest values of SiO₂. As silica increases and MgO decreases, the rocks become more isotopically primitive (Fig. 7C, D). This observation is further supported by the low εNdi ratios which, for the most MgO-rich endmembers, reach -18.5 (Fig. 5A) and have the highest HFSE and LILE element contents (Fig. 7E,F). The Nd model ages ranging up to 2.5 Ga (Fig. 5D) indicate a probable Paleoproterozoic to latest Archean source.

A Tibetan SCLM origin for the trachytes was suggested by Yang et al. (2016). They considered that devolatilization of the subducting Indian crust would have metasomatized the overlying wedge of subcontinental lithospheric mantle, ultimately producing ultrapotassic and/or alkaline mafic magmas. The major problem with this model is that no evidence exists for Tibetan SCLM beneath the Gangdese arc during the Paleocene or Eocene. Accordingly, the mantle wedge should have been asthenospheric and the resultant trachytic magmas should be much less evolved. However, it is possible that ancient Tibetan SCLM was underthrust from the forearc region beneath the Gangdese arc during Oligocene collision, and subsequent

746 devolatilization during ongoing subduction would have resulted in progressive fluid-fluxed
747 melting of the metasomatized SCLM.

748 Guo et al. (2015) focused on the chemical and isotopic nature of the most primitive of
749 these post-collisional ultrapotassic (trachytic) magmas with $\text{MgO} > 6$ wt. %. These only crop
750 out west of 87°E . They proposed a two-stage model: During the first-stage (55–25 Ma),
751 fluids and melts released from the subducting Indian crust resulted in the formation of
752 pyroxenites through metasomatism of the overlying mantle wedge. During the second-stage
753 (25–8 Ma), partial melting of pyroxenites caused by slab roll-back and slab break-off
754 generated the trachytic magmas. They argued that the absence of these primitive endmembers
755 of Miocene ultrapotassic magmatism east of 87°E indicates different subduction geometries.
756 The critical problem of this model is that Guo et al (2015) assume that the decreases in Sr_i
757 and Pb_i , and increasing Nd_i of the Miocene rocks from the western to eastern Gangdese belt,
758 result from an eastward-decreasing crustal component in the mantle source region. However,
759 as we have shown above (Figs. 5 and 7), these changes are the result of an *increasing* crustal
760 component to the east, because the crustal (Gangdese arc) component in the high-Sr/Y
761 magmas is more juvenile than the mantle component in the trachytic magmas (see section
762 6.6).

763 Wang et al. (2016, 2017a) showed that the ϵNdi values for southern Tibet trachytes
764 increase with increasing SiO_2 . The positive slope is more likely to be part of a mixing array
765 between mafic trachytic magmas derived from an isotopically evolved source with felsic
766 magmas derived from the isotopically unevolved southern Tibetan (Gangdese) crust, as
767 suggested by xenolith evidence (Wang et al., 2017a).

768 Hybrid origins have also been proposed to explain the trachytic (UPV) suite. For example,
769 direct melting of subducted (Indian) crustal rocks followed by interaction with mantle
770 peridotite has been proposed to explain the origin of post-collisional Eocene UPVs in eastern

Tibet (Campbell et al., 2014; Stepanov et al., 2014). Stepanov et al. (2017) suggested this model could be applied to the Miocene trachyte suite of Tibet. The model requires two principal stages: melting of blocks of continental crust within the mantle and variable reaction between the rising crustal melts and the adjacent peridotitic mantle. Thus, felsic, K-rich melts derived from continental crust thrust into the mantle interact with the overlying mantle wedge during ascent to become mafic in composition (Stepanov et al., 2017).

However, several lines of evidence from the trachytic suites of southern Tibet preclude this hypothesis (Wang et al., 2017a). For example, their ϵNd_i values increase with increasing SiO_2 and do not trend toward Indian metasedimentary crust, as represented isotopically by Himalayan leucogranites (Fig. 7C). Rather, the positive slope of SiO_2 with Nd(i) in the trachyte suites from southern Tibet (Fig. 7D) is more likely to be part of an array between mafic magmas derived from an isotopically evolved mantle source, mixing with felsic magmas derived from the isotopically unevolved southern Tibetan (Gangdese arc) crust. This is consistent with the xenolith evidence from the trachytic suites (Wang et al., 2016).

Another critical point that conflicts with the Campbell et al. (2014) model is the variation of trace elements on Harker diagrams. The trachytic suites show that the most mafic alkaline rocks (with 10–12 wt. % MgO) have the highest concentrations of incompatible trace elements (Figs. 2A–C, 4F, 8A). This incompatible enrichment in mafic trachytic rocks exists across the entire spectrum of incompatible elements (Wang et al., 2017a, their Fig. 3B), and shows that an enriched mantle source, not continental crust, controlled the primary trace element geochemistry of the alkaline suite.

The consistently old Nd model ages (1.2–2.5 Ga) and relatively low zircon O isotopic compositions ($\delta^{18}\text{O} = 5\text{--}8.4\text{‰}$; Wang et al., 2015a) for the trachytic suite, especially for the more primitive variants (Fig. 7), suggest that these magmas were derived from low-degree melting of an ancient (Proterozoic or Archean) SCLM. Furthermore, the SCLM must have

undergone melt infiltration during the Proterozoic to explain the high HFSE and LILE contents of the parental high-MgO but isotopically evolved magmas (sample T2A/98: MgO = 11.78 wt. %, $\epsilon\text{Nd}_i = -18.5$; Table A1). Melt infiltration, rather than hydrothermal fluid metasomatism, is necessary because only melts can carry significant amounts of HFSE at high P-T conditions (Spandler and Pirard, 2013). This melt infiltration may have occurred during Proterozoic subduction-related magmatism, and is consistent with the typical subduction-modified geochemical pattern of the trachytic rocks (Fig. 3D).

We propose therefore that the trachytic rocks originated from low degree partial melting of SCLM at differing mantle depths. Two groups of trachytic suites can be distinguished on La/Yb vs MgO and Sr/Y vs MgO plots (Fig. 8A and B). The eastern trachytic suite and approximately half of the western suite plot on a very steep trend, with La/Yb ratios varying between 30–200 for MgO <4 wt.%. By contrast, the other half of the suite, including the transitional monzonitic types, have La/Yb ratios varying between 30–100 over an extended MgO range (2–12 wt. % MgO). This suggests that the high-La/Yb trachytic magmas formed in the garnet stability field, requiring depths of melting >70 km (Robinson and Wood, 1998), whereas the low-La/Yb group probably formed at shallower mantle depths. This is consistent with the presence of olivine in some rocks, suggesting the low-pressure melting reaction: pyroxene + phlogopite = olivine + melt. The Sr/Y vs MgO plot (Fig. 8B) shows a similar division into two groups. Overall, the contrasting La/Yb and Sr/Y ratios suggest that the trachytic suites formed in a SCLM source region near the spinel–garnet transition.

The spinel–garnet transition implies mantle melting occurred between 60–80 km depth (~2 GPa; Kinzler, 1997; Klemme and O'Neill, 2000). The geotherm for Tibet during the Miocene, derived from xenoliths in the trachytic magmas, is ~16°C/km (Chen et al., 2009; Wang et al., 2016), which suggests mantle temperatures at the Moho (~70 km depth) were ~1100–1150°C. Recent melting experiments on phlogopite-bearing lherzolites and

harzburgites (Condamine et al., 2016) showed that partial melting will occur in this range, beginning at ~1000°C for 1 GPa, or at ~1150°C for 3 GPa, depending on fluorine content. The K₂O content of low-degree melts from phlogopite-lherzolite and phlogopite-harzburgite is buffered between 6–8 wt.% (Condamine et al., 2016) similar to the values for the trachyandesites (Fig. 2B). Also, the high K₂O/Na₂O ratios (2–8) of the trachytic suites, typical of ultrapotassic rocks (Fig. 2D), are usually formed at low degrees of melting (Condamine et al., 2016). The ~2 GPa (70 km) estimate for mantle melting suggested above, combined with the relatively low inferred melting temperatures (~1100°C) and high K₂O/Na₂O ratios, is in reasonable agreement with melting experiments on phlogopite-bearing peridotites. Accordingly, the trachytic magmas are interpreted to have been produced by partial melting of phlogopite-bearing (enriched) harzburgitic SCLM, which originally formed in a supra-subduction environment during the Proterozoic.

6.4 Tibetan or Indian lithospheric mantle melting as a source for trachytes?

Evidence for the derivation of trachytic melts from an ancient, metasomatized lithospheric mantle can be interpreted in two different ways: either the source was Tibetan SCLM in the fore-arc region of the Gangdese arc, or Indian SCLM. Several authors, including some of us (e.g., Wang et al., 2014c; Wang et al., 2015a), have proposed that the trachyte suites were derived from Tibetan SCLM (Ding et al., 2003; Yang et al., 2015, 2016; Lu et al., 2015). Here, we suggest the Indian plate SCLM as an alternative source.

Metasomatized Tibetan SCLM is an obvious potential source for the trachytic magmas, but there are some issues with this model. Seismic studies show no evidence for the presence of SCLM beneath Tibet today (Nábělek et al., 2009), and the isotopic record does not indicate the participation of an older, evolved continental crust or underlying lithospheric mantle throughout the magmatic history of the Gangdese arc, from ~200 Ma. Instead, the positive Hf

isotopic composition of Gangdese arc magmas from Jurassic to early Eocene show repeated reworking of juvenile crust with no ancient SCLM involvement (see Fig. 10 of Ji et al., 2009; Fig. 4 of Liu et al., 2017).

A further point is that, if the trachyte suites originated from the Tibetan SCLM, it would be difficult to keep producing these alkaline magmas over a ~20 m.y. period. As demonstrated from experimental petrology (e.g., Wood and Turner, 2009; Condamine and Médard, 2014; Condamine et al., 2016), generation of these magmas is by phlogopite breakdown, producing low percentage melts derived from metasomatized SCLM (Foley, 1987), leaving a refractory harzburgitic residuum that cannot melt again under the moderate 16°C/km geothermal gradient constrained by the xenolith evidence.

From this we conclude that there was no old SCLM beneath the arc itself during its growth. We argue instead that, if the evolved isotopic signal in the trachytes was derived from Tibetan SCLM, it must have originally been part of the fore-arc region. We suggest that during continental collision, the fore-arc lithosphere may have been thrust under the arc and smeared northwards (Fig. 12c). Subsequent Miocene magmatism could then have involved melting of this Tibetan SCLM and overlying Gangdese lower crust.

An alternative model, that the trachytes were derived from the Indian SCLM, is suggested by the 20 m.y.-period of trachyte generation, which seems to require a continuously rejuvenated source. We suggest that the subducting metasomatized Indian plate provides such a source. Seismic and numerical models suggest that the Indian plate middle and upper crust were mostly scraped off prior to subduction to form the Greater Himalaya accretionary prism (e.g., Nábělek et al., 2009; Capitanio et al., 2010), leaving only the underlying mantle lithosphere and part of lower crust as the main subducting component. The Indian plate SCLM is thought to have undergone subduction metasomatism during the Proterozoic (Miller et al., 2000), which led to its evolved Nd and Sr isotopic signature and K-rich, phlogopitic

character (France-Lanord et al., 1988; Inger and Harris, 1993). Low-degree partial melting of this material could have produced trachytic melts during subduction.

At this time we cannot distinguish between these two possible sources of Miocene trachytic magmatism in Tibet (underthrust for-arc Tibetan SCLM or Indian plate SCLM).

6.5 Fluid-fluxed melting and oxidation of Tibetan lower crust in the Miocene: the origin of high-Sr/Y granitoids

In this section, we demonstrate the importance of water in generating the Miocene high-Sr/Y granitoids, and that the source was the Gangdese arc root. Zircons from the Miocene high-Sr/Y granitoids provide temperatures that are generally $<750^{\circ}\text{C}$ (Fig. 6D, E). Maximum zircon saturation temperatures (T_{Zr}) for the eastern Miocene high-Sr/Y granitoids are also $<750^{\circ}\text{C}$ (Fig. 9B), and the western high-Sr/Y group is marginally higher, up to 770°C (although this difference is well within expected error for the method).

A requirement for accurate T_{Zr} estimates is that the magma must be saturated in zircon (Watson & Harrison, 1983). Calc-alkaline magmas generally reach zircon saturation when SiO_2 reaches values above 65 wt.% (Collins et al., 2016), which is reflected by a systematic decrease in Zr content with silica increase in both the western and eastern high-Sr/Y granites, from $\sim 63\text{--}65$ wt.% SiO_2 to higher silica values (Fig. 9A). Given the presence of inherited Paleogene zircons in high-Sr/Y granitoids (Wang et al., 2014a, Li et al. 2014), T_{Zr} marks an upper bound for temperature. A comparison of Ti-in-zircon temperatures with T_{Zr} estimates (Fig. 9C) shows they yield similarly low-T values. The same does not hold for the Paleocene-Eocene Gangdese arc rocks, which show poor agreement between Ti-in-zircon and T_{Zr} temperature estimates in Figure 8C. However, many of these samples were undersaturated in zircon, as shown by their increasing Zr content up to ~ 65 wt.% SiO_2 . The comparisons

between T_{zr} and Ti-in-zircon temperature estimates and silica contents reinforces the point that the high-Sr/Y granitoids were formed from cool magmas.

Given that dehydration melting of the crust requires temperatures of at least 850°C to generate reasonable granitic magma volumes, the consistently low temperatures for the Miocene high-Sr/Y granitoids and transitional monzonites (Fig. 9B,C), requires additional water-fluxed melting (cf. Weinberg and Hasalová, 2015; Collins et al., 2016). Plagioclase compositions in the eastern high-Sr/Y granitoids further support this interpretation because they show excess aluminium (Fig. 10), which has been linked to high melt water contents (Williamson et al., 2016).

Evidence from the Paleocene–Eocene Gangdese arc rocks suggests that the Tibetan arc root was relatively reduced, but became moderately oxidized and strongly hydrated during Oligocene–Miocene flat continental subduction. This lithospheric metasomatism is thought to have played an important role in the subsequent magmatic flare-up and associated porphyry copper mineralization in the Miocene (Wang et al., 2014b). The oxidation process can be dated back to the start of Indian plate subduction in the Eocene, when a range of sediments, including evaporites and carbonates that might have existed on the leading edge of the Indian passive margin were underthrust beneath Tibet. These variably oxidized metasedimentary rocks had the potential to oxidize the arc root as the underthrust Indian plate progressively dehydrated during continental collision (e.g., Massonne, 2016).

6.6 Mixing model for Miocene high-Sr/Y magmas

Whole-rock and zircon isotopic compositions for Miocene high-Sr/Y granitoid samples are generally similar to those of the Paleocene–Eocene Gangdese arc (Wang et al., 2015a), suggesting derivation by partial melting of the arc root (Hou et al., 2004, 2015). The distinctively higher La/Yb of the eastern granitoids compared to the Gangdese arc rocks (Fig.

7B, 9A) accords with their distinctively high-Sr/Y contents (Fig. 4A, B, 7A), but many other major and trace elements overlap with the felsic endmembers of the Gangdese arc (Figs. 2, 3, 4, 8). The high La/Yb and Sr/Y ratios demonstrate that these Miocene granitoids formed by melting of the Paleocene-Eocene arc, within the garnet stability field at depths >30 km.

In detail, however, there are some subtle but significant differences between the high-Sr/Y granitoids in eastern and western Tibet, best revealed by the variation of ϵNd_i values (Figs. 5, 7). Although the eastern high-Sr/Y granitoids have values that overlap with those of the Paleocene-Eocene Gangdese arc (+8 to -5), the range extends beyond the Gangdese envelope toward the trachyte suites. This is also evident geographically, with the high-Sr/Y granitoids being most primitive in the east, and becoming progressively more evolved toward the west (Fig. 5B, C). Chemically and geographically, the trend is toward the evolved isotopic compositions of the trachytic suite, indicating that some high-Sr/Y granitoids have incorporated trachytic components.

The Sr/Y vs Nd_i plot (Fig. 7A) most convincingly shows the chemical-isotopic interrelationship. High-Sr/Y Miocene granitoids are chemically distinctive from the Gangdese arc rocks, but isotopically similar. On the other hand, the trachytic suite varies between low- and high-Sr/Y at evolved Nd isotopic compositions, with a general trend toward the eastern high-Sr/Y Miocene granitoids. This suggests that variable degrees of mixing occurred between low-Sr/Y evolved trachyandesites, and high-Sr/Y crustal melts derived from Gangdese crust.

Isotopic variations in the eastern Miocene high-Sr/Y granitoids are mimicked by other compositional variations. A clear demonstration is the compositional overlap of MgO and SiO_2 between the felsic members of the trachytic suites and the mafic endmembers of the eastern Miocene high-Sr/Y granitoids (Fig. 7C, D). The variation is also evident for trace elements such as Cr (Fig. 7E) and Th (Fig. 7F), and with Zr (Fig. 9A): Zr drops from ~1000

ppm to 100 ppm as SiO₂ increases from 55–70 wt. %. The order of magnitude drop in Zr content corresponds to a change from εNd of -15 to +2 (Fig. 9D), demonstrating the extreme effect that mixing had on trace element abundance, rather than crystal fractionation.

Intermediate between the mantle-derived (trachytic) endmember and the crustally derived most felsic, silica-rich endmembers of the high-Sr/Y granitoid suite, lie the western Miocene, high-Sr/Y granitoids and the transitional monzonite suite. These granitoids tend to overlap with the lower silica, lower alkali group of the eastern granitoids (Fig. 2), also evident in their slightly higher CaO, MgO, Ni (Fig. 4) and Zr (Fig. 9D) contents. Considering the two hypothetical endmembers defined in Fig. 5A, most of the eastern Miocene granitoids contain 5–10 % trachytic magmatic component, whereas most of the western Miocene granitoids contain 15–20 % of that component. Overall, the Miocene high-Sr/Y magmas are dominated by a Gangdese arc source, with 5–20 % contamination by mantle-derived, alkaline magmas of the coeval trachytic suites.

An antithetic geographical relationship exists between Miocene trachytic and high-Sr/Y granitoid suites in southern Tibet. Whereas the high-Sr/Y granitoids are voluminous in the east, they are sparse in the west. Conversely, trachytic rocks are sparse in the east, but much more voluminous in the west. The isotopic array indicates the two endmembers mixed more effectively in the east (Fig. 5B, C), producing the greater range in isotopic compositions of the eastern high-Sr/Y granitoids, and the limited number of erupted alkaline magmas were much more thoroughly mixed than those in the west. No eastern trachytic magmas have εNd values <-9, whereas the isotopic range extends to -18 farther west, in regions where high-Sr/Y plutons are not present. The antithetic relationship suggests that the more voluminous high-Sr/Y crustal melts in the east acted as a rheological and probably density barrier to ascending mantle-derived melts.

In summary, there is evidence for variable degrees of hybridization between mantle-derived trachytic magmas and high-Sr/Y granitoid melts formed by anatexis of the older Gangdese magmatic arc in a water-fluxed environment (Wang et al., 2016, 2017a). This model is most similar to that of Yang et al. (2015, 2016), and contrasts with many other petrogenetic models (Qu et al., 2004, 2007; Gao et al., 2007, 2010; Chung et al., 2003; Hou et al., 2004; Guo et al., 2007; Hou et al., 2009; Li et al., 2011; Wang et al., 2014a, b; Zheng et al., 2012; Liu et al., 2017). Yang et al.'s (2015) model was based on the chemical features of the transitional Qulong “high Mg-diorite” (our transitional monzonite group) (Fig. 1). It differs from the model presented here in that we suggest the mantle source was the Indian SCLM or Tibetan fore-arc SCLM. In addition, our model differs from Yang and co-workers in that we suggest the steepening of the subducting Indian plate in the early Miocene allowed temperatures to rise in the lower Tibetan crust as an asthenospheric mantle wedge began to open, which induced voluminous deep crustal melting in the eastern Gangdese. Trachytic magmas would have transported additional heat and fluid into these lower crustal melting zones, and may have enhanced the melting process.

A mixing model has also been proposed by Liu et al. (2017) for the Miocene magmatic rocks of southern Tibet, but their model contrasts with that presented herein, because they consider that the Miocene high-Sr/Y granitoids were derived from the Indian plate and the potassic volcanic rocks from Tibetan crust. Both schools of thought agree the “ultrapotassic” component of the trachytic alkaline magmas (see subdivision between potassic and ultrapotassic in Fig. 2D) were mantle derived, but Liu et al. (2017) discriminate the “potassic rocks” from the “ultrapotassic group” (our trachytic suite) and suggest the former ultimately had a crustal origin. The authors argued that “poorly varying” (presumably meaning a narrow range of values) and negative zircon $\epsilon\text{Hf}(t)$ values of the potassic volcanic rocks provided clear evidence for derivation from ancient Lhasa terrane crust with minor input from related

ultrapotassic magma. However, as shown in Fig. 7, both the Indian crust (represented by the Himalayan leucogranites) and the Indian SCLM (represented by the 3.35 Ga komatiites, Jayananda et al., 2008), have highly negative $\epsilon\text{Nd}(t)$ values. Thus, although Liu et al. (2017) assume that the dramatic decrease of co-magmatic zircon $\epsilon\text{Hf}(t)$ values since ~35 Ma is strong evidence for the enhanced mass transfer from underthrust Indian continental crust, it is equally possible that it represents an influx of trachytic magma (their ultrapotassic magmas) from Indian or Tibetan ancient SCLM.

Most significantly, the diagrams in Fig. 7 indicate that the silicic endmember involved in the process is close to juvenile in terms of its isotopic signature, similar to the Paleocene-Eocene Gangdese granitoids, whereas the most mafic, Mg-rich magmas were the most isotopically evolved. Thus, Indian crustal magmas with evolved signatures, such as the Himalayan leucogranites (Fig. 7A, C, D) could not be a significant endmember in the hybridization process that generated the high-Sr/Y granitoids, whereas granitic magmas derived from anatexis of the Paleocene-Eocene Gangdese arc could. Conversely, the trachyte suites, derived from melting of harzburgite of the Indian SCLM, are both Mg-rich and isotopically evolved and would explain both the compositional and isotopic variation in the Miocene high-Sr/Y granitoids.

Liu et al. (2017) also used variation in the alkali ratio ($\text{K}_2\text{O}/\text{Na}_2\text{O}$) against Y and SiO_2 (their fig. 10) to suggest that the SCLM-derived trachytic (their ultrapotassic) melts only played a minor role in Miocene granitoid magmatism. They suggested that $\text{K}_2\text{O}/\text{Na}_2\text{O}$ in the high-Sr/Y granitoids (their adakites) increases with increasing SiO_2 and decreasing Y. However, this increase only applies to the low-K, Paleocene-Eocene Gangdese arc rocks, not to the Miocene granitoids (Fig. 11); the Miocene trachyte-granitoid array shows a steady decrease of $\text{K}_2\text{O}/\text{Na}_2\text{O}$ with increasing silica and decreasing Y, as predicted by magma mixing models.

Liu et al. (2017) further suggest that the potassic volcanism is dominated by recycling of the Lhasa terrane crust because the negative and variable co-magmatic zircon Hf isotopic variations are comparable with detrital zircon records and magmatic zircons from the Mesozoic granitoids outcropping in the central and northern Lhasa subterrane (cf., Liu et al., 2014). We concur with Liu et al. (2014) that such zircons are mostly crust-derived (high U/Yb) xenocrysts entrained within mantle-derived ultrapotassic (trachytic) magmas and that their heterogeneous Hf isotopes indicate assimilation of Lhasa terrane crust during ascent of those magmas. Indeed, the highlighted granitic xenoliths (Liu et al., 2014, their Fig. 1) are non-foliated, upper crustal fragments, indicating late entrainment of Lhasa terrane within the crustal column rather than derivation from lower crustal sources. The presence of these upper crustal xenoliths and xenocrysts in the trachytic suites does not indicate that the potassic (or ultrapotassic) magmas were derived from Tibetan crust.

6.7 Thermal structure of the Miocene Gangdese belt

Mantle xenoliths entrained in the Miocene trachytic magmas place constraints on petrological and geophysical models for that time interval in southern Tibet. Mafic granulite xenoliths from within the trachytic suites in the western Gangdese belt yielded temperatures of 1130–1330° C and pressures between 22 and 26 kbar, defining a geotherm of $\sim 16^{\circ}\text{C km}^{-1}$, suggesting that mafic crust extended to between 70–85 km depth beneath Tibet during the Miocene (Wang et al., 2016, 2017a). Hydrous ultramafic xenoliths have abundant hornblende and contain ~ 85 Ma-old zircons typical of the Gangdese arc (Chan et al., 2009), likely representing a deep cumulate section of the arc. Felsic granulite xenoliths indicate that the Miocene Tibetan arc root had a basal temperature of $\sim 850^{\circ}\text{C}$ (Wang et al., 2016), close to biotite dehydration melting temperatures. Assuming a 50 km thick Tibetan crust, as indicated by seismic data for the present (Nábelek et al., 2009), the felsic granulite xenoliths yield a geothermal gradient of 17°C /km . We use this gradient to

constrain the 750°C isotherm at shallower crustal levels (Fig. 12), which is the approximate temperature of the high-Sr/Y granitoid magmas estimated above. Farther north, deep seismic experiments beneath the Qiangtang and Songpan-Ganzi terranes identified the lithosphere-asthenosphere boundary (LAB) at ~80 km depth (Owens and Zandt, 1997). Assuming the LAB (lithosphere-asthenosphere boundary) is a thermal boundary layer at ~1100°C, the geothermal gradient is ~16°C/km, similar to the other estimated gradients. We use this to locate the LAB beneath central Tibet.

Another thermal constraint for Fig. 12 comes from experimental melting models for phlogopite-bearing peridotites. Wendlandt and Eggler (1980) showed that the beginning of melting of a phlogopite-bearing spinel lherzolite under anhydrous conditions was at ~1075 °C at 10 kbar and ~1120 °C at 20 kbar, suggesting that under Tibet at ~70 km depth (~20 kbar), the temperature was approximately 1100 °C in agreement with the 16 °C geothermal gradient determined from xenoliths *within* the trachytic magmas. This result provides confidence for the inferred thermal structure beneath Tibet, and is also consistent with the geochemical/petrological arguments that trachyte generation occurred near the garnet-spinel transition, at ~70 km.

The thermal structure constrained by petrological arguments appears to be unlike the structure given in the classical papers by Toksöz et al. (1971), Bird et al. (1975), and Peacock (1990), and more recently by Beaumont and co-workers (Warren et al., 2008; Beaumont et al., 2009). All these models project a cold slab extending deep into the mantle, where temperatures can remain at ~600°C to at least 100 km depth, but also suggest the lithospheric mantle wedge is much less than 1000°C, for any condition involving continental collision. Therefore, such models cannot predict the generation of hot, trachytic magmas beneath southern Tibet. If the trachytic magmas are derived from the slab (our hypothesis), then the slab interior heats up much more rapidly than predicted by the thermal models (Fig. 12). In

the next section, we use these petrological constraints to derive a geodynamic model for Tibet between 15–20 Ma.

6.8 Geodynamic model

Receiver-function images (Kumar et al., 2006; Zhao et al., 2010) and body and surface wave tomographic models (Nunn et al., 2014), suggest a west to east increase in the angle of dip of the Indian plate lithosphere, and a decrease in thickness of the Indian plate lithosphere, both west and east (Fig. A1). The flat subduction inferred for the early stages of collision (between ~50 and 30 Ma, section 3.2) differs from present-day geometry, particularly for the east. The geometries of the subducting Indian plate today (Fig. A1) are equivalent to type IIa “continental subduction” in the east, versus type IIb “continental underthrusting” in the west (Massonne, 2016, his Fig. 1). We suggest that the steepening of the Indian plate in eastern Tibet occurred in the middle Miocene, and was related to the generation of voluminous high-Sr/Y granitoid magmatism in that region. A coherent geodynamic model must not only take into account the contrasting geometry of the subducting Indian plate from west to east, but also the increased volumes of high-Sr/Y granitoids and the greater numbers of PCDs in the east, and the diminished volumes of trachytic rocks.

The following scenario is proposed:

1. During the Paleocene–Eocene (pre-50 Ma), normal, subduction-related Gangdese arc magmatism occurred. The medium- to high-K calc-alkaline arc magmas (Fig. 2) were relatively reduced (Fig. 6). Starting at ~50 Ma, the Eocene magmas are characterized by higher Th/Y and La/Yb ratios, suggesting crustal thickening.
2. The slab began to flatten during the Oligocene as Indian lithosphere entered the subduction zone and a period of magmatic quiescence ensued. Crustal thickening occurred and the Himalayan orogenesis began. Although some metasedimentary

materials reach the lower crust based on the high $\delta^{18}\text{O}$ values (up to 8.03) of olivine from xenoliths hosted by trachytes (Liu C et al., 2014), most of the upper crust of the Indian plate was scraped off (Capitanio et al., 2010) and formed the accretionary wedge of Tethyan metasedimentary rocks south of the Indus-Yarlung Tsangpo suture zone. Strong coupling between the two plates during this flat subduction event removed ancient Tibetan SCLM beneath southern Tibet, consistent with the seismic evidence (Nábělek et al., 2009).

3. During this flat subduction mode, the geothermal gradient in the Tibetan crust decreased from typically 30–40°C/km or greater during Gangdese arc magmatism to ~16°C/km by the Miocene during continental underthrusting, based on xenoliths from the western Gangdese belt (Chan et al., 2009; Wang et al., 2016).
4. During ongoing continental underthrusting, the remnant subducted Indian lower crust and some retained metasediments from upper crust progressively dehydrated as it converted to eclogite facies. Massonne (2016) demonstrated that sedimentary rocks in a subducting slab can release up to 2.5 wt. % water at ~600 °C over a wide range of pressures, with the aqueous fluids rising into and hydrating the overlying rocks. Serpentinised peridotites also released significant water volumes during serpentine breakdown, which occurs at <650°C for $P < 2.0$ GPa. At ~50 km depth, the mantle is saturated at 1.8 wt. % H_2O at 600 °C (Massonne et al., 2016), allowing a free aqueous phase to rise into the overlying lithosphere.
5. The northern margin of the Indian continent was covered by carbonates and evaporitic sediments (Mukherjee et al., 2003; Scheibner and Speijer, 2008; Johnston et al., 2011). They are also the most ductile of supracrustal rocks, and commonly define fault structures. Although most of upper crust has been scrapped off, some of these sediments can persist to great depths. During Indian flat subduction, dehydration of

these carbonates and evaporites (and other sediments) led to further hydration and oxidation of the base of the Gangdese arc. This oxidation step is critical to subsequent metallogeny, because the Gangdese arc lower crust is thought to have been relatively reduced prior to this time, and did not generate magmas that were fertile for porphyry formation.

6. Steepening of the Indian subduction in the east (Fig. 12B, C) resulted in the opening of an asthenospheric mantle wedge, and caused temperatures to rise in the overlying lower Tibetan crust (compare Fig. 12A, B, C). This induced melting of water-fluxed (or hydrated) lower crust at the ambient temperature of $\sim 800^{\circ}\text{C}$ at depths of 45–50 km.
7. Early Miocene trachytic magmatism began along the southern margin of Tibet as a result of phlogopite breakdown at $\sim 1100^{\circ}\text{C}$, near the garnet-spinel transition (~ 70 km), producing low volume, K-rich, trachytic partial melts (Condamine et al., 2016). The location of the trachytic magmas in southern Tibet suggests that the $\sim 1100^{\circ}\text{C}$ isotherm was at shallower depths than estimated from thermo-mechanical models of subduction (Fig. 12).
8. The highly evolved Nd and Sr isotopic signature of the trachytic magmas, yielding Early Proterozoic T_{DM} model ages (Fig. 5), and depletions for Nb and Ta in mantle-normalized trace element patterns (Fig. 3), indicate that the SCLM was originally metasomatised during Proterozoic suprasubduction zone magmatism. As mentioned in section 6.4, there are two possible sources for trachytic melts: ancient Indian SCLM, or ancient Tibetan SCLM in the fore-arc region.
9. The impact of hot, rising trachytic magmas into Tibetan crust differs from west to east. In the west, the melts rose into a cool, relatively rigid lower crust still cool because of ongoing flat slab subduction (Fig. 12A). Accordingly, extensive crustal

- melting did not occur and trachytic melts could continue toward the surface virtually unmodified. This explains the relatively high proportion of trachytic intrusions relative to high-Sr/Y granitoids in western Tibet.
10. By contrast, the resultant crustal melting was extensive caused trapping of trachytic melts, resulting in their sparse eruption at surface, but evidence for mixing with the granitoid melts. Fluids released from these trachytes may have enhanced fluid-fluxed melting of the metasomatized and now warm Tibetan lower crust.
11. Trachytic magmas were not the oxidizing agent of the Gangdese lower crust, because the dominant (western) trachytic suite rocks are significantly more reduced than the high-Sr/Y granitoids (Fig. 6C). The western trachytic and transitional monzonitic magma have much higher $\text{Ce}^{4+}/\text{Ce}^{3+}$ ratios but broadly similar $\text{Eu}_\text{N}/\text{Eu}_\text{N}^*$ ratios with the western trachytic magmas, suggesting that neither of them was significantly oxidized. Instead, we propose that the oxidation evident in the high-Sr/Y granitoids occurred during metasomatism of the Tibetan lower crust by fluids released from the Indian plate during flat subduction.
12. Ascent of trachytic magma into the lower Tibetan crust was accompanied by high degrees of olivine fractionation until the magmas reached low-MgO (~2 wt. %) and high silica (~65–70 wt. %) contents (Fig. 7C, D). At this stage, the magmas were able to release water to stimulate crustal melting, and at the same time were capable of mixing with lower crustal melts (Figs. 5, 7) at ~750–800°C, producing some high-Sr/Y granitoid magmas with high Cr-Ni-Mg[#] contents (Figs. 2D, 7F, 8D).
13. The high-Sr/Y granitoid magmas derived from partial melting of hydrated and oxidized Gangdese arc base were capable of scavenging Cu from originally sulphide-rich, probably metalliferous portions of the Gangdese arc cumulates in the lower crust and/or lithospheric mantle. The metals were remobilized under these relatively

oxidised melting conditions, and transported into the upper crust by the high-Sr/Y
granitoid magmas to become the key components of the PCDs in eastern Tibet. The
more extensive crustal melting in the eastern Gangdese (compared to the west)
explains the occurrence of PCDs

6.9 Metallogenic implications

Similar to PCDs in arc settings, Gangdese post-collisional PCDs are also associated with
hydrous and oxidized magmas (Hou et al., 2015; Lu et al., 2015; Yang et al., 2015; Wang et
al., 2015a). Although partial melting of subduction-modified lower crust has been proposed
to generate such magmas, recent studies (Lu et al., 2015; Yang et al., 2015) question the
ability of dehydration melting of garnet amphibolite in a thickened lower crust to generate
sufficient quantities of hydrous magma to form porphyry deposits upon upper crustal
emplacement. In contrast with Yang et al. (2015), we suggest the shallow-subduction
metasomatism was not enough to cause melting until slab steepening in the Miocene caused
heating. However, the shallow subduction was a very important precursor event, which
rendered the lower crust fusible (and oxidized) when temperatures rose as the asthenospheric
mantle wedge opened. This process of hydrating the Gangdese arc base can be dated back to
the Eocene, when the Indian plate flat subduction started, and lasted till the Miocene. We
have also suggested above that mixing with trachytic magmas is necessary to explain some
Miocene granitoid magmas with enriched Cr and Ni contents, and high $Mg^\#$ at 56–70 wt. %
 SiO_2 . The arrival of trachytic magmas at the base of the Tibetan arc was broadly coincident
with the melting of the hydrated base of arc. Trachytic magmas may have been at least in part
the heat and fluid source that triggered or enhanced melting at the base of the arc.

A key question is how did Miocene high-Sr/Y granitoid magmas, derived from the melting
of reduced cumulates of the Gangdese arc root (ΔFMQ -1.2 to +0.8; Wang et al., 2014c)

become oxidized? As discussed in sections 6.2, 6.5 and 6.8, we consider that subduction of a range of Tethyan sediments from the Indian plate oxidized the roots of the arc ahead of Miocene melting.

Miocene high-Sr/Y magmas are oxidized and can carry more sulphur than their reduced counterparts (Wang et al., 2014b; Hou et al., 2015, Tomkins et al., 2012), and could have scavenged sulphides and their metals that became trapped within the roots of the reduced Gangdese arc. The assimilation of sulphides would have limited reducing effect on the high-Sr/Y magmas (Tomkins et al., 2012), which were capable of transporting metals to give rise to PCDs (Richards, 2011; Chiaradia et al., 2012).

The observation that PCDs are restricted to the eastern section of the Gangdese belt is a direct result of the increased crustal melting in the east as the asthenospheric mantle wedge opened during the transition from flat to steep subduction. In contrast, the lack of asthenospheric mantle wedge in the west restricted the degree of crustal melting and limited the ability to trap trachytic melts, leading to the generation of few poorly mineralized granitoids but the eruption of large volumes of trachytic volcanic rocks at surface.

Acknowledgements

This research was financially cosupported by the MOST of China (2016YFC0600304 and 2016YFC0600407), the Chinese National Natural Science Foundation (91755207 and 4122500), and the 111 Project (B18048). William J. Collins was supported by ARC grant DP120104004, and Jeremy P. Richards was supported by Discovery Grant from the Natural Sciences and Engineering Research Council of Canada. Wen-yan He and Qiuyun Li are thanked for zircon trace element analysis, and Andrew Locock is thanked for assisting EPMA analysis. Andreas Audétat is thanked for reviewing an early version of the manuscript.

Figures Captions and Tables

Figure 1. Geology of the Gangdese magmatic belt in the Lhasa terrane, showing the distribution of Paleocene-Eocene Gangdese magmatism (including intrusions and Linzizong volcanic successions), Miocene high-Sr/Y granitoids, and western (W) Miocene trachytic rocks, and eastern (E) Miocene trachydacites (sparse). Notice how Miocene granitoids west of ~88°E are sparse and mostly barren, whereas in the east they are more abundant and commonly associated with PCDs. Blank areas are Quaternary successions. Map modified from: Hou et al. (2004); Zhao et al. (2009); Wang et al. (2015a).

Figure 2. (A) Total alkali-silica (TAS) diagram, (B) K₂O vs SiO₂ plot, (C) K₂O vs MgO plot and (D) K₂O vs Na₂O plot for the six main Cenozoic suites in the Gangdese belt. References for data provided in Table A1.

Figure 3. (A-C) Chondrite-, and (B-D) N-MORB-normalized trace element diagrams for the six main Cenozoic suites in the Gangdese belt. Normalization values are from Sun and McDonough (1989). References for data provided in Table A1.

Figure 4. Major and trace element plots showing the features of the six main Cenozoic suites in the Gangdese belt: (A) Sr/Y vs Y, (B) Sr/Y vs La/Yb, (C) Mg# vs SiO₂, (D) CaO vs Al₂O₃, (E) MgO vs SiO₂, and (F) Th vs Ni. References for data provided in Table A1.

Figure 5. (A) εNd_i (T=15Ma) vs (⁸⁷Sr/⁸⁶Sr)_i (T=15Ma). (B) εNd_i (T=15Ma) vs. longitude and (C) Nd_{TDM2} vs longitude for the six main Cenozoic suites in the Gangdese belt. Note: the

Paleocene-Eocene Gangdese arc calc-alkaline values were calculated at 15 Ma for comparison to Miocene rocks. In A, grey line shows mixing between a primitive end-member for the arc root, and a primitive trachyte for melts derived from Indian lithospheric mantle or ancient fore-arc Tibetan SCLM. The values for end-members used in this mixing model are: $(^{87}\text{Sr}/^{86}\text{Sr})_i = 0.703$ and $\epsilon\text{Ndi} = +8.5$ (the most primitive Gangdese Paleocene-Eocene Gangdese arc sample), and average Sr (623 ppm) and Nd (20.3 ppm) values from eastern Miocene high-Sr/Y granitoids. Values for the primitive trachytic melts are taken from the western Miocene suite: $(^{87}\text{Sr}/^{86}\text{Sr})_i = 0.726$ and $\epsilon\text{Ndi} = -17$, average Sr (916 ppm) and Nd (137 ppm). References for data provided in Table A1.

Figure 6. Trace element composition of zircons from the six main Cenozoic suites in the Gangdese belt: (A) Chondrite-normalized REE diagram; inset is a plot of Dy/Yb vs. Yb indicating that the western trachytes have low Yb contents and a Dy/Yb ratio close to unity, contrasting with all other suites; (B) $\text{Ce}^{4+}/\text{Ce}^{3+}$ histogram showing all individual analyses; (C) $\text{Ce}^{4+}/\text{Ce}^{3+}$ vs. Eu/Eu^* ; (D) Th/U vs T(ti-zr) (Ti-in-zircon temperature based on equations from Watson and Harrison, 2005); (E) $\text{Ce}^{4+}/\text{Ce}^{3+}$ vs. T(ti-zr); (F) $\text{Ce}^{4+}/\text{Ce}^{3+}$ vs Th/U. Normalization values are from Sun and McDonough (1989). Chemical values for zircons in C-F are averages of several spots in single sample from which averages and errors are calculated. References for data provided in Table A2. Averages of Qulong and Jiama ore-forming samples are from Lu et al. (2016).

Figure 7. Major and trace element plots for the six main Cenozoic suites in the Gangdese belt: (A) Sr/Y vs. ϵNdi (T=15Ma), (B) La/Yb vs. ϵNdi (T=15Ma), (C) SiO_2 vs. ϵNdi (T=15Ma), (D) MgO vs. ϵNdi (T=15Ma), (E) Cr vs. ϵNdi (T=15Ma); (F) Th vs. ϵNdi (T=15Ma). References for data provided in Table A1.

Figure 8. Major and trace element plots for the six main Cenozoic suites in the Gangdese belt:

(A) La/Yb vs. MgO and (B) Sr/Y vs MgO. References for data provided in Table A1.

Figure 9. Zr content and T estimates: (A) whole rock Zr vs SiO₂ plot; (B) T_{zr} (Zr saturation

temperature) vs SiO₂; (C) T(ti-zr) (Ti-in-zircon temperature) vs T_{zr}; (D) whole rock Zr vs

εNdi (T=15Ma) for the six main Cenozoic suites in the Gangdese belt. T(ti-zr) estimation

based on equations from Watson and Harrison (2005), T_{zr} temperature estimate based on Zr

saturation (Boehnke et al., 2013).

Figure 10. Al/(Ca+Na+K) vs. An% for plagioclase from different suites. Plagioclase crystals

from eastern Miocene high-Sr/Y rocks plot above the line, indicating they have excess Al

(Williamson et al., 2016), unlike Paleocene-Eocene Gangdese arc and western trachyte

plagioclase. References for data in plots provided in Table A3.

Figure 11. Major and trace element plots for the six main Cenozoic suites in the Gangdese

belt: (A) K₂O/Na₂O vs. SiO₂ and (B) K₂O/Na₂O vs. Y. References for data provided in Table

A1.

Figure 12. Cartoon illustrating the contrasting subduction geometry associated with Miocene

magmatism in the Gangdese belt: (A) Flat subduction and continental underthrusting in the

western Gangdese belt, and (B-C) steeper subduction in the eastern Gangdese belt, consistent

with deep seismic experiments. Both geometries led to underplating of oxidized supracrustal

rocks, and generated a thermal structure capable of hydrating and oxidizing the overlying

Tibetan plate lithosphere. Upon opening of the asthenospheric mantle wedge in the east in the Miocene, the hydrated and oxidized Tibetan lower crust began to melt to form high-Sr/Y magmas. This process was accompanied by the formation of trachytic partial melts in the underthrust Indian plate SCLM (B) or for-arc Tibetan SCLM (C), which also invaded the Tibetan lower crust. In the east, these hydrous, alkaline magmas were trapped by the lower crustal melt sheets, where they released fluids that contributed to further fluid-fluxed crustal melting, and variably mixed with these crustal melts. The increased oxidation state of the Tibetan lower crust caused metals trapped in sulfides from previous subduction-related magmatism to be remobilized, generating magmas that were fertile for porphyry Cu deposit formation. In contrast, the lack of an asthenospheric mantle wedge in the west caused more limited crustal melting that failed to trap the ascending trachytic magmas. Consequently, only small volumes of crustal melt (high-Sr/Y granitoid) were generated, with only Zhunuo Cu-Mo deposit and a few intrusions with mineralization, but large volumes of trachytic volcanic rocks were erupted.

Table 1 Geochemical comparison of Gangdese Cenozoic igneous rocks and their zircons.

References

- Aitchison, J. C., Ali, J. R., Davis, A. M., 2007. When and where did India and Asia collide? *J. Geophys. Res.* 112, B05423, doi. 10.1029/2006JB004706.
- Ali, J. R., Aitchison, J. C., 2005. Greater India. *Earth-Sci. Rev.* 72, 169–188.
- Audétat, A., Simon, A.C., 2012. Magmatic controls on porphyry Cu genesis. In *Geology and Genesis of Major Copper Deposits and Districts of the World: A Tribute to Richard Sillitoe* (eds. J. W. Hedenquist, M. Harris and F. Camus). *Econ. Geol.* S16, 553–572.
- Ayyıldız, T., Varol, B., Önal, M., Tekin, E., Gündoğan, İ. 2015. Cretaceous-Tertiary (K-T) boundary evaporites in the Malatya Basin, eastern Turkey. *Carbonate. Evaporite.* 4, 461–476.
- Ballard, J.R., Palin, J.M., Campbell, I.H., 2002. Relative oxidation states of magmas inferred from Ce(IV)/Ce(III) in zircon: Application to porphyry copper deposits of northern Chile. *Contrib. Mineral. Petrol.* 144, 347–364.
- Beaumont, C., Jamieson, R.A., Nguyen, M.H., Lee, B., 2001. Himalayan tectonics explained by extrusion of a low-viscosity crustal channel coupled to focused surface denudation. *Nature* 414, 738–742.

- Beaumont, C., Jamieson, R.A., Butler, J.P., Warren, C.J., 2009. Crustal structure: A key constraint on the mechanism of ultra-high-pressure rock exhumation. *Earth and planet. Sci. Let.* 287, 116–129.
- Bird, P., Toksöz, M.N., Sleep, N.H., 1975. Thermal and mechanical models of continent-continent convergence zones. *J. Geophys. Res.* 80, 4405–4416.
- Boehnke, P., Watson, E.B., Trail, D., Harrison, T.M., Schmitt, A.K., 2013. Zircon saturation re-visited. *Chem. Geol.* 351, 324–334.
- Burnham, C.W., 1979. Magmas and hydrothermal fluids, in Barnes, H.L., ed., *Geochemistry of hydrothermal ore deposits*, 2nd edition: New York, John Wiley and Sons, 71–136.
- Campbell, I.H., Stepanov, A.S., Liang, H.Y., Allen, C.M., Norman, M.D., Zhang, Y.Q., Xie, Y.W., 2014. The origin of shoshonites: new insights from the Tertiary high-potassium intrusions of eastern Tibet. *Contrib. Mineral. Petrol.* 167: 983.
- Candela, P.A., 1992. Controls on ore metal ratios in granite-related ore systems: An experimental and computational approach: *Trans. R. Soc. Edinb. Earth Sci.* 83, 317–326.
- Capitanio, F.A., Morra, G., Goes, S., Weinberg, R.F., Moresi, L., 2010. India-Asia convergence driven by the subduction of the Greater Indian continent. *Nature Geo.* 3, 136–139.
- Chan, G.H.N., Waters, D.J., Searle, M.P., Aitchison, J.C., Horstwood, M.S.A., Crowley, Q., Lo, C.H., Chan, J.S.L., 2009. Probing the basement of southern Tibet: Evidence from crustal xenoliths entrained in a Miocene ultrapotassic dyke. *J. Geol. Soc. London* 166, 45–52.
- Chiaradia, M., Ulianov, A., Kouzmanov, K., Beate, B., 2012. Why large porphyry Cu deposits like high-Sr/Y magmas? *Sci. Rep.* 2, 685.
- Chen, J.L., Xu, J.F., Zhao, W.X., Dong, Y.H., Wang, B.D., Kang, Z.Q., 2011. Geochemical variations in Miocene adakitic rocks from the western and eastern Lhasa terrane: Implications for lower crustal flow beneath the southern Tibetan Plateau. *Lithos* 125, 928–939.
- Chu, M. F., Chung, S. L., Song, B., Liu, D. Y., O'Reilly, S. Y., Pearson, N. J., Ji, J. Q., Wen, D. J., 2006. Zircon U-Pb and Hf isotope constraints on the Mesozoic tectonics and crustal evolution of southern Tibet. *Geology* 34, 745–748.
- Chung, S. L., Liu, D., Ji, J. Q., Chu, M. F., Lee, H. Y., Wen, D. J., Lo, C. H., Lee, T. Y., Qian, Q., Zhang, Q., 2003. Adakites from continental collision zones: melting of thickened lower crust beneath southern Tibet. *Geology* 31, 1021–1024.
- Chung, S.L., Chu, M.F., Zhang, Y.Q., Xie, Y.W., Lo, C. H., Lee, T.Y., Lan, C. Y., Li, X.H., Zhang, Q., Wang, Y.Z., 2005. Tibetan tectonic evolution inferred from spatial and temporal variations in post-collisional magmatism. *Earth Sci. Rev.* 68, 173–196.
- Chung, S.L., Chu, M.F., Ji, J., O'Reilly, S.Y., Pearson, N.J., Liu, D., Lee, T.Y., Lo, C.H., 2009. The nature and timing of crustal thickening in Southern Tibet: geochemical and zircon Hf isotopic constraints from postcollisional adakites. *Tectonophysics* 477, 36–48.
- Clark, M.K., Royden, L.H., 2000. Topographic ooze: Building the Eastern margin of Tibet by lower crustal flow. *Geology* 28, 703–706.
- Cogan, M.J., Nelson, K.D., Kidd, W. S.F., Wu, C.D., Project INDEPTH Team, 1998. Shallow structure of the Yadong-Gulu rift, southern Tibet, from refraction analysis of Project INDEPTH common midpoint data. *Tectonics* 17, 46–61.
- Collins, W.J., Huang, H.Q., Jiang, X.Y., 2016. Water-fluxed crustal melting produces Cordilleran batholiths. *Geology* 2, 143–146.
- Corrie, S.L., Kohn, M.J., and Vervoort, J.D., 2010. Young eclogite from the Greater Himalayan sequence, Arun Valley, eastern Nepal: P-T-t path and tectonic implications. *Earth and Planetary Science Letters* 289, 406–416.
- Davidson, J., Turner, S., Handley, H., Macpherson, C., Dosseto, A., 2007. Amphibole

- “sponge” in arc crust? *Geology* 35, 787–790.
- Defant, M. J., Drummond, M. S., 1990. Derivation of some modern arc magmas by melting of young subducted lithosphere. *Nature* 347, 662–665.
- de Sigoyer, J., Chavagnac, V., Blichert-Toft, J., Villa, I. M., Luais, B., Guillot, S., Cosca, M., Mascle, G., 2000. Dating the Indian continental subduction and collision thickening in the northwest Himalaya: Multichronology of the Tso Moriri eclogites. *Geology* 28, 487–490.
- DeCelles, P.G., Gehrels, G.R., Najman, Y., Martin, A.J., Carter, A., Garzanti, E., 2004. Detrital geochronology and geochemistry of Cretaceous–Early Miocene strata of Nepal: implications for timing and diachroneity of initial Himalayan orogenesis. *Earth Planet. Sci. Lett.* 227, 313–330.
- Dilles, J.H., Ken, A.J.R., Wooden, J.L., Tosdal, R.M., Koleszar, A., Lee, R.G., Farmer, L.P., 2015. Zircon compositional evidence for sulfur-degassing from ore-forming arc magmas. *Eco. Geol.* 110, 241–251.
- Ding, H.X., Zhang, Z.M., Dong, X., Tian, Z.L., Xiang, H., Mu, H.C., Gou, Z.B., Shui, X.F., Li, W.C., Mao, L.J., 2016. Early Eocene (c. 50Ma) collision of the Indian and Asian continents: Constraints from the North Himalayan metamorphic rocks, southeastern Tibet. *Earth Planet. Sci. Lett.* 435, 64–73.
- Ding, L., Kapp, P., Zhong, D., Deng, W., 2003. Cenozoic volcanism in Tibet: evidence for a transition from oceanic to continental subduction. *J. Petrol.* 44, 1833–1865.
- Foley, S.F., Venturelli, G., Green, D.H., Toscani, L., 1987. The ultrapotassic rocks: characteristics, classification, and constraints for petrogenetic models. *Earth-Sci. Rev.* 24, 81–134.
- France-Lanord, C., Sheppard, S. M. F., Le Fort, 1988. Hydrogen and oxygen isotope variations in the High Himalaya peraluminous Manaslu leucogranites: evidence for heterogeneous sedimentary source. *Geochim. Cosmochim. Acta* 52, 513–526.
- Gao, Y.F., Hou, Z.Q., Kamber, B., Wei, R.H., Meng, X.J., Zhao, R.S., 2007. Adakite-like porphyries from the southern Tibetan continental collision zones: evidence for slab melt metasomatism. *Contrib. Mineral. Petrol.* 153, 105–120.
- Gao, Y.F., Yang, Z.S., Santosh, M., Hou, Z.Q., Wei, R.H., Tian, S.H., 2010. Adakitic rocks from slab melt-modified mantle sources in the continental collision zone of southern Tibet. *Lithos* 119, 651–663.
- Guillot, S., Maheo, G., de Sigoyer, J., Hattori, K.H., Pecher, A., 2008. Tethyan and Indian subduction viewed from the Himalayan high-to ultrahigh-pressure metamorphic rocks. *Tectonophysics* 451, 225–241.
- Guan, Q., Zhu, D.C., Zhao, Z.D., Zhang, L.L., Liu, M., Li, X.W., Yu, F., Mo, X.X., 2010. Late Cretaceous adakites in the eastern segment of the Gangdese Belt, southern Tibet: Products of Neo-Tethyan ridge subduction? *Acta Geol. Sin.* 26, 2165–2179.
- Guo, Z.F., Wilson, M., Liu, J.Q., 2007. Post-collisional adakites in south Tibet: products of partial melting of subduction-modified lower crust. *Lithos* 96, 205–224.
- Guo, Z.F., Wilson, M., Zhang, M.L., Cheng, Z.H., Zhang, L.H., 2013. Post-collisional, K-rich mafic magmatism in south Tibet: constraints on Indian slab-to-wedge transport processes and plateau uplift. *Contrib. Mineral. Petrol.* 165, 1311–1340.
- Guo, Z.F., Wilson, M., Zhang, M.L., Cheng, Z.H., Zhang, L.H., 2015. Post-collisional ultrapotassic mafic magmatism in South Tibet: Products of partial melting of pyroxenite in the mantle wedge induced by roll-back and delamination of the subducted Indian continental lithosphere slab. *J. Petrol.* 56, 1365–1406.
- Harris, N.B.W., Pearce, J.A., Tindle, A.G., 1986. Geochemical characteristics of collisional-zone magmatism, in Coward, M.P., Reis, A.C., eds., *Collision tectonics*. *Geol. Soc. London Spec. Publ.* 19, 67–81.
- Harris, N., 2007. Channel flow and the Himalayan-Tibetan orogen: a critical review. *J. Geol.*

- Soc. 164(3), 511–523.
- Hattori, K., 2014. What makes plate convergent zones fertile in metals? *Acta Geol. Sin.* 88 (s2), 543–544.
- Hearn, T.M., Wang, H., Chen, Y.J., Sandvol, E.A., Ni, J.F., 2011. Three-dimensional variations in the Tibetan mantle lid velocity from Pn tomography. In: AGU Fall Meeting. San Francisco. pp. T43A-2293.
- Hébert, R., Guilmette, C., Dostal, J., Bezard, R., Lesage, G., Bédard, É., Wang, C.S., 2014. Miocene post-collisional shoshonites and their crustal xenoliths, Yarlung Zangbo Suture Zone southern Tibet. *Geodynamic implications. Gondwana Res.* 25, 1263–1271.
- Hou, Z.Q., Gao, Y.F., Qu, X.M., Rui, Z.Y., Mo, X.X., 2004. Origin of adakitic intrusives generated during mid-Miocene east-west extension in southern Tibet. *Earth Planet. Sci. Lett.* 220, 139–155.
- Hou, Z.Q., Yang, Z.M., Lu, Y.J., Kemp, A., Zheng, Y.C., Li, Q.Y., Tang, J.X., Yang, Z.S., Duan, L.F., 2015. A genetic linkage between subduction- and collision-related porphyry Cu deposits in continental collision zones. *Geology* 43, 247–250.
- Hoskin, W.P., Black, L.P., 2000. Metamorphic zircon formation by solid state recrystallization of protolith igneous zircon. *J. Metam. Geol.* 18, 423–439.
- Hu, M.Y., He, H.L., Zhan, X.C., Fan, X.T., Wang, G., Jia, Z.R., 2008. Matrix normalization from in-situ multi-element quantitative of zircon in Laser Ablation-Inductively Coupled Plasma Mass Spectrometry. *Chinese J. Analy. Chem.* 36, 947–983. (in Chinese with English abstract)
- Hu, X.M., Garzanti, E., Wang, J., Huang, W., An, W., Webb, A., 2016. The timing of India-Asia collision onset – Facts, theories, controversies: *Earth-Sci. Rev.* 160, 264–299.
- Huang, G. C., Wu, F. T., Roecker, S. W., Sheehan, A. F., 2009. Lithospheric structure of the central Himalaya from 3-D tomographic imaging. *Tectonophysics* 475, 524–543.
- Ingalls, M., Rowley, D., Currie, B., Colman, A.S., 2016. Large-scale subduction of continental crust implied by India-Asia mass-balance calculation. *Nat. Geosci.* 9, 848–853.
- James, D.E. Sacks, S., 1999. Cenozoic formation of the Central Andes: a geophysical perspective. In: Skinner, B. et al. (eds) *Geology and Mineral Deposits of Central Andes*. Society of Economic Geology, Special Publication, 7, 1–25.
- Jayananda, M., Kano, T., Peucat, J.J., Channabasappa, S., 2008. 3.35 Ga komatiite volcanism in the western Dharwar craton, southern India: Constraints from Nd isotopes and whole-rock geochemistry. *Precambrian Res.* 162, 160–179.
- Ji, W.Q., Wu, F. Y., Chung, S. L., Li, J. X., Liu, C. Z., 2009. Zircon U-Pb geochronology and Hf isotopic constraints on petrogenesis of the Gangdese batholith, southern Tibet. *Chem. Geol.* 262, 229–245.
- Jiménez-Munt, I., Fernández, M., Vergés, J., Platt, J.P., 2008. Lithosphere structure underneath the Tibetan Plateau inferred from elevation, gravity and geoid anomalies. *Earth Planet Sci. Lett.* 267, 276–289.
- Johnston, F.K.B., Turchyn, A.V., Edmonds, M., 2011. Decarbonation efficiency in subduction zones: implications for warm Cretaceous climates. *Earth Planet. Sci. Lett.* 303, 143–152.
- Kapp, P., Yin, A., Harrison, T. M., Ding, L., 2005. Cretaceous–Tertiary shorting, basin development, and volcanism in central Tibet. *GSA Bulletin* 117, 865–878.
- Kay, S.M., Mpodozis, C., 2001. Central Andean ore deposits linked to evolving shallow subduction systems and thickening crust. *GSA Today*, 11, 4–9.
- Kay, S.M., Mpodozis, C., and Coira, B., 1999. Neogene magmatism, tectonism, and mineral deposits of the Central Andes (22° to 33°S latitude), in Skinner, B.J., ed., *Geology and ore deposits of the Central Andes: Society of Economic Geologists, Special Publication 7*, 27–59.

- Kelley, K.A., Cottrell, E., 2012. The influence of magmatic differentiation on the oxidation state of Fe in a basaltic arc magma. *Earth Planet. Sci. Lett.* 329–330, 109–121.
- Kind, R., Yuan, X., Saul, J., Nelson, D., Sobolev, S., Mechie, J., Zhao, W., Kosarev, G., Ni, J., Achauer, U., 2002. Seismic images of crust and upper mantle beneath Tibet: evidence for Eurasian plate subduction. *Science* 298, 1219–1221.
- Kind, R., Yuan, X.H., 2010. Seismic images of the biggest crust on earth. *Science* 329, 1479–1480.
- Kinzler, R.J., 1997. Melting of mantle peridotite at pressures approaching the spinel to garnet transition: Application to mid-ocean ridge basalt petrogenesis. *J Geophys. Res.* 102, 853–874.
- Kirkland, C.L., Smithies, R.H., Taylor, R.J.M., Evans, N., McDonald, B., 2015. Zircon Th/U ratios in magmatic environs. *Lithos* 212–215, 397–414.
- Klemme, S., O'Neill, H.S., 2000. The near-solidus transition from garnet lherzolite to spinel lherzolite. *Contrib. Mineral Petrol.* 138, 237–248.
- Kumar, P., Yuan, X., Kind, R., Ni, J., 2006. Imaging the colliding Indian and Asian lithospheric plates beneath Tibet. *J. Geophys. Res.* 111, B6. doi 10.1029/2005JB003930.
- Lange, R.A., Frey, H.M., Hector, J., 2009. A thermodynamic model for the plagioclase-liquid hygrometer/thermometer. *Am. Mineral.* 94, 494–506.
- Le Bas, M.L., Streckeisen, A.L., 1991. The IUGS systematics of igneous rocks. *J. Geol. Soc. London*, 148, 825–833.
- Leech, M.L., Singh, S., Jain, A.K., Klemperer, S.L., and Manickavasagam, R.M., 2005. The onset of India-Asia continental collision: Early, steep subduction required by the timing of UHP metamorphism in the western Himalaya. *Earth and Planetary Science Letters*, 234, 83–97.
- Li, J.X., Qin, K.Z., Li, G.M., Xiao, B., Chen, L., Zhao, J.X. Post-collisional ore-bearing adakitic porphyries from Gangdese porphyry copper belt, southern Tibet: Melting of thickened juvenile arc lower crust. *Litho* 126, 265–277.
- Li, Z.Y., Ding, L., Lippert, P.C., Song, P.P., Yue, Y.H., van Hinsbergen, D.J.J., 2016. Paleomagnetic constraints on the Mesozoic drift of the Lhasa terrane (Tibet) from Gondwana to Eurasia. *Geology*, 44, 727–730.
- Lister, G., Kennett, B., Richards, S., and Forster, M., 2008. Boudinage of a stretching slablet implicated in earthquakes beneath the Hindu Kush. *Nature Geoscience*, 1, 196–201.
- Lee, T.Y., Lawver, L.A., 1995. Cenozoic plate reconstruction of Southeast Asia. *Tectonophysics* 251, 85–138.
- Lee, H.Y., Chung, S.L., Lo, C.H., Ji, J., Lee, T.Y., Qian, Q., Zhang, Q., 2009. Eocene Neotethyan slab breakoff in southern Tibet inferred from the Linzizong volcanic record. *Tectonophysics* 477, 20–35.
- Leeder, M.R., Zeidan, R., 1977. Giant late Jurassic sabkhas of Arabian Tethys. *Nature* 268, 42–44.
- Li, C., van der Hilst, R. D., Meltzer, A. S., Engdahl, E. R., 2008. Subduction of the Indian lithosphere beneath the Tibetan plateau and Burma. *Earth Planet. Sci. Lett.* 274, 157–168.
- Li, J.X., Qin, K.Z., Li, G.M., Xiao, B., Chen, L., Zhao, J.X., 2011. Post-collisional ore-bearing adakitic porphyries from Gangdese porphyry copper belt, southern Tibet. Melting of thickened juvenile arc lower crust. *Lithos* 126, 264–277.
- Liang, X.F., Sandvol, E., Chen, J., Hearn, T., Ni, J., Klemperer, S., Shen, Y., Tilmann, F., 2012. A complex Tibetan upper mantle: a fragmented Indian slab and no south-verging subduction of Eurasian lithosphere. *Earth Planet. Sci. Lett.* 333–334, 101–111.
- Liang, X.F., Chen, Y., Tian, X.B., Chen, Y.J., Ni, J., Gallegos, A., Klemperer, S.L., Wang, M.L., Xu, T., Sun, C.Q., Si, S.K., Lan, H.Q., Teng, J.W., 2016. 3D imaging of subducting and fragmenting Indian continental lithosphere beneath southern and central Tibet using

- body-wave finite-frequency tomography: *Earth Planet. Sci. Lett.* 443, 162–175.
- Liu, C.Z., Wu, F.Y., Chung, S.L., Zhao, Z.D., 2011. Fragments of hot and metasomatized mantle lithosphere in Middle Miocene ultrapotassic lavas southern Tibet. *Geology* 39: 923–926.
- Liu, C.Z., Wu, F.Y., Chung, S. L., Li, Q.L., Sun, W.D., Ji, W.Q., 2014. A ‘hidden’ ^{18}O -enriched reservoir in the sub-arc mantle. *Sci. Rep.*, 4, 4232, DOI: 10.1038/srep04232.
- Liu, D., Zhao, Z.D., Zhu, D.C., Niu, Y.L., Harrison, T. M., 2014. Zircon xenocrysts in Tibetan ultrapotassic magmas: imaging the deep crust through time. *Geology* 42, 43–46.
- Liu, D., Zhao, Z.D., Zhu, D.C., Niu, Y.L., Widom, E., Teng, F.Z., DePaolo, D.J., Ke, S., Xu, J.F., Wang, Q., Mo, X.X., 2015. Identifying mantle carbonatite metasomatism through Os–Sr–Mg isotopes in Tibetan ultrapotassic rocks. *Earth Planet. Sci. Lett.* 430, 458–469.
- Liu, D., Zhao, Z.D., DePaolo, D.J., Zhu, D.C., Meng, F.Y., Shi, Q.S., Wang, Q., 2017. Potassic volcanic rocks and adakitic intrusions in southern Tibet: Insights into mantle-crust interaction and mass transfer from Indian plate. *Lithos* 268–271, 48–64.
- Lu, Y.J., Loucks, R.B., Fiorentini, M.L., Yang, Z.M., Hou, Z.Q., 2015. Fluid flux melting generated postcollisional high-Sr/Y copper ore-forming water-rich magmas in Tibet, *Geology* 43, 583–586.
- Lu, Y.J., Loucks, R.R., Fiorentini, M.L., McCuaig, T.C., Evans, N.J., Yang, Z.M., Hou, Z.Q., Kirkland, C.L., Parra-Avila, L.A., Kobussen, A., 2016. Zircon Compositions as a Pathfinder for Porphyry $\text{Cu} \pm \text{Mo} \pm \text{Au}$ Deposits, Society of Economic Geologists Special Publication 19, pp. 329–347.
- Lu, Y.J., Hou, Z.Q., Yang, Z.M., Parra-Avil, L.A., Fiorentini, M., McCuaig, T.C., Loucks, R.R., 2017. Terrane-scale porphyry Cu fertility in the Lhasa terrane, southern Tibet, *GSWA Record* 2017/6, 95–100.
- Macpherson, C.G., Dreher, S.T., Thirlwall, M.F., 2006. Adakites without slab melting: High pressure differentiation of island arc magma, Mindanao, the Philippines. *Earth Planet. Sci. Lett.* 243, 581–593.
- Massonne, H.J., 2016. Hydration of the lithospheric mantle by the descending plate in a continent-continent collisional setting and its geodynamic consequences. *J. Geodyn.* 96, 50–61.
- McDowell, S.M., Miller, C.F., Mundil, R., Ferguson, C.A., Wooden, J.L., 2014. Zircon evidence for a ~200 k.y. supereruption-related thermal flare-up in the Miocene southern Black Mountains, western Arizona, USA. *Contrib. Mineral. Petrol.* 168, 1031, 21p.
- Meng, J., Wang, C., Zhao, X., Coe, R., Li, Y.L., Finn, D., 2012. India-Asia collision was at 24°N and 50 Ma: Paleomagnetic proof from southern Asia: *Sci. Rep.* 2, 925; doi: 10.1038/srep00925.
- Miller, C., Schuster, R., Klotzli, U., Mair, V., Frank, W., Purtscheller, F., 1999. Post-collisional potassic and ultrapotassic magmatism in SW Tibet: geochemical Sr–Nd–Pb–O isotopic constraints for mantle source characteristics and petrogenesis. *J. Petrol.* 40, 1399–1424.
- Miller, C., Klotzli, U., Frank, W., Martin Thoni, M., Grasemann, B., 2000. Proterozoic crustal evolution in the NW Himalaya (India) as recorded by circa 1.80 Ga mafic and 1.84 Ga granitic magmatism. *Precambrian Research* 103, 191–206.
- Mo, X. X., Niu, Y. L., Dong, G. C., Zhao, Z. D., Hou, Z. Q., Zhou, S., Ke, S., 2008. Contribution of syncollisional felsic magmatism to continental crust growth: a case study of the Paleogene Linzizong volcanic succession in southern Tibet. *Chem. Geol.* 250, 49–67.
- Mukherjee, B.K., Sachan, H.K., Ogasawara, Y., Muko, A., and Yoshioka, N., 2003. Carbonate-bearing UHPM rocks from the Tso-Morari region, Ladakh, India: petrological implications. *Int. Geol. Rev.* 45, 49–69.

- Nábělek, J., Hetényi, G., Vergne, J., Sapkota, S., Kafle, B., Jiang, M., Su, H., Chen, J., Huang, B.S., the Hi-CLIMB team, 2009. Underplating in the Himalaya-Tibet collision zone revealed by the Hi-CLIMB experiment. *Science* 325, 1371–1374.
- Naney, M.T., 1983. Phase equilibria of rock-forming ferromagnesian silicates in granitic systems, *Am. J. Sci.*, 283, 993–1033.
- Neiva, A.M.R., 1995. Distribution of trace elements in feldspars of granitic aplites and pegmatites from Alijó-Sanfins, northern Portugal. *Miner. Mag.* 59, 35–45.
- Nunn, C., Roecker, S.W., Priestley, K.F., Liang, X.F., and Gilligan, A., 2014. Joint inversion of surface waves and teleseismic body waves across Tibetan collision zone: the fate of subducted Indian lithosphere. *Geophys. J. Int.* 198, 1526–1542.
- Owens, T.J., Zandt, G., 1997. Implications of crustal property variations for models of Tibetan plateau evolution. *Nature* 387, 37–43.
- Pan, G. T., Ding, J., Yao, D., Wang, L., 2004, The Guide Book of 1:1,500,000 Geologic map of the Qinghai-Xizang (Tibet) Plateau and adjacent Areas. Chengdu Cartographic Publishing House, 44 p (in Chinese).
- Peacock, S.M., 1990. Numerical simulation of metamorphic pressure-temperature-time paths and fluid production in subducting slabs. *Tectonics* 9, 1197–1121.
- Pearce, N.J.G., Perkins, W.T., Westgate, J.A., Gorton, M.P., Jackson, S.E., Neal, C.R., Chenery, S.P., 1997. A compilation of new and published major and trace element data for NIST SRM 610 and NIST SRM 612 glass reference materials. *Geostandards Newslett.* 21, 115–144.
- Phillips, E., Waters, C.N., Ellison, R.A., 2013. The Jurassic-Cretaceous depositional and evolution of the southernwestern margin of the Neotethys Ocean, Northern Oman and United Arab Emirates. *Front. Earth Sci.* 5, 61–100.
- Qu, X., Hou, Z., Li, Y., 2004. Melt components derived from a subducted slab in late orogenic ore-bearing porphyries in the Gangdese copper belt, southern Tibetan Plateau. *Lithos* 74, 131–148.
- Qu, X., Hou, Z., Khin Z., Li, Y., 2007. Characteristics and genesis of Gangdese porphyry copper deposits in the southern Tibetan Plateau: preliminary geochemical and geochronological results. *Ore Geol. Rev.* 31, 205–223.
- Replumaz, A., Negredo, A.M., Villaseñor, A., Guillot, S., 2010. Indian continental subduction and slab breakoff during Tertiary collision. *Terra Nova* 22, 290–296.
- Richards, J.P., 2003. Tectono-magmatic precursors for porphyry Cu-(Mo-Au) deposit formation. *Econ. Geol.* 98, 1515–1533.
- Richards, J.P., 2011. High-Sr/Y arc magmas and porphyry Cu±Mo±Au deposits: Just add water. *Econ. Geol.* 106, 1075–1081.
- Richards, J.P., Kerrich, R., 2007. Adakite-like rocks: Their diverse origins and questionable role in metallogenesis. *Econ. Geol.* 102, 537–576.
- Robinson, J.A., Wood, B.J., 1998. The depth of the spinel to garnet transition at the peridotite solidus. *Earth Planet. Sci. Lett.* 164, 277–284.
- Rowley, D.B., Currie, B.S., 2006. Palaeo-altimetry of the late Eocene to Miocene Lunpola basin, central Tibet. *Nature* 439, 677–681.
- Rubatto, D., 2002, Zircon trace element geochemistry: partitioning with garnet and the link between U-Pb ages and metamorphism, *Chem. Geol.* 184, 123–138.
- Scheibner, C., and Speijer, R.P., 2008. Late Paleocene-early Eocene Tethyan carbonate platform evolution – A response to long- and short term paleoclimatic change, *Earth-Science Rev.* 90, 71–102.
- Shen, X.K., Yuan, X.H., and Liu, M., 2015. Is the Asian lithosphere underthrusting beneath northeastern Tibetan Plateau? Insights from seismic receiver functions. *Earth Planet Sci. Lett.* 428, 172–180.

- Singh, B.P., Singh, S.P., Sachan, H.K., 2006. Post-depositional transformations during burial and exhumation in the Neoproterozoic evaporite sequences, NW Himalaya, India. *Journal of Geological Society of India*, 68, 1058–1068.
- Saha, D., 2013. Lesser Himalayan sequences in Eastern Himalaya and their deformation: Implications for Paleoproterozoic tectonic activity along the northern margin of India. *Geoscience Frontiers*, 4, 289–304.
- Shokoohi Razi, A., Levin, V., Roecker, S. W., Huang G. D., 2014. Crustal and uppermost mantle structure beneath western Tibet using seismic traveltime tomography. *Geochem Geophys* 15, 434–452.
- Sommer, H., and Gauert, C., 2011. Hydrating laterally extensive regions of continental lithosphere by flat subduction: A pilot study from the North American Cordillera. *J. Geodyn.* 51, 17–24.
- Spandler, C., Pirard, C. 2013. Element recycling from subducting slabs to arc crust: a review. *Lithos* 170, 208–223.
- Stern, R.J., 2002. Subduction zones. *Rev. Geophys.* 40 (4), 1012, doi: 10.1029/2001RG000108.
- Stepanov, A.S., Campbell, I., Rapp, R., Lowczak, J., Korsakov, A.V. 2017. Discussion: “Xenoliths in ultrapotassic volcanic rocks in the Lhasa block: direct evidence for crust-mantle mixing and metamorphism in the deep crust” by Wang et al. 2016. (*Contributions to Mineralogy and Petrology*) 171:62. *Contrib. Mineral. Petrol.* 172: 19.
- Stepanov, A.S., Hermann, J., Korsakov, A.V., Rubatto, D. 2014. Geochemistry of ultrahigh-pressure anatexis: fractionation of elements in the Kokchetav gneisses during melting at diamond-facies conditions. *Contrib. Mineral. Petrol.* 167, 1002.
- Sun, S.S., McDonough, W.F., 1989. Chemical and isotopic systematics of oceanic basalts: implications for mantle composition and processes. *Geol. Soc. London Spec. Publ.* 42, 313–345.
- Tafti, R., Mortensen, J.K., Lang, J.R., Rebagliati, M., Oliver, J.L., 2009. Jurassic U–Pb and Re–Os ages for the newly discovered Xietongmen Cu–Au porphyry district, Tibet, PRC: implications for metallogenic epochs in the southern Gangdese belt. *Econ. Geol.* 104, 127–136.
- Tafti, R., 2011. Metallogeny, geochronology and tectonic setting of the Gangdese belt, southern Tibet, China. Unpublished Ph.D. thesis, University of British Columbia, Canada, 451 p.
- Tafti, R., Lang, J.R., Mortensen, J.K., Oliver, J., Rebagliati, C.M., 2014. Geology and geochronology of the Xietongmen (Xiongcu) Cu–Au porphyry district, Southern Tibet, China. *Econ. Geol.* 109, 1967–2001.
- Tang, J.X., Lang, X.H., Xie, F.W., Gao, Y.M., Li, Z.J., Huang, Y., Ding, F., Yang, H.H., Zhang, L., Zhou, Y., 2015. Geological characteristics and genesis of the Jurassic No. I porphyry Cu–Au deposit in the Xiongcu district, Gangdese porphyry copper deposit, Tibet. *Ore Geol. Rev.* 70, 438–456.
- Tapponnier, P., Xu, Z., Roger, F., Meyer, B., Anaud, N., Wittlinger, G., Yang, J., 2001. Oblique stepwise rise and growth of the Tibet Plateau. *Science* 294, 1671–1677.
- Taylor, R.J.M., Kirkland, C.L., Clark, C., 2016. Accessories after the facts: Constraining the timing, duration and conditions of high-temperature metamorphic processes. *Lithos* 264, 239–257.
- Toksöv, M.N., Minear, J.W., Julian, B.R., 1971. Temperature field and geophysical effects of a downgoing slab. *J. Geophys. Res.* 76, 1113–1138.
- Trail, D., Watson, E.B., Tailby, N.D., 2012. Ce and Eu anomalies in zircon as proxies for the oxidation state of magmas. *Geochim. Cosmochim. Acta*, 97, 70–87.
- Turner, S., Arnaud, N., Liu, J., Rogers, N., Hawkesworth, C., Harris, N., Kelley, S., 1996.

- Post-collision, shoshonitic volcanism on the Tibetan Plateau: implications for convective thinning of the lithosphere and the source of ocean island basalts. *J. Petrol.* 37, 45–71.
- Tilmann, F., Ni, J., INDEPTH III Seismic Team, 2003. Seismic imaging of the downwelling Indian lithosphere beneath Central Tibet. *Science* 300, 1424–1427.
- Tomkins, A.G., Weinberg, R.F., McFarlane, C.R.M., 2009. Preferential magma extraction from K- and metal-enriched source regions in the crust. *Miner. Deposita* 44, 171–181.
- Van der Voo, R., Spakman, W., Bijwaard, H., 1999. Tethyan subducted slabs under India. *Earth Planet. Sci. Lett.* 171, 7–20.
- van Hinsbergen, D.J.J., Lippert, C., Dupont-Nivet, G., McQuarrie, N., Doubrovine, V., Spakman, W., Torsvik, T.H., 2012. Greater India basin hypothesis and a two-stage Cenozoic collision between India and Asia. *PNAS* 109, 7659–7664.
- Wagner, L.S., Beck, S., Zandt, G., 2005. Upper mantle structure in the south central Chilean subduction zone (30° to 36°S). *J. Geophys. Res.* 110, B01308.
- Wang, R., Richards, J.P., Hou, Z.Q., Yang, Z.M., DuFrane, S.A., 2014a. Increased magmatic water content—the key to Oligo-Miocene porphyry Cu–Mo ± Au formation in the eastern Gangdese belt, Tibet. *Econ. Geol.* 109, 1315–1339.
- Wang, R., Richards, J.P., Hou, Z.Q., Yang, Z.M., Gou, Z.B., DuFrane, S.A., 2014b. Increasing magmatic oxidation state from Paleocene to Miocene in the eastern Tibetan Gangdese belt: implication for collision-related porphyry Cu–Mo±Au mineralization. *Econ. Geol.* 109, 1943–1965.
- Wang, R., Richards, J.P., Hou, Z.Q., Yang, Z.M., 2014c. Extent of underthrusting of the Indian plate beneath Tibet controlled of Miocene porphyry Cu–Mo±Au deposits. *Miner. Deposita* 49, 165–173.
- Wang, R., Richards, J.P., Zhou, L.M., Hou, Z.Q., Stern, R.A., Creaser, R.A., Zhu, J.J., 2015a, the Role of Indian and Tibetan lithosphere in spatial distribution of Cenozoic magmatism and porphyry Cu–Mo±Au deposits in the Gangdese belt, southern Tibet. *Earth-Sci. Rev.* 150, 68–94.
- Wang, R., Richards, J.P., Hou, Z.Q., An, F., Creaser, R.A., 2015b. Zircon U–Pb age and Sr–Nd–Hf–O isotope geochemistry of the Paleocene–Eocene igneous rocks in western Gangdese: Evidence for the timing of Neo-Tethyan slab breakoff. *Lithos*, 224–225, 179–194.
- Wang, R., Collins, W.J., Weinberg, R.F., Li, J.X., Li, Q.Y., He, W.Y., Richards, J.P., Hou, Z.Q., Zhou, L.M., Stern, R.A., 2016. Xenoliths in ultrapotassic volcanic rocks in the Lhasa block: direct evidence for crust–mantle mixing and metamorphism in the deep crust. *Contrib. Mineral. Petrol.*, 171, 62.
- Wang, R., Collins, W.J., Weinberg, R.F., Richards, J.P., He, W.Y., 2017a, Reply to the comments on “Xenoliths in ultrapotassic volcanic rocks in the Lhasa block: direct evidence for crust–mantle mixing and metamorphism in the deep crust”. *Contrib. Mineral. Petrol.*, 170:20.
- Wang, R., Tafti, R., Hou, Z.Q., Shen, Z.C., Guo, N., Evans, N., Jeon, H., Li, Q.Y., Li, W.K., 2017b. Across-arc geochemical variation in the Jurassic magmatic zone, Southern Tibet: Implication for continental arc-related porphyry Cu–Au mineralization. *Chem. Geol.*, 451, 116–134.
- Warren, C.J., Beaumont, C., Jamieson, R.A., 2008. Deep subduction and rapid exhumation: the role of crustal strength and strain weakening in continental subduction and ultrahigh pressure rock exhumation. *Tectonics* 27, TC6002. doi:10.1029/2008TC002292
- Waters, L.E., Lange, R.A., 2015. An updated calibration of the plagioclase–liquid hygrometer–thermometer applicable to basalts through rhyolites. *Am. Mineral.* 100, 2172–2184.
- Watson, E.B., Harrison, T.M., 2005. Zircon thermometer reveals minimum melting

- conditions on earliest Earth. *Science* 308, 841–844.
- Weinberg, R.F. and Dunlap, W.J., 2000, Growth and deformation of the Ladakh Batholith, NW Himalayas: implications for timing of continental collision and origin of calc-alkaline batholiths. *J. Geol.* 108, 303–320
- Weinberg, R.F., Hasalová, P., 2015, Water-fluxed melting of the continental crust: A review. *Lithos* 212–215, 158–188.
- Wen, D.R., 2007. The Gangdese batholith, Southern Tibet. Ages, geochemical characteristics and petrogenesis. Unpublished Ph.D. thesis, National Taiwan University, 120 p.
- Wen, D.R., Liu, D.Y., Chung, S.L., Chu, M.F., Ji, J.Q., Zhang, Q., Song, B., Lee, T.Y., Yeh, M.W., Lo, C.H., 2008. Zircon SHRIMP U-Pb ages of the Gangdese Batholith and implications for Neotethyan subduction in southern Tibet. *Chem. Geol.*, 252, 191–201.
- Wendlandt, R.F., Eggler, D.H., 1980. The origins of potassic magmas; 2, Stability of phlogopite in natural spinel lherzolite and in the system $\text{KAlSiO}_4\text{-MgO-SiO}_2\text{-H}_2\text{O-CO}_2$ at high pressures and high temperatures. *Am. J. Sci.* 280, 421–458.
- Willet, S.D., Beaumont, C., 1994. Subduction of Asian lithospheric mantle beneath Tibet inferred from models of continental collision. *Nature* 369, 642–645.
- Williams, H.M., 2000. Magmatic and tectonic evolution of Southern Tibet and the Himalaya: Ph.D. thesis, The Open University, 329 p.
- Williams, H.M., Turner, S.P., Kelley, S.P., Harris, N.B.W., 2001. Age and composition of dikes in Southern Tibet: new constraints on the timing of east–west extension and its relationship to post-collisional volcanism. *Geology* 29, 339–342.
- Williams, H.M., Turner, S.P., Pearce, J.A., Kelley, S.P., Harris, N.B.W., 2004. Nature of the source regions for post-collisional, potassic magmatism in southern and northern Tibet from geochemical variations and inverse trace element modelling. *J. Petrol.* 45, 555–607.
- Williamson, B.J., Herrington, R.J., Morris, A., 2016, Porphyry copper enrichment linked to excess aluminium in plagioclase. *Nature Geosci.* 9, 237–241.
- Wood, B.J., Turner, S.P., 2009. Origin of primitive high-Mg andesite: constraints from natural examples and experiments. *Earth Planet. Sci. Lett.* 283, 59–66.
- Xu, B., Griffin, W.L., Xiong, Q., Hou, Z.Q., O'Reilly, S.Y., Guo, Z., Pearson, N.J., Gréau, Y., Yang, Z.M., Zheng, Y.C., 2016. Ultrapotassic rocks and xenoliths from South Tibet: Contrasting styles of interaction between lithospheric mantle and asthenosphere during continental collision. *Geology* doi: 10.1130/g38466.1
- Yang, Z.M., Hou, Z.Q., White, N.C., Chang, Z.S., Li, Z.Q., Song, Y.C., 2009. Geology of the post-collisional porphyry copper-molybdenum deposit at Qulong, Tibet: *Ore Geol. Rev.* 36, 133–159.
- Yang, Z.M., Lu, Y.J., Hou, Z.Q., Chang, Z.S., 2015. High-Mg diorite from Qulong in Southern Tibet: Implications for the genesis of Adakite-like intrusions and associated porphyry Cu deposits in collisional orogens. *J. Petrol.* 56, 227–254.
- Yang, Z.M., Goldfarb, R., Chang, Z.S., 2016. Generation of postcollisional porphyry copper deposits in southern Tibet triggered by subduction of the Indian continental plate. *Econ. Geol.* 119, 279–300.
- Ye, Z., Gao, R., Li, Q., Zhang, H., Shen, X., Liu, X., Gong, C., 2015. Seismic evidence for the North China plate underthrusting beneath northeastern Tibet and its implications for plateau growth. *Earth Planet. Sci. Lett.* 426, 109–117.
- Yin, A., 2010. Cenozoic tectonic evolution of Asia: a preliminary synthesis. *Tectonophysics*, 488, 293–325.
- Yin, A., Harrison, T. M., 2000. Geologic evolution of the Himalayan-Tibetan orogen. *Annu. Rev. Earth Planet. Sci.* 28, 211–280.
- Ying, L. J., Wang, C. S., Tang, J. X., Wang, D. H., Qu, W. J., Li, C., 2014. Re-Os systematics of sulfides (chalcopyrite, bornite, pyrite and pyrrhotite) from the Jima Cu–Mo

- deposit of Tibet, China. *J. Asian Earth Sci.* 79, 497–506.
- Zhang, Z.M., Zhao, G.C., Santosh, M., Wang, J.L., Dong, X., Shen, K., 2010. Late Cretaceous charnockite with adakitic affinities from the Gangdese batholith, southeastern Tibet: evidence for Neo-Tethyan mid-ocean ridge subduction? *Gondwana Res.*, 17, 615–631.
- Zhao, J., Yuan, X., Liu, H., Kumar, Pei, S., Kind, R., Zhang, Z., Teng, J., Ding, L., Gao, X., Xu, Q., Wang, W., 2010. The boundary between the Indian and Asian tectonic plates below Tibet. *PANS* 107, 11229–11233.
- Zhao, J. X., Qin, K. Z., Li, G. M., Li, J. X., Xiao, B., Chen, L., Yang, Y. H., Li, C., Liu, Y. S., 2014. Collision-related genesis of the Sharang porphyry molybdenum deposit, Tibet: evidence from zircon U-Pb ages, Re-Os ages and Lu-Hf isotopes. *Ore Geol. Rev.* 56, 312–326.
- Zhao, W., Kumar, P., Mechie, J., Kind, R., Meissner, R., Wu, Z., Shi, D., Su, H., Xue, G., Karplus, M., Tilmann, F., 2011. Tibetan plate overriding the Asian plate in central and northern Tibet. *Nat. Geosci.* 4, 870–873.
- Zhao, Z.D., Mo, X.X., Dilek, Y., Niu, Y.L., DePaolo, D.J., Robinson P., Zhu, D.C., Sun, C.G., Dong, G.C., Zhou, S., Luo, Z.H., Hou, Z.Q., 2009. Geochemical and Sr-Nd-Pb-O isotopic compositions of the post-collisional ultrapotassic magmatism in SW Tibet: petrogenesis and implications for India-continental subduction beneath southern Tibet. *Lithos* 113, 190–212.
- Zheng, W.B., Tang, J.X., Zhong, K.H., Ying, L.J., Leng, Q.F., Ding, S., Lin, B., 2016, Geology of the Jiama porphyry copper-polymetallic systems, Lhasa Region, China. *Ore Geol. Rev.* 74, 151–169.
- Zheng, Y. C., Hou, Z. Q., Li, W., Liang, W., Huang, K. X., Li, Q. Y., Sun, Q. Z., Fu, Q., Zhang, S., 2012. Petrogenesis and geological implications of the Oligocene Chongmuda-Mingze adakite-like intrusions and their mafic enclaves, southern Tibet. *J. Geol.* 120, 647–669.
- Zheng, Y.Y., Zhang, G.Y., Xu, R.K., Gao, S.B., Pang, Y.C., Cao, L., Du, A.D., Shi, Y.R., 2007. Geochronologic constraints on magmatic intrusions and mineralization of the Zhunuo porphyry copper deposit in Gangdese, Tibet. *Chin. Sci. Bull.* 52, 3139–3147.
- Zheng, Y. Y., Sun, X., Gao, S. B., Zhao, Z. D., Zhang, G. Y., Wu, S., You, Z. M., Li, J. D., 2014. Multiple mineralization events at the Jiru porphyry copper deposit, southern Tibet: implications for Eocene and Miocene magma sources and resource potential. *J. Asian Earth Sci.* 79, 842–857.
- Zheng, Y.C., Hou, Z.Q., Gong, Y.L., Liang, W., Sun Q.Z., Zhang, S., Fu, Q., Huang, K.X., Li, Q.Y., Li, W., 2014. Petrogenesis of Cretaceous adakite-like intrusions of the Gangdese plutonic belt, southern Tibet: Implications for mid-ocean ridge subduction and crustal growth. *Lithos* 190–191, 240–263.
- Zhou, S., Mo, X.X., Zhao, Z.D., Qiu, R.Z., Niu, Y.L., Guo, T.Y., Zhang, S.Q., 2010. $^{40}\text{Ar}/^{39}\text{Ar}$ geochronology of post-collisional volcanism in the middle Gangdese Belt, southern Tibet. *J. Asian Earth Sci.*, 37, 246–258.
- Zhu, D.C., Mo, X.X., Zhao, Z.D., Niu, Y.L., Wang, L.Q., Chu, Q.H., Pan, G.T., Xu, J.F., Zhou, C.Y., 2010. Presence of Permian extension- and arc-type magmatism in southern Tibet: petrogeographic implications. *Geol. Soc. Am. Bull.* 122, 979–993.
- Zhu, D.C., Zhao, Z.D., Niu, Y.L., Dilek, Y., Mo, X.X., 2011. Lhasa terrane in southern Tibet came from Australia. *Geology* 39, 727–730.
- Zhu, D.C., Zhao, Z.D., Niu, Y., Dilek, Y., Hou, Z.Q., Mo, X.X., 2013. Origin and pre-Cenozoic evolution of the Tibetan plateau. *Gondwana Res.* 23, 1429–1454.
- Zhu, D.C., Wang, Q., Zhao, Z.D., Chung, S.L., Cawood, P.A., Niu, Y.L., Liu, S.A., Wu, F.U., Mo X.X., 2015. Magmatic record of India-Asia collision. *Sci. Rep.* 5: 14289.

Zhu, D.C., Li, S.M., Cawood, P.A., Wang, Q., Zhao, Z.D., Liu, S.A., Wang, L.Q., 2016. Assembly of the Lhasa and Qiangtang terranes in central Tibet by divergent double subduction. *Lithos* 245, 7–17

Zhu, D.C., Wang, Q., Cawood, P.A., Zhao, Z.D., Mo, X.X., 2017. Raising the Gangdese Mountains in southern Tibet. *J Geophys. Res. Solid Earth* 122, 214–223.

Appendix-Analytical methods

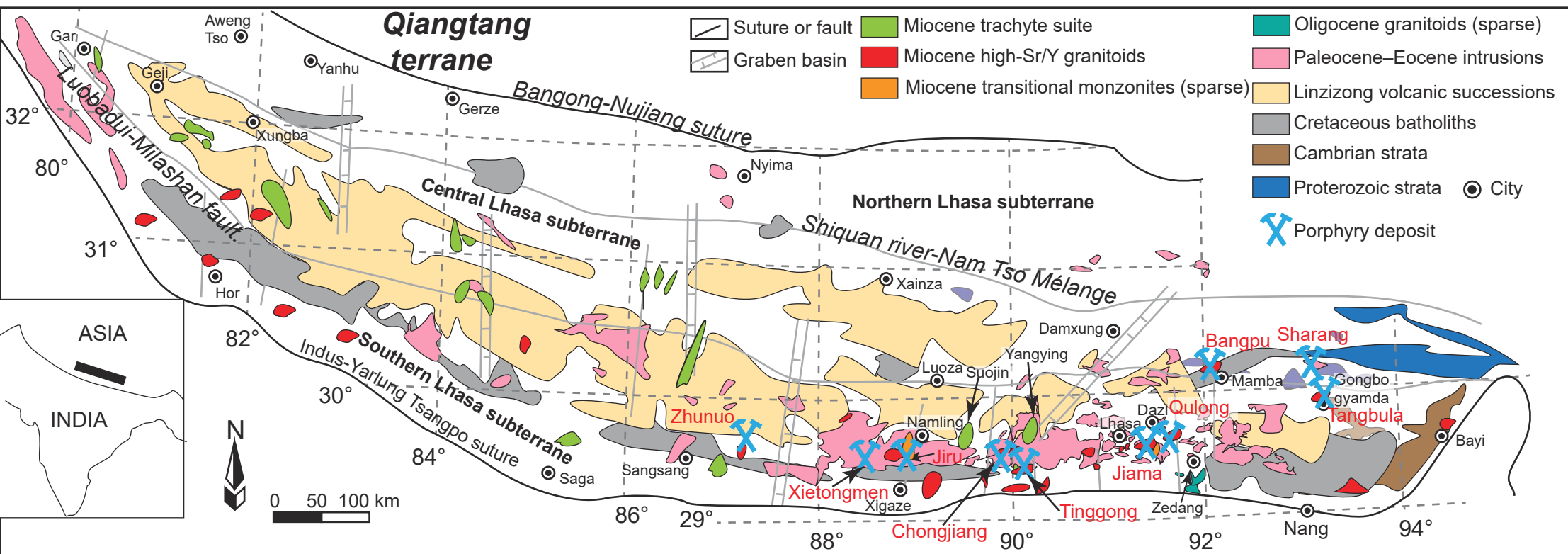
Zircon trace element analysis

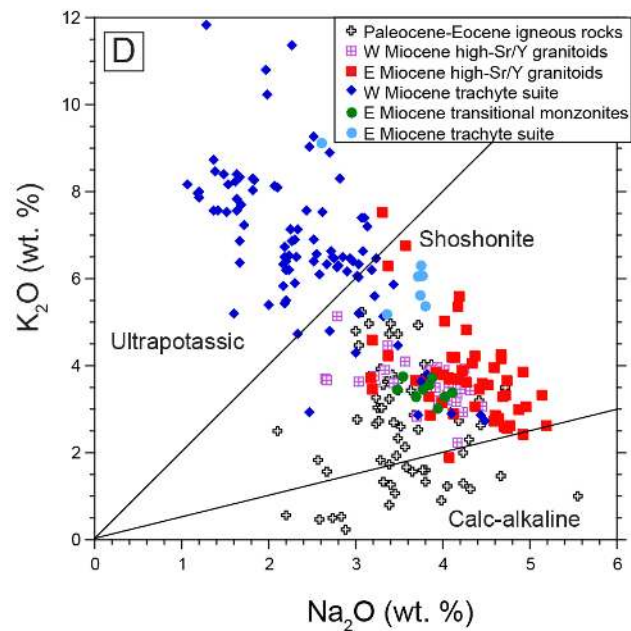
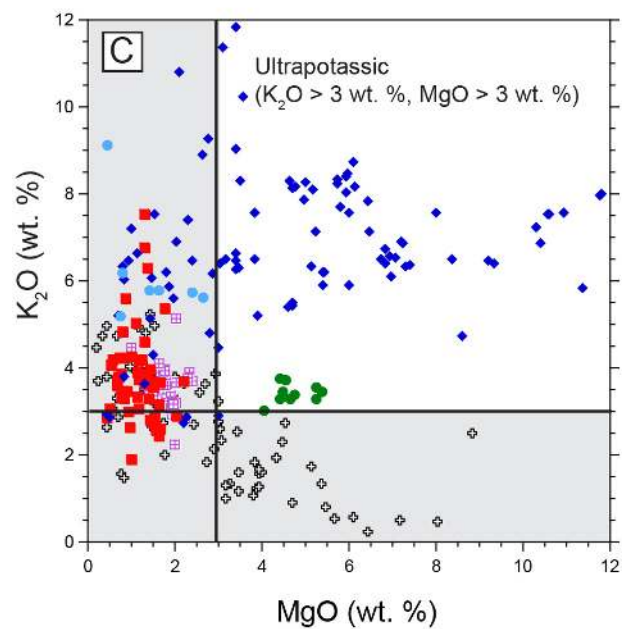
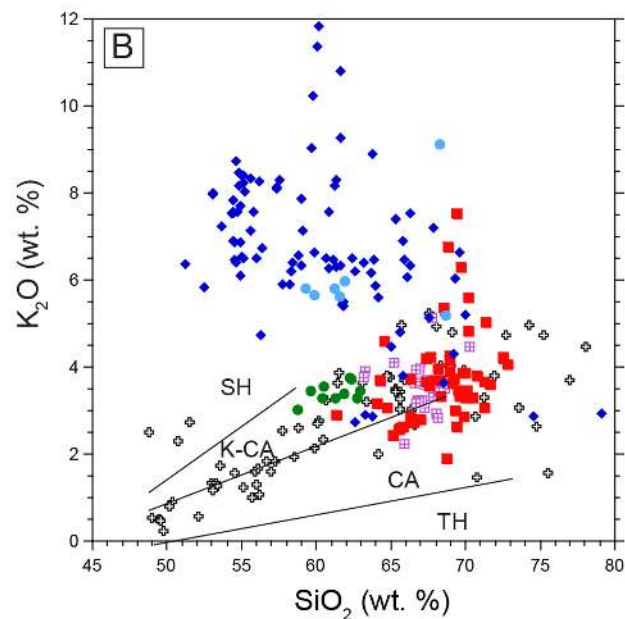
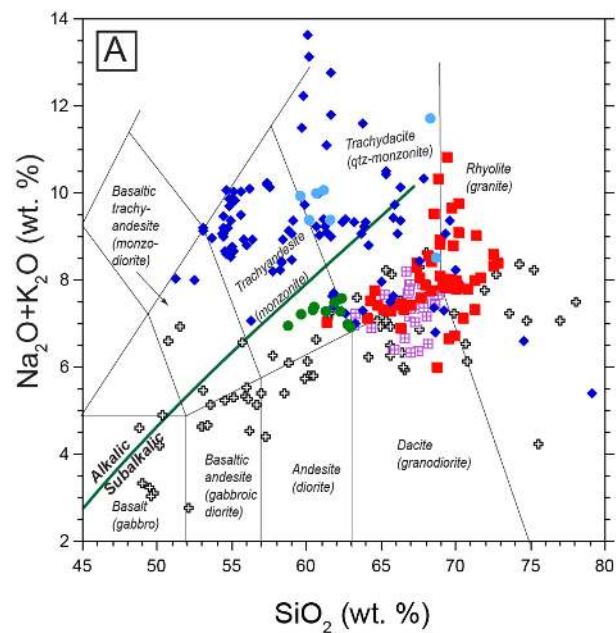
Here, we add new zircon chemistry results to compiled data in order to determine the magmatic temperatures, water contents, and oxidation states of the magmatic rocks. Zircons were mounted in epoxy with chips of standard ATHO-G and NIST 612 glass. A frequency quintupled Nd-YAG laser (UP 213, New Wave Research) was used to ablate the zircons and standard, and ablated material was carried by He-Ar gas (flow rates of 0.73 L He/min and 0.85 L Ar/min) to a Finnigan MAET ELEMENT II high-resolution inductively coupled plasma mass spectrometer (HR-ICP-MS) at the National Research Center for Geoanalysis, Beijing, China. Laser ablation pits were approximately 40 μm wide and 20 μm deep. Data were acquired for 12 s with the laser off, and 43 s with the laser on, then the system was flushed with He-Ar gas for 15 s with the laser off. Each block of ten zircon analyses was bracketed by analysis of standard glass NIST 612, which was used to correct for mass bias drift during analysis (Pearce et al., 1997). The calibration procedure using internal standards and matrix normalization followed Hu et al. (2008). Calibration was conducted by normalizing count rates for each analysed element with Si to obtain its concentration, and assuming SiO_2 to be stoichiometric in zircon (ZrSiO_4) with a concentration of ca. 32.8 wt.%. Accuracy for selected elements, as determined by reproducibility of laboratory standards and duplicates, is within 10 relative %.

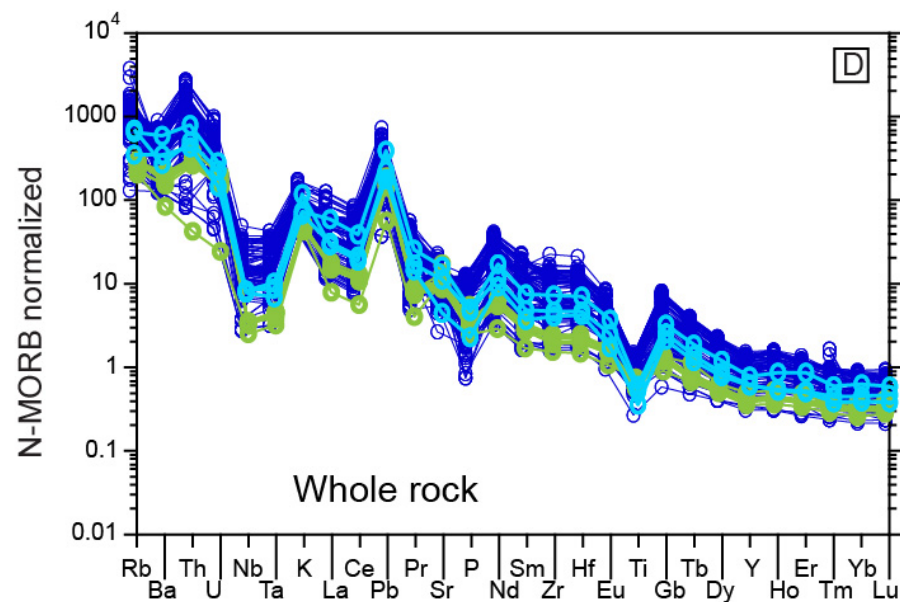
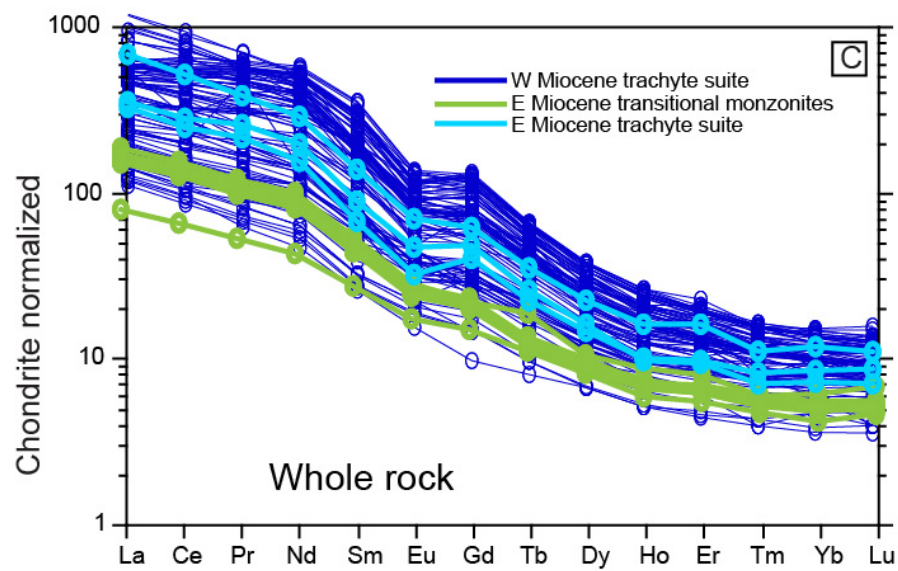
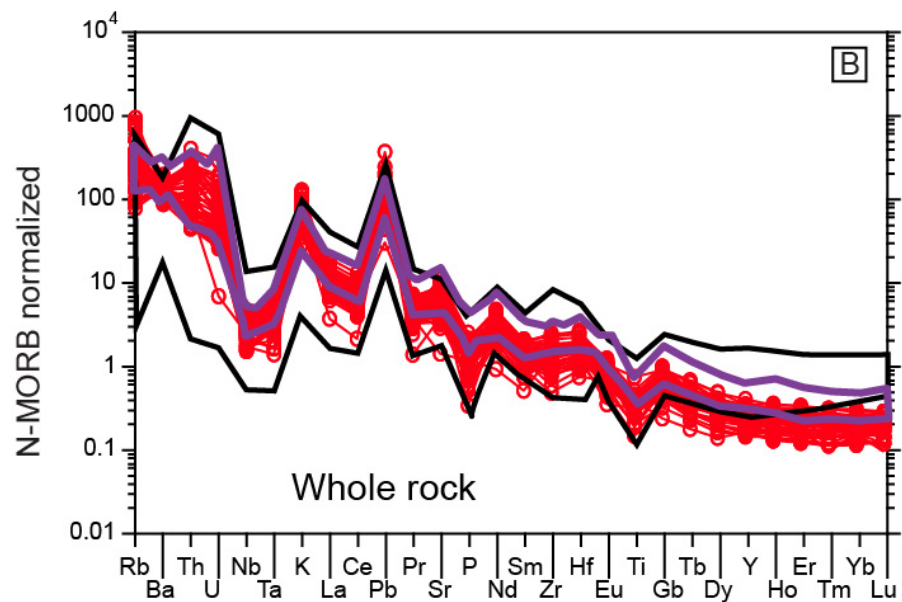
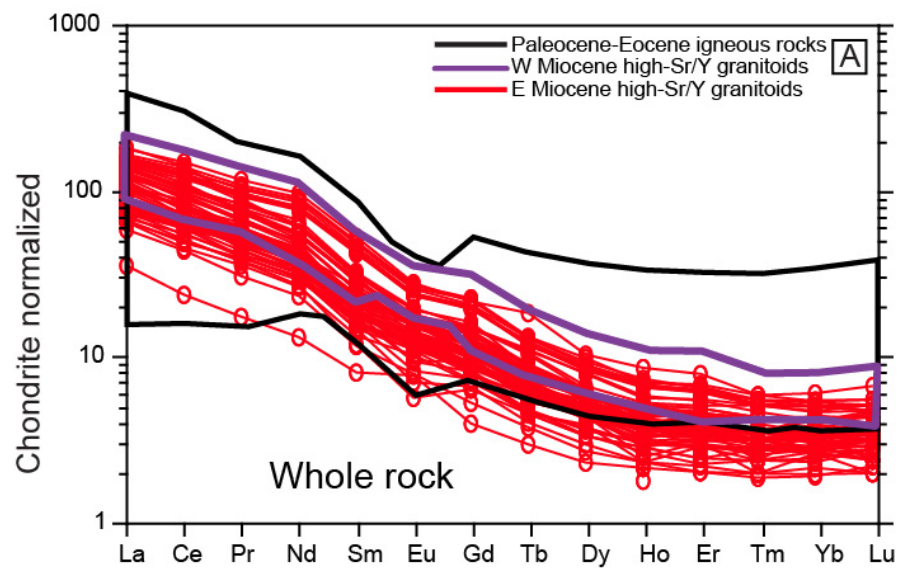
In order to avoid mineral and glass inclusions, inherited cores, and fractures, the laser ablation spots in zircon were selected carefully. Apatite inclusions are common in zircon

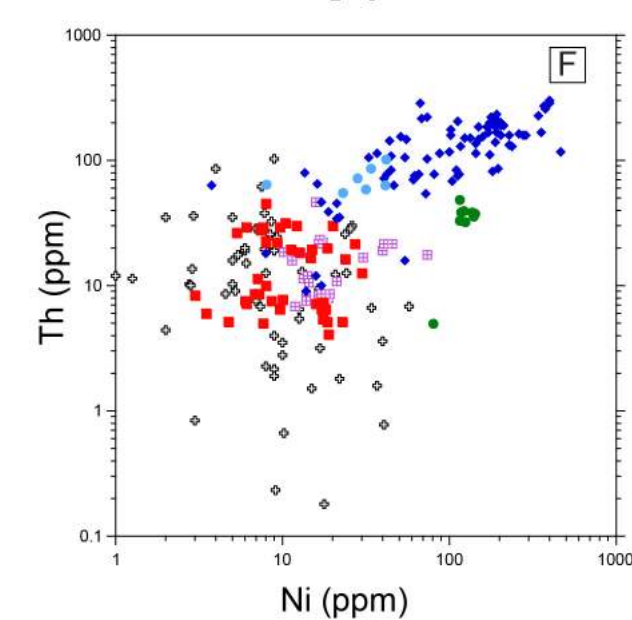
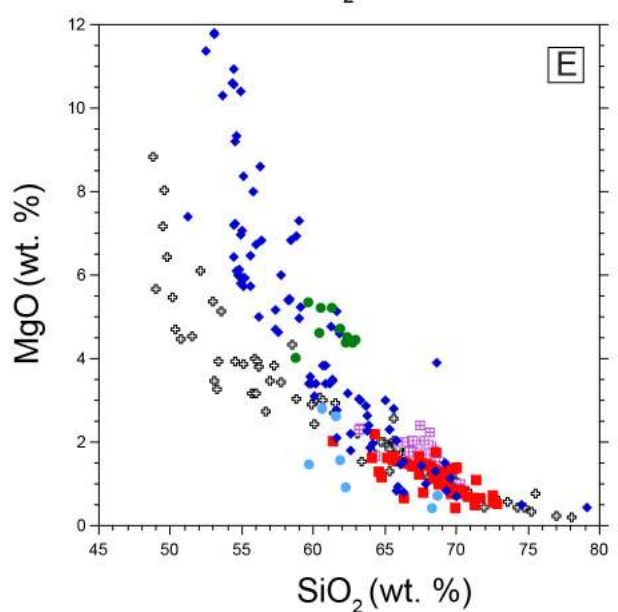
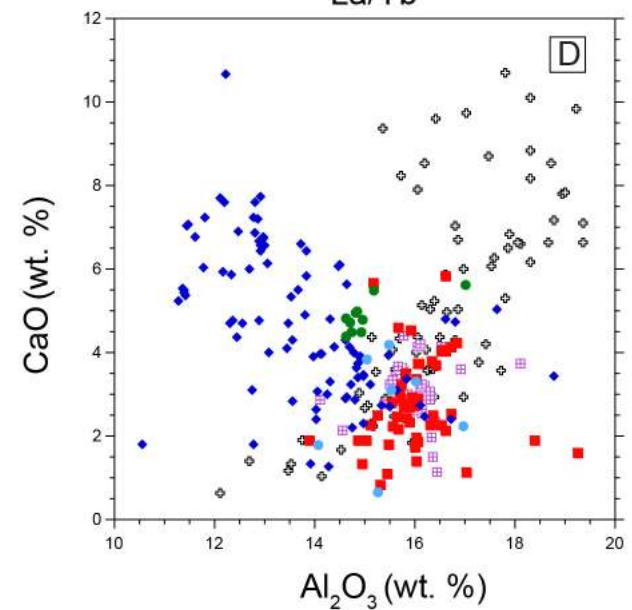
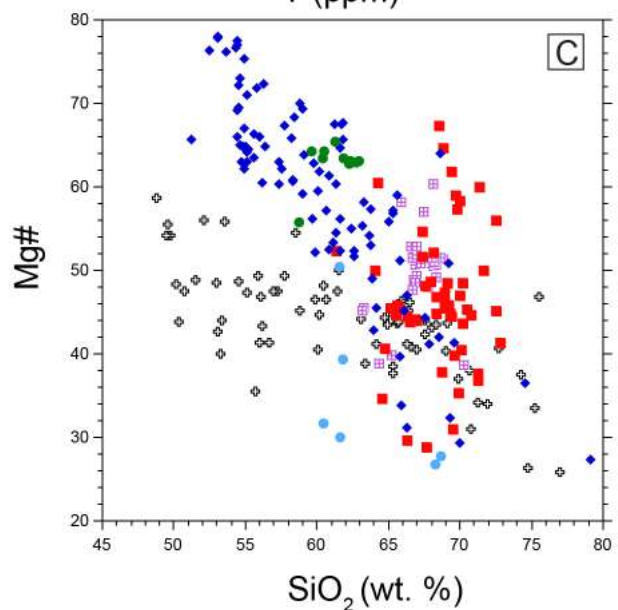
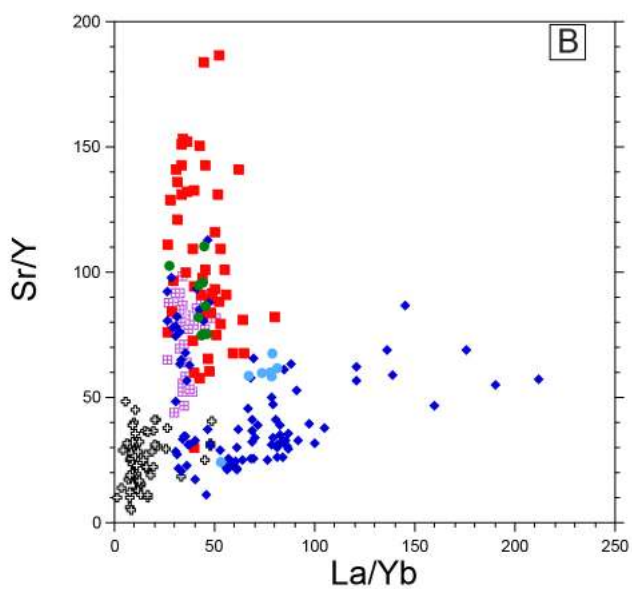
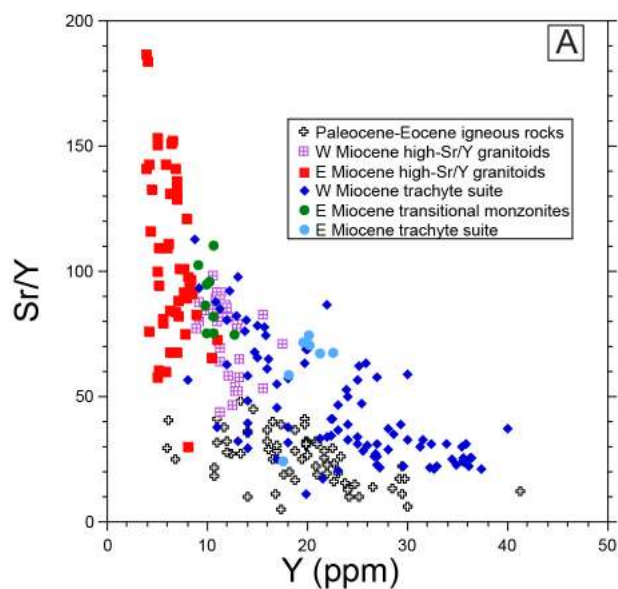
3777
3778
3779 1858 grains and can strongly affect REE contents, so phosphorus and calcium were included in the
3780
3781 1859 list of elements measured in order to monitor for apatite inclusions.
3782
3783
3784 1860
3785
3786 1861 Electron microprobe analyses, plagioclase data
3787
3788 1862 Plagioclase in igneous rocks from the Gangdese belt were analysed by electron
3789
3790 1863 microprobe at the University of Alberta, Canada. Electron microprobe data were acquired on
3791
3792 1864 a JEOL 8900 instrument operated at 15 kV accelerating voltage and 15 nA probe current, and
3793
3794 1865 with a beam diameter of 1 to 5 μm . A variety of minerals, oxides, and elemental standards
3795
3796 1866 were used for calibration, and data reductions were undertaken with the CITZAF routine of
3797
3798 1867 J.T. Armstrong (as implemented by P. Carpenter in the JEOL software). The limits of
3799
3800 1868 detection are typically lower than 500 ppm (≤ 800 ppm for Mn, Fe, Ti, Cr, and Ni; ≤ 5000 ppm
3801
3802 1869 for F), and analytical precision for major elements is better than one relative percent.
3803
3804 1870 The Al composition of plagioclase can be used to estimate magmatic water contents
3805
3806 1871 (Lange et al., 2009; Waters and Lange, 2015; Williamson et al., 2016). We analysed EPMA
3807
3808 1872 compositions of plagioclase from Paleocene-Eocene Gangdese arc intrusions, Miocene PCD-
3809
3810 1873 bearing intrusions, and Miocene volcanic rocks, and combined these data with analyses of
3811
3812 1874 plagioclase from the Qulong deposit (Xiao, 2011). These data are listed in Table A3.
3813
3814 1875
3815
3816 1876 Figure A1 Two profiles of the geometry of the colliding lithospheres discussed in Zhao et al.
3817
3818 1877 (2010): (A) Underthrusting of Indian lithosphere along the western profile along longitude
3819
3820 1878 $\sim 80^\circ\text{E}$; (B) northward subduction of Indian lithosphere along the eastern profile along
3821
3822 1879 longitude $\sim 87^\circ\text{E}$. Abbreviations: BNS = Bangong-Nujiang suture; MBT = Main central thrust;
3823
3824 1880 YZS = Indus-Yarlung Tsangpo suture.
3825
3826 1881
3827
3828
3829
3830
3831
3832
3833
3834
3835

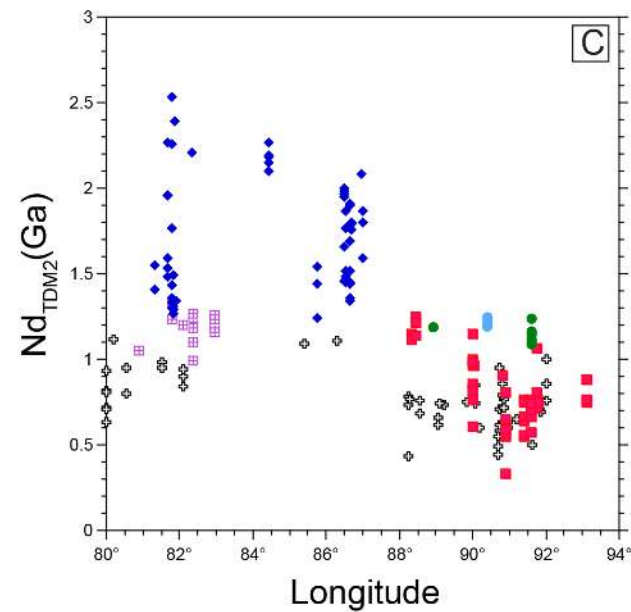
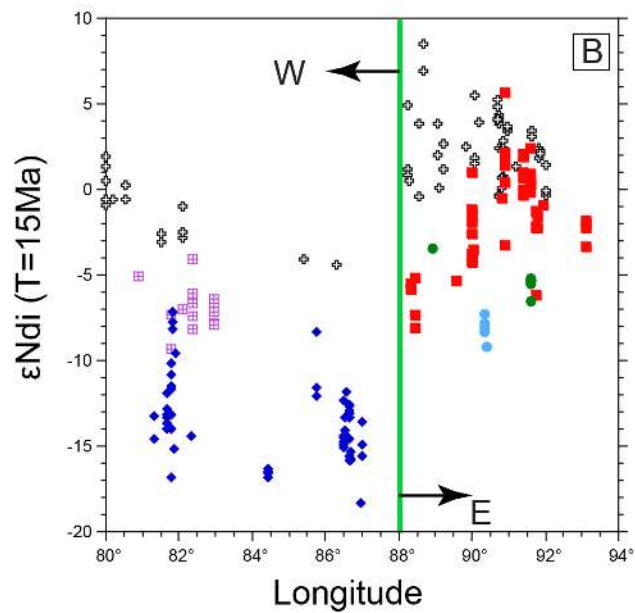
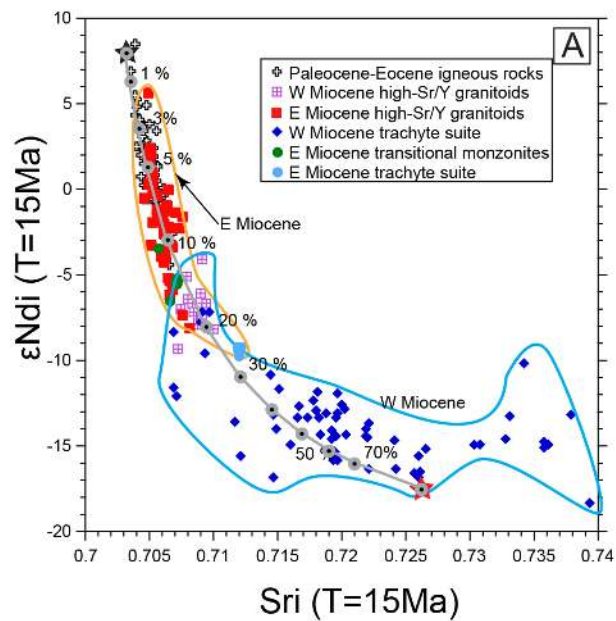
3836
3837
3838
3839 1882 Figure A2 Trace element composition of zircons from the six main Cenozoic suites in the
3840
3841 1883 Gangdese belt: (A) Ce^{4+}/Ce^{3+} vs. Eu/Eu^* ; (B) Th/U vs. $T(ti-zr)$; (C) Ce^{4+}/Ce^{3+} vs. $T(ti-zr)$; (D)
3842
3843 1884 Ce^{4+}/Ce^{3+} vs. Th/U . References for data provided in Table A2.
3844
3845 1885
3846
3847 1886 Figure A3 Chondrite normalized REE diagram for zircons from the six main Cenozoic suites
3848
3849 1887 in the Gangdese belt: (A) W Miocene trachytes, E Miocene trachytes, and E Miocene
3850
3851 1888 transitional monzonites; (B) Paleocene-Eocene Gangdese arc calc-alkaline rocks, W Miocene
3852
3853 1889 high-Sr/Y granitoids, and E Miocene high-Sr/Y granitoids. References for data provided in
3854
3855 1890 Table A1.
3856
3857 1891
3858
3859
3860 1892 Figure A4 Trace element composition of zircons from Paleocene-Eocene Gangdese arc
3861
3862 1893 igneous rocks: (A) $T(ti-zr)$ vs. age; (B) Eu/Eu^* vs. age; (C) Ce^{4+}/Ce^{3+} vs. age. Note that
3863
3864 1894 zircons from 53–50 Ma igneous rocks show significantly higher $T(ti-zr) = 800–900\text{ }^{\circ}C$
3865
3866 1895 compared to older igneous rocks ($<800C$), but lower Eu/Eu^* and Ce^{4+}/Ce^{3+} ratios indicating
3867
3868 1896 input of mantle-derived melts with low oxidation states. References for data provided in
3869
3870 1897 Tables A1, A2.
3871
3872 1898
3873
3874 1899 Table A1. Published major and trace element compositions of Cenozoic igneous rocks from
3875
3876 1900 the Gangdese Belt
3877
3878
3879 1901
3880
3881 1902 Table A2. Zircon trace element compositions for Cenozoic igneous rocks from the Gangdese
3882
3883 1903 Belt..
3884
3885 1904
3886
3887 1905 Table A3. EPMA compositions for plagioclase from Cenozoic igneous rocks from the
3888
3889 1906 Gangdese Belt.
3890
3891
3892
3893
3894

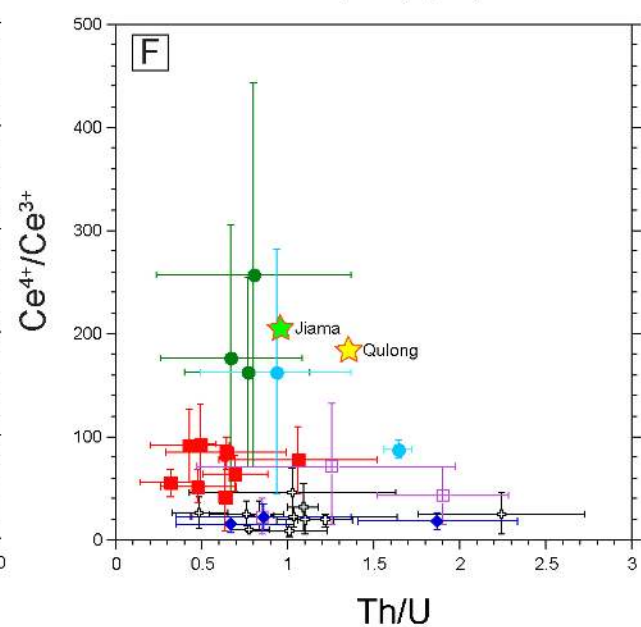
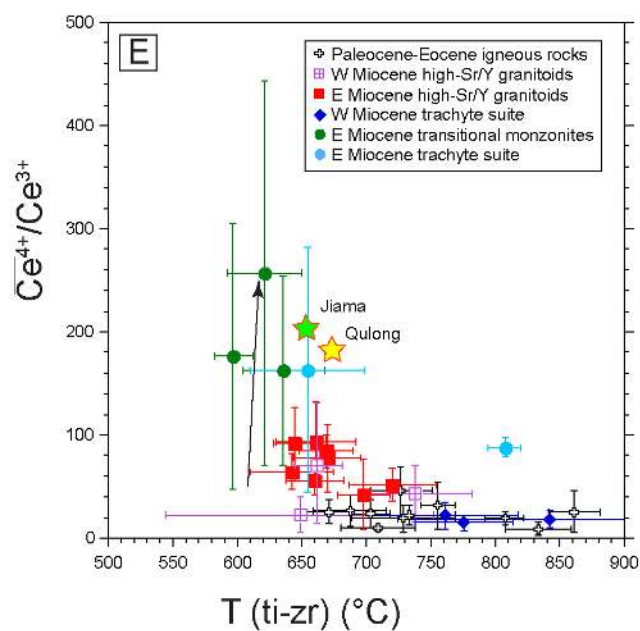
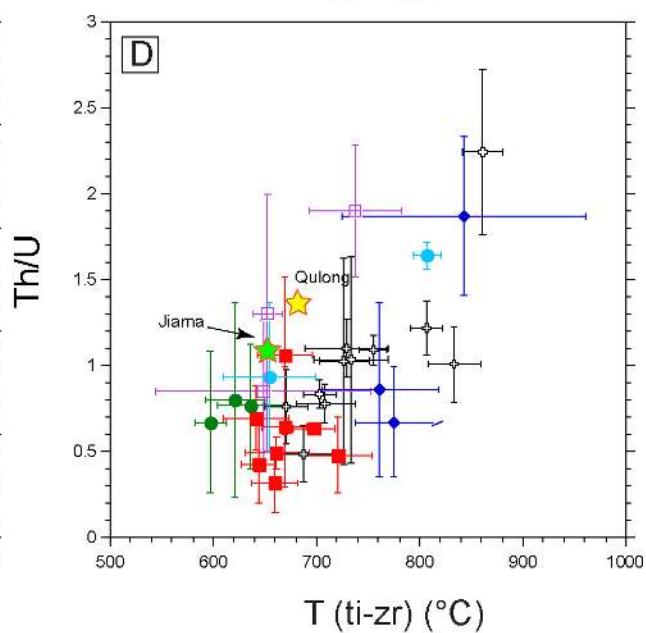
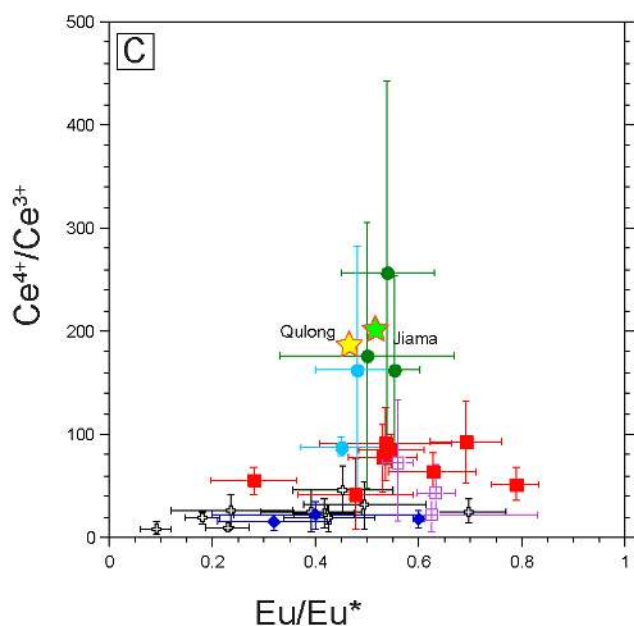
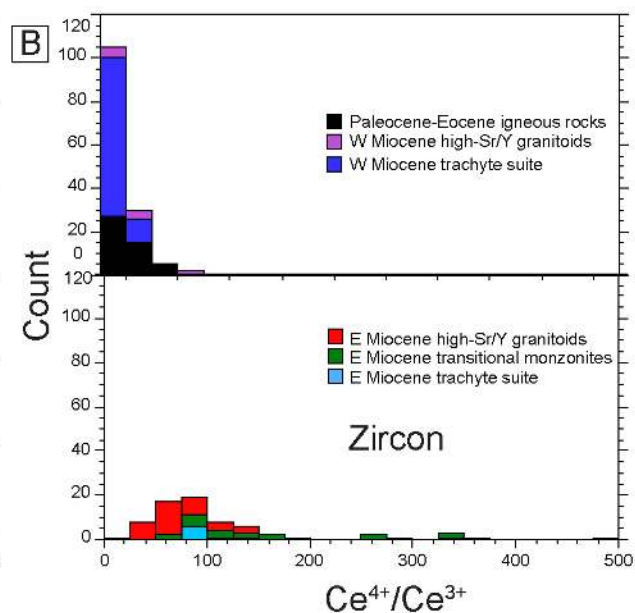
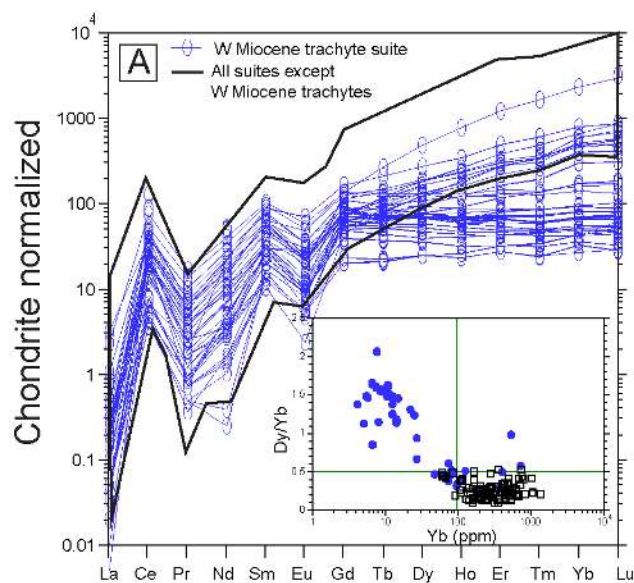


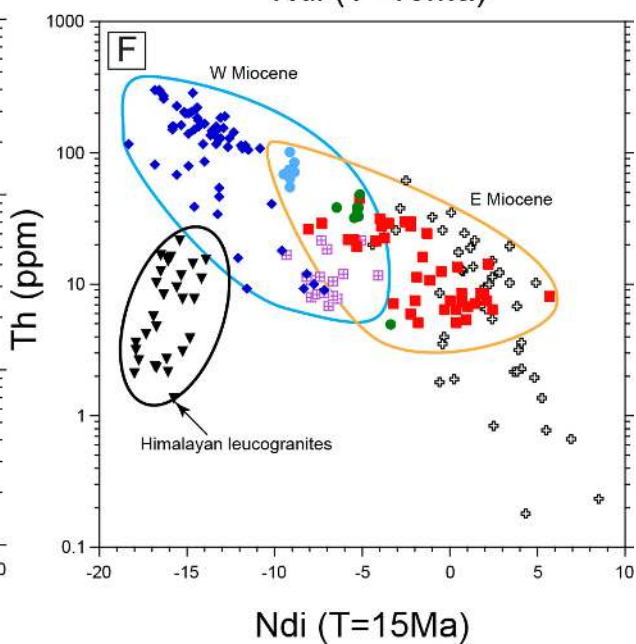
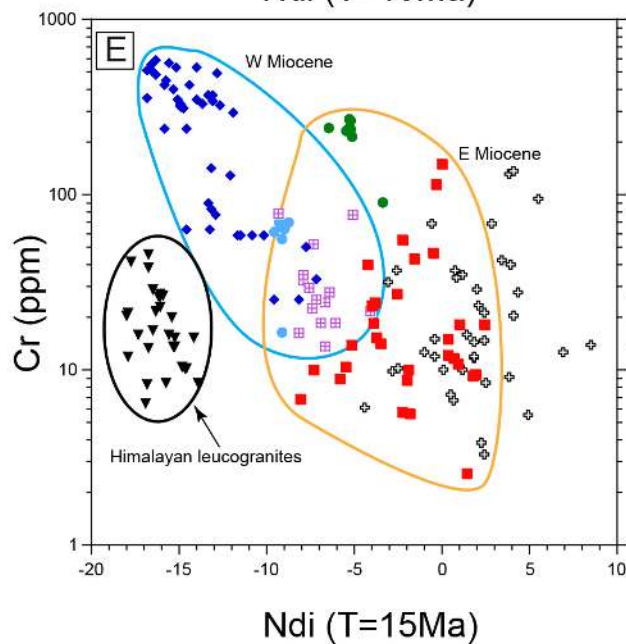
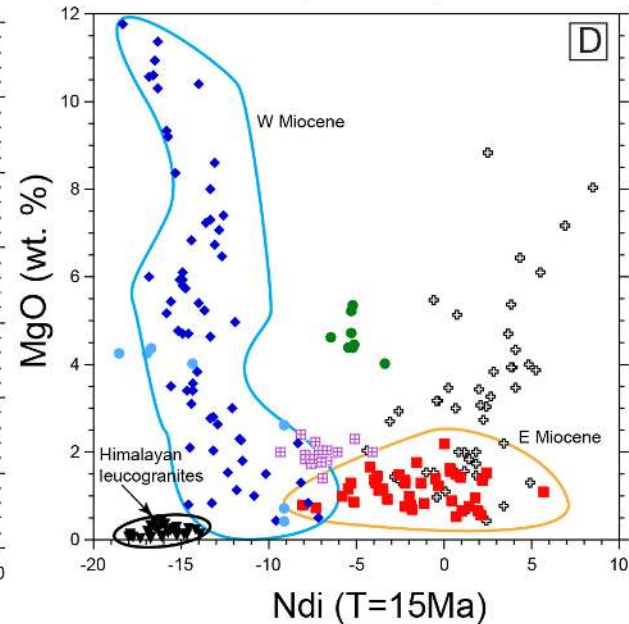
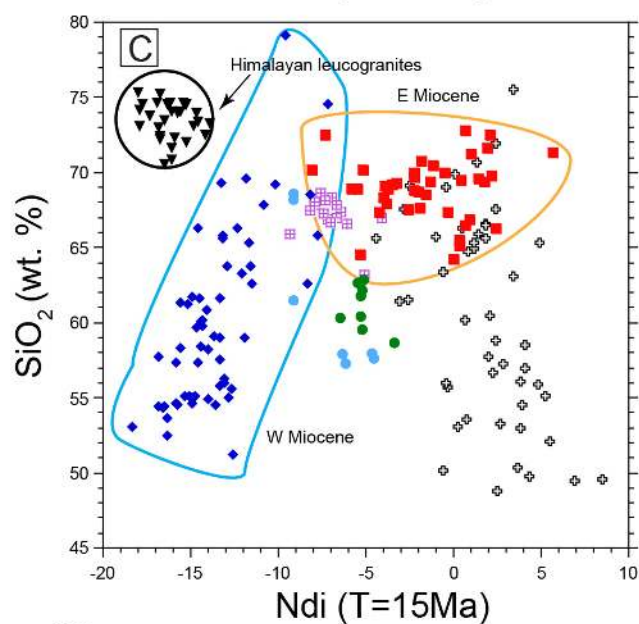
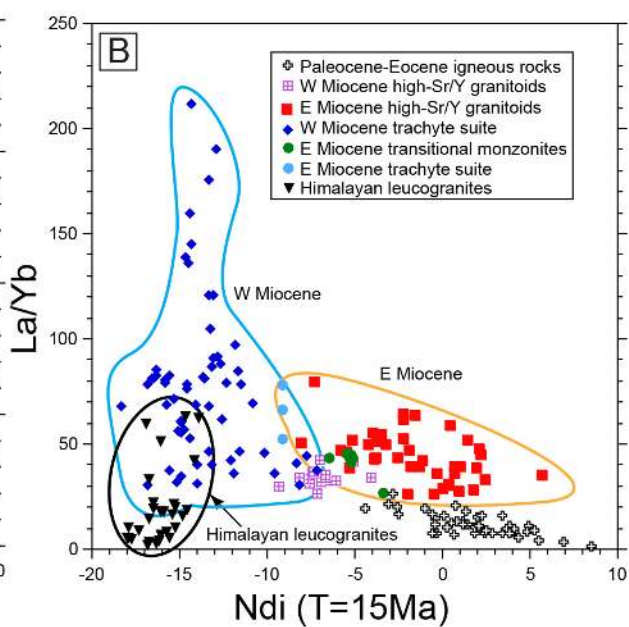
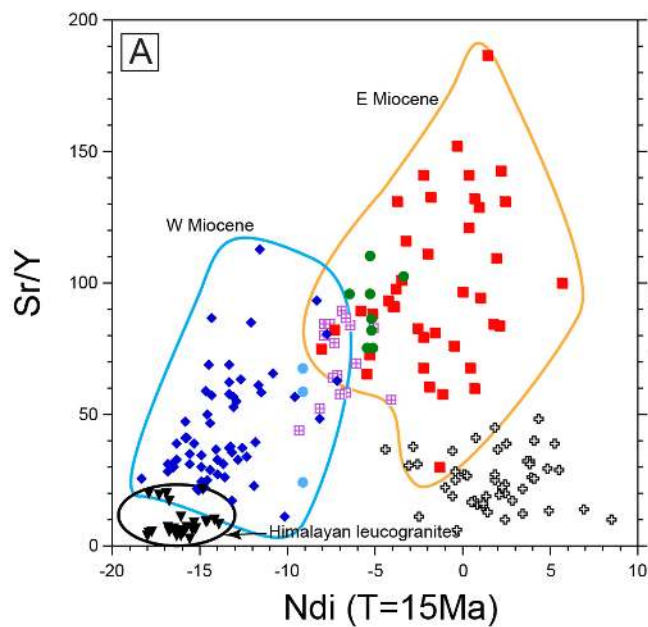


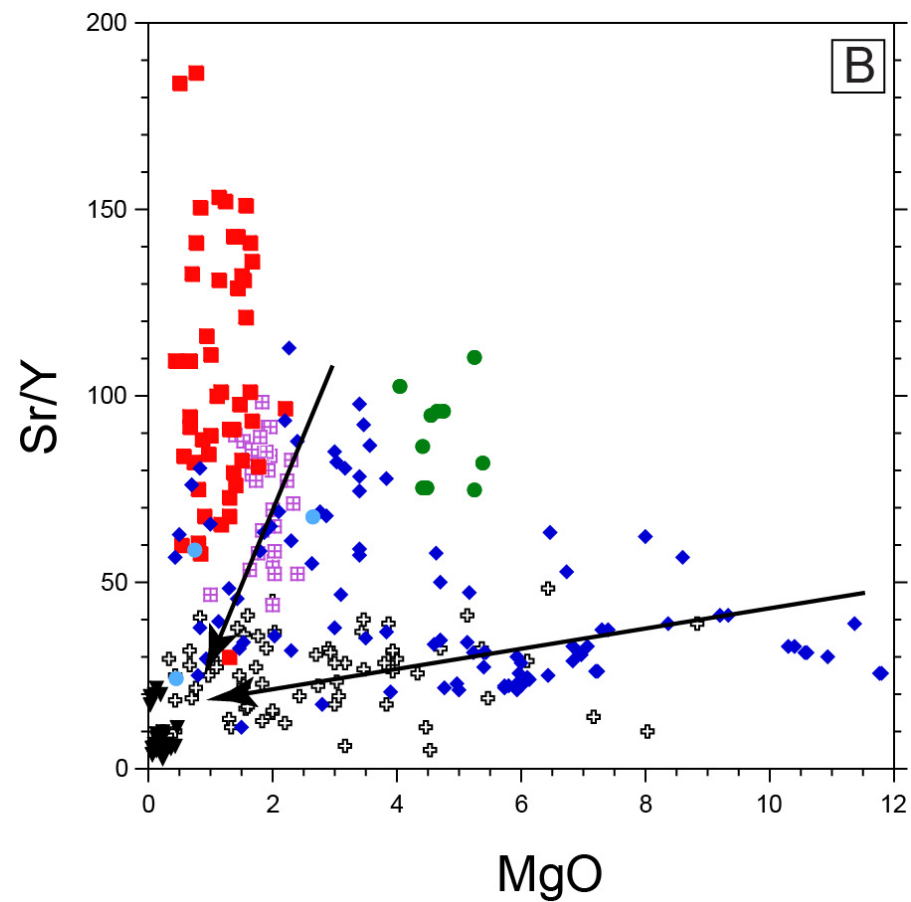
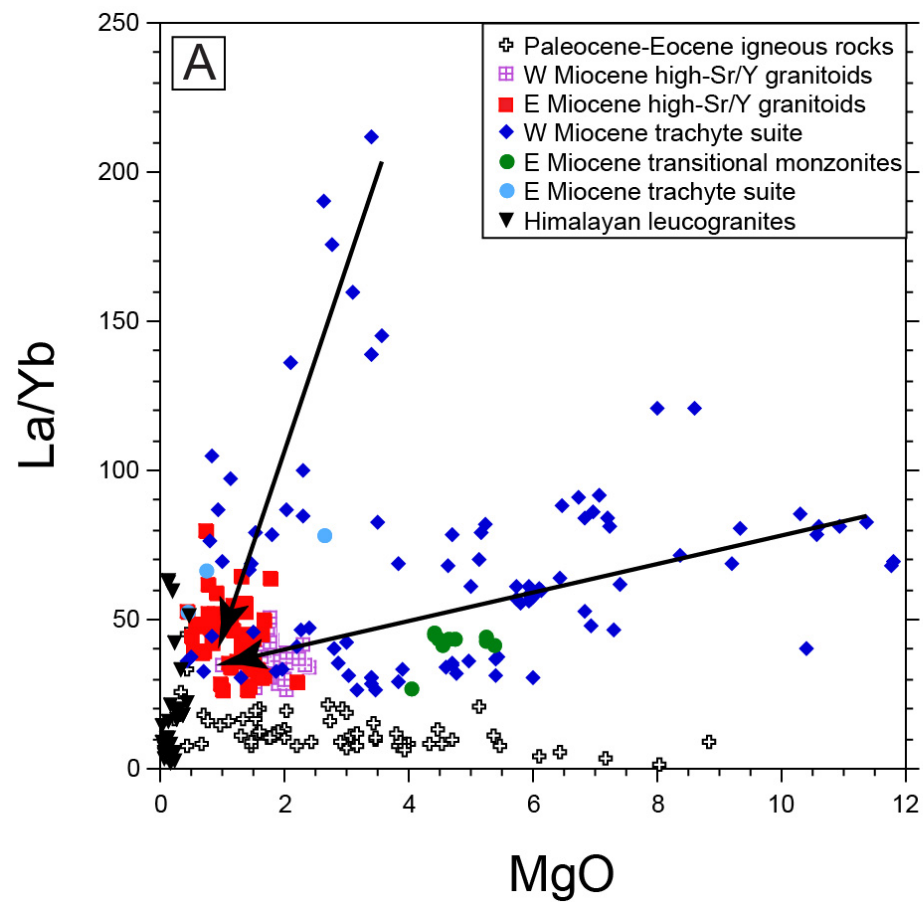


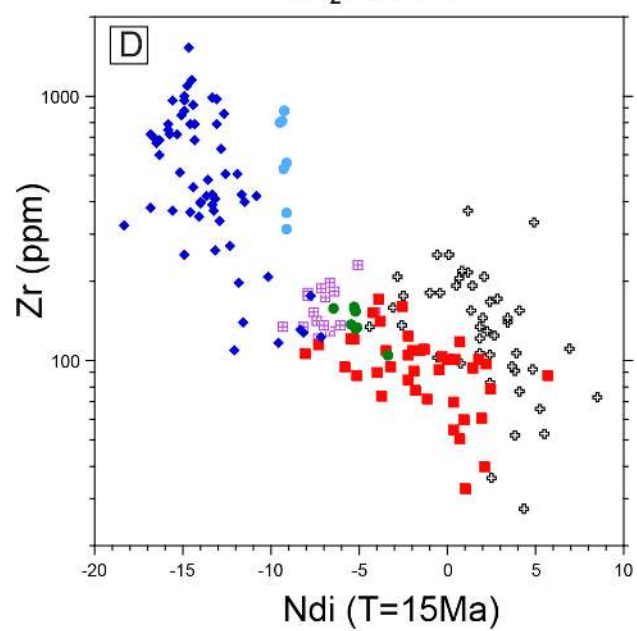
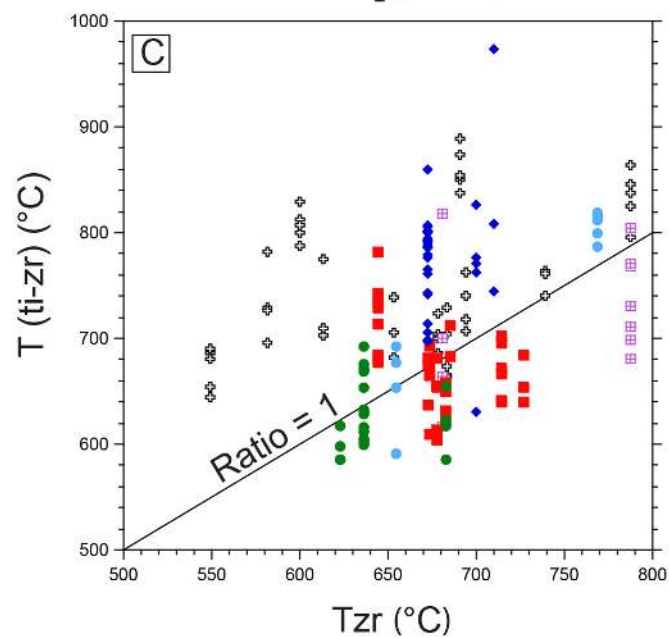
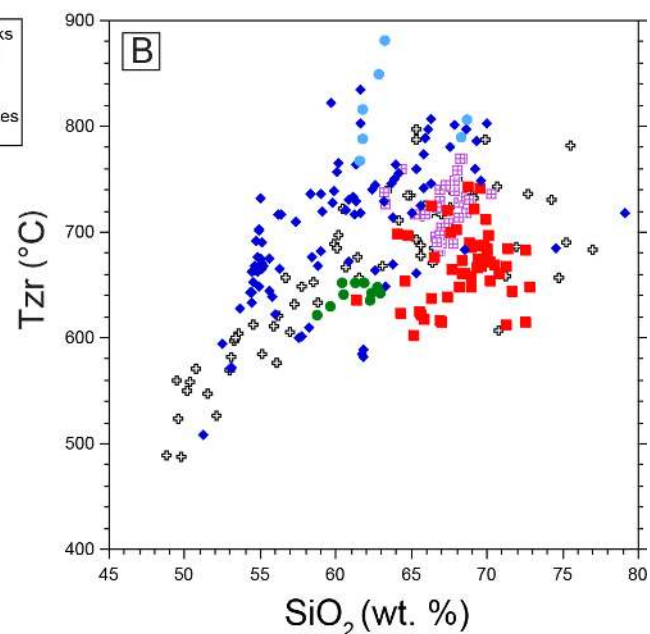
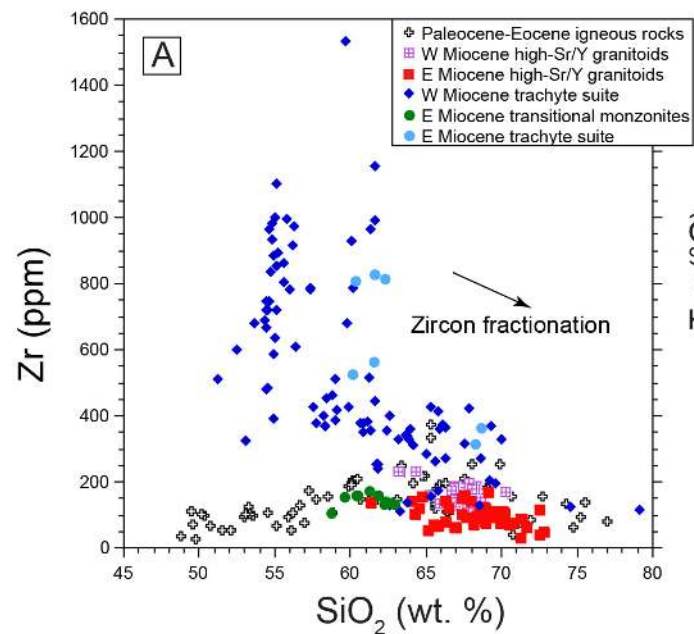


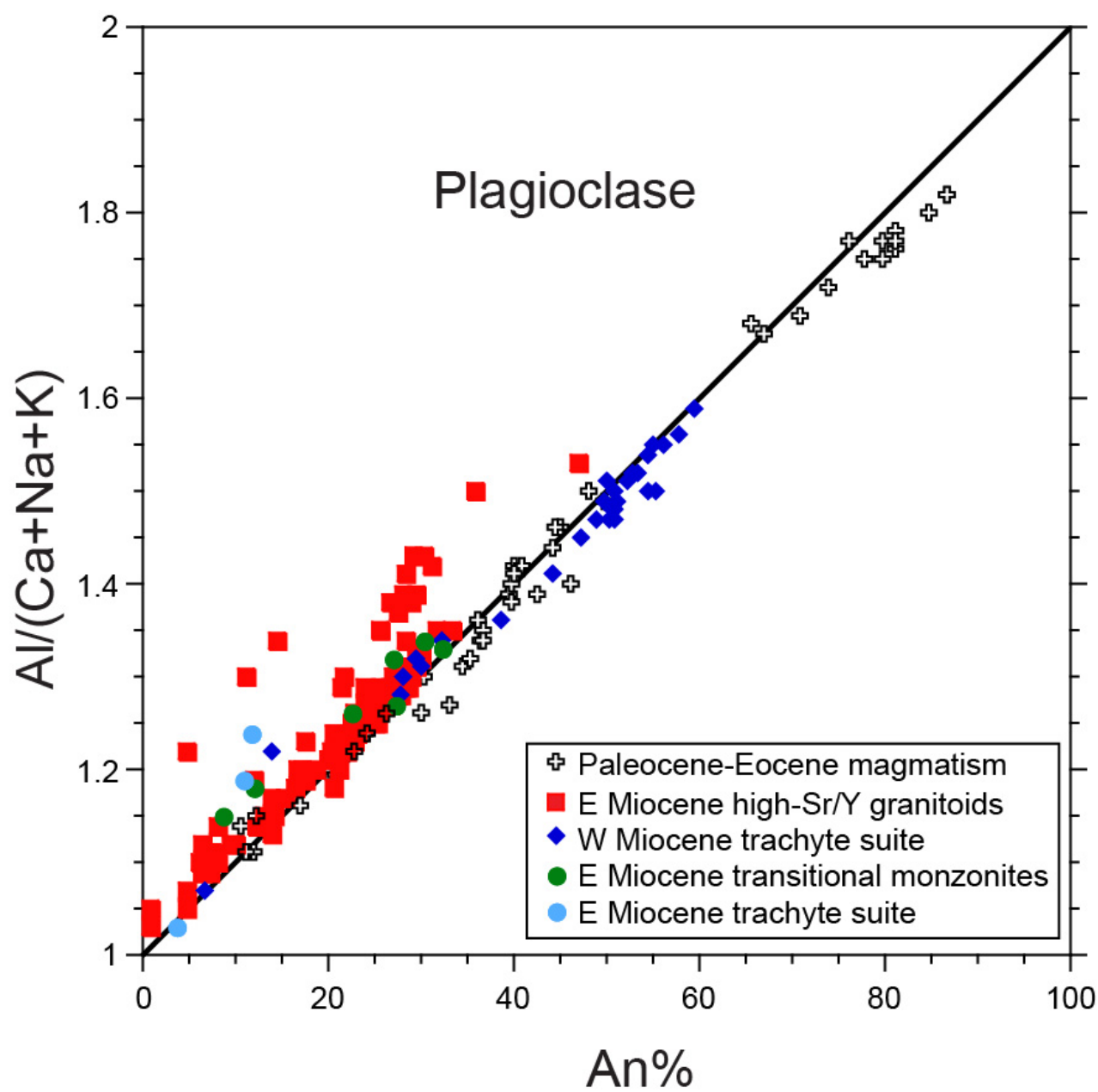


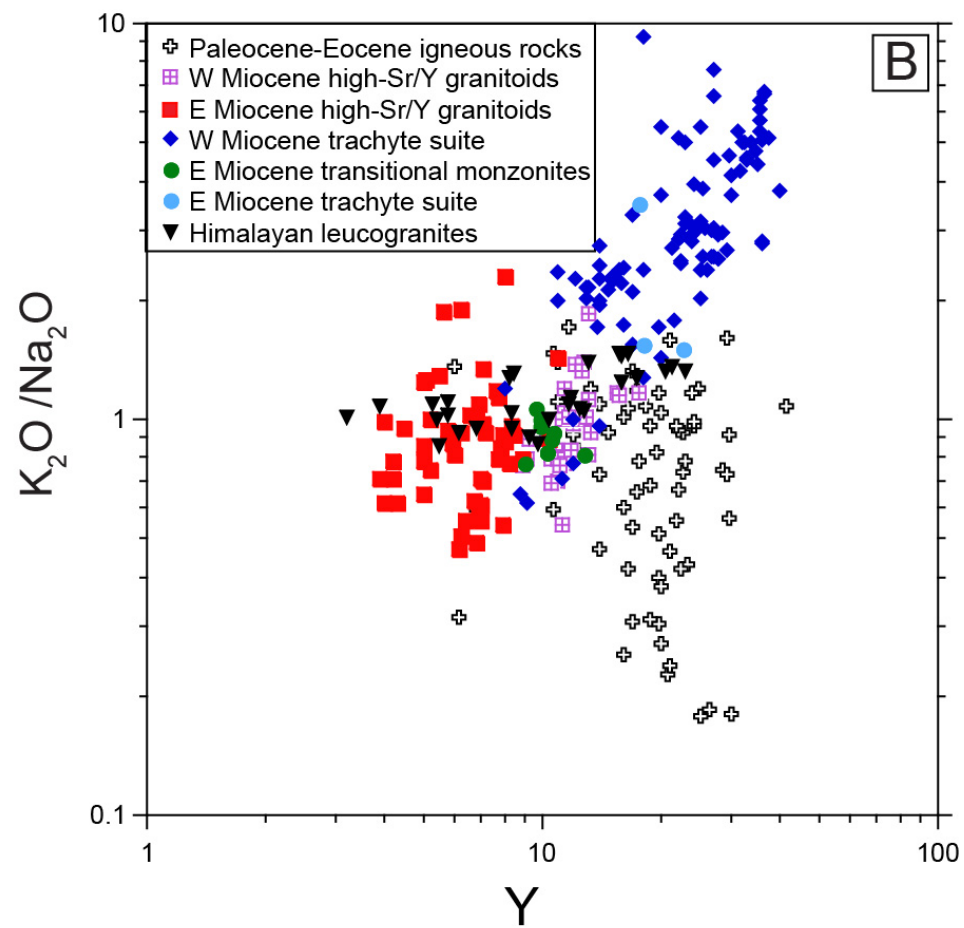
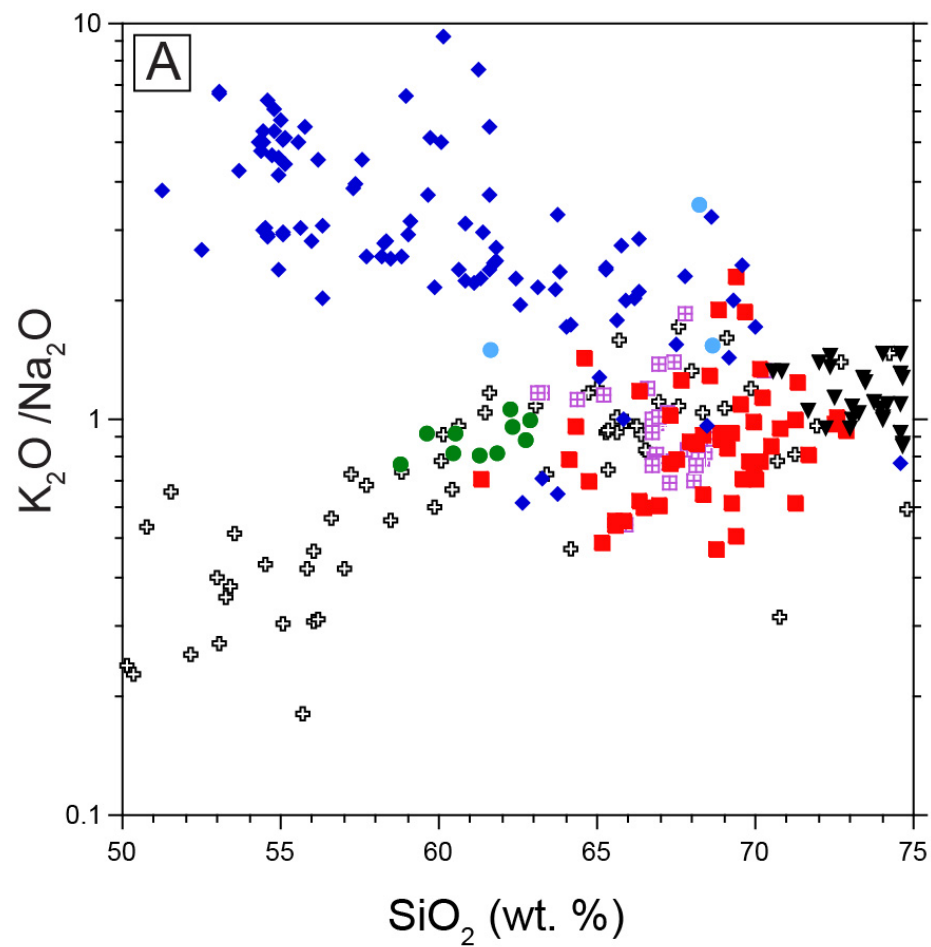




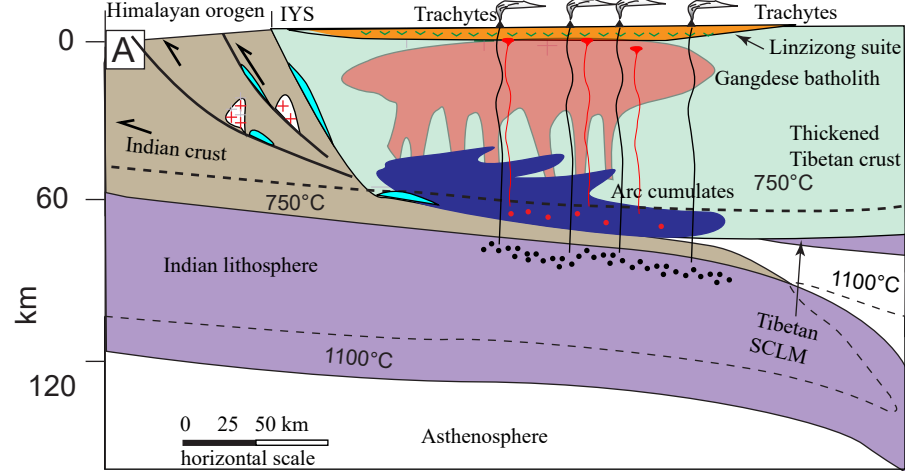




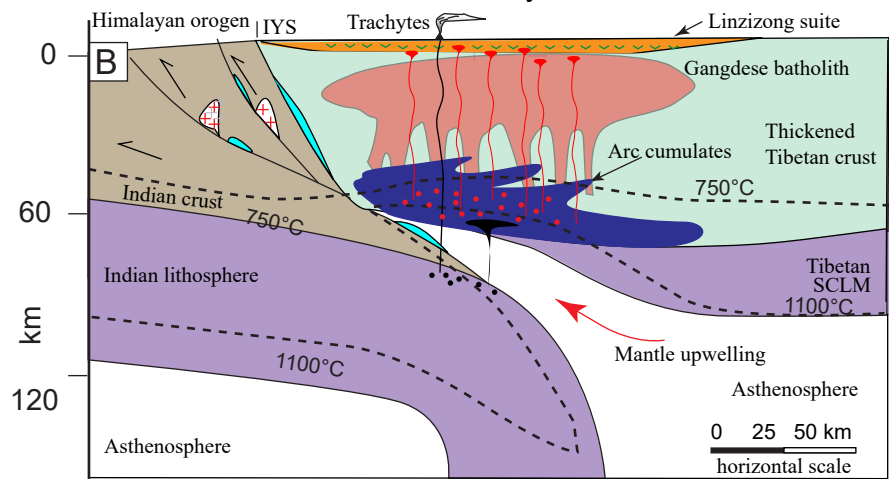




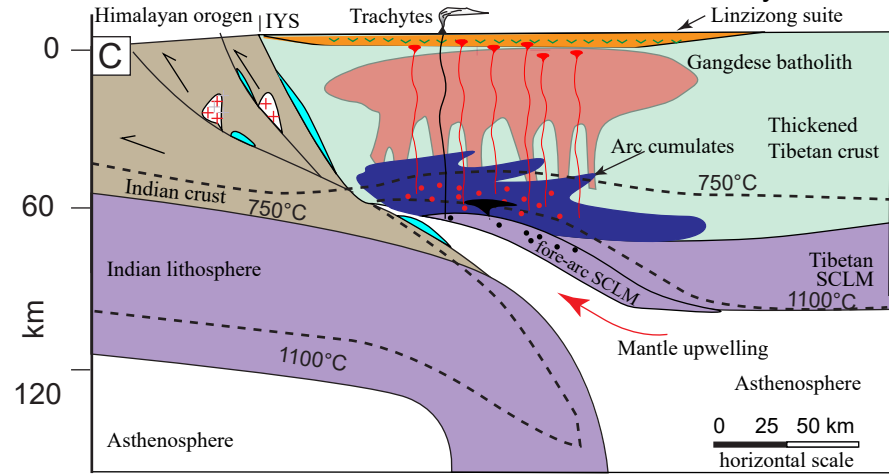
Continental underthrusting (flat subduction) (Western Gangdese)



Continental subduction (Eastern Gangdese):
Indian SCLM is source of trachytic melts



Continental subduction (Eastern Gangdese):
underthrust Tibetan SCLM is source of trachytic melts



... trachytic melts ... high-Sr/Y melts --- geotherm red triangle high-Sr/Y granitoids
trachytes leucogranite oxidized carbonate and evaporitic sediments

